

## Journal Pre-proofs

Double-edged Swords: Diaryl Pyrazoline Thiazolidinediones Synchronously Targeting Cancer Epigenetics and Angiogenesis

Neha Upadhyay, Kalpana Tilekar, Sabreena Safuan, Alan P. Kumar, Markus Schweipert, Franz-Josef Meyer-Almes, Ramaa C S

PII: S0045-2068(21)00727-6  
DOI: <https://doi.org/10.1016/j.bioorg.2021.105350>  
Reference: YBIOO 105350

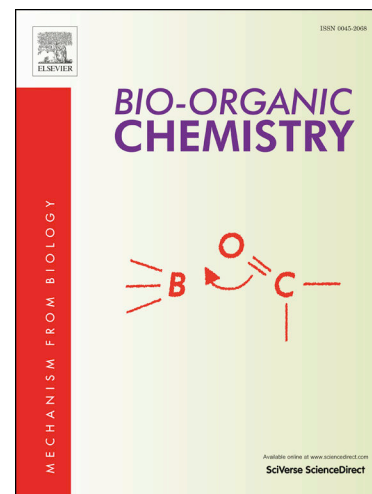
To appear in: *Bioorganic Chemistry*

Received Date: 22 March 2021  
Revised Date: 13 July 2021  
Accepted Date: 7 September 2021

Please cite this article as: N. Upadhyay, K. Tilekar, S. Safuan, A.P. Kumar, M. Schweipert, F-J. Meyer-Almes, R. C S, Double-edged Swords: Diaryl Pyrazoline Thiazolidinediones Synchronously Targeting Cancer Epigenetics and Angiogenesis, *Bioorganic Chemistry* (2021), doi: <https://doi.org/10.1016/j.bioorg.2021.105350>

This is a PDF file of an article that has undergone enhancements after acceptance, such as the addition of a cover page and metadata, and formatting for readability, but it is not yet the definitive version of record. This version will undergo additional copyediting, typesetting and review before it is published in its final form, but we are providing this version to give early visibility of the article. Please note that, during the production process, errors may be discovered which could affect the content, and all legal disclaimers that apply to the journal pertain.

© 2021 Published by Elsevier Inc.



# Double-edged Swords: Diaryl Pyrazoline Thiazolidinediones Synchronously Targeting Cancer Epigenetics and Angiogenesis

Neha Upadhyay<sup>1</sup>, Kalpana Tilekar<sup>1</sup>, Sabreena Safuan<sup>2</sup>, Alan P. Kumar<sup>3</sup>, Markus Schweipert<sup>4</sup>, Franz-Josef Meyer-Almes<sup>\*4</sup>, Ramaa C S<sup>\*1</sup>

<sup>1</sup>Department of Pharmaceutical Chemistry, Bharati Vidyapeeth's College of Pharmacy, Navi Mumbai, India.

<sup>2</sup>School of Health Sciences, Health Campus Universiti Sains Malaysia 16150 Kubang Kerian Kelantan.

<sup>3</sup>Cancer Science Institute of Singapore and Department of Pharmacology, Yong Loo Lin School of Medicine, National University of Singapore, Singapore

<sup>4</sup>Department of Chemical Engineering and Biotechnology, University of Applied Sciences, Darmstadt, Germany.

\*Corresponding authors. E-mail address: [sinharamaa@yahoo.in](mailto:sinharamaa@yahoo.in), [franz-josef.meyer-almes@h-da.de](mailto:franz-josef.meyer-almes@h-da.de)

**Keywords:** Anti-tumor, HDAC, Multi-targeting, Synthesis, VEGFR-2

## ABSTRACT

In the present study, two novel series of compounds incorporating naphthyl and pyridyl linker were synthesized and biological assays revealed 5-(((6-(2-(5-(2-chlorophenyl)-3-(4-fluorophenyl)-4,5-dihydro-1H-pyrazol-1-yl)-2-oxoethoxy) naphthalene-2-yl)methylene)thiazolidine-2,4-dione (**14b**) as the most potent dual inhibitors of vascular endothelial growth factors receptor-2 (VEGFR-2) and histone deacetylase 4 (HDAC4). Compounds **13b**, **14b**, **17f**, and **21f** were found to stabilize HDAC4; where, pyridyl linker swords were endowed with higher stabilization effects than naphthyl linker. Also, **13b** and **14b** showed best inhibitory activity on VEGFR-2 as compared to others. Compound **14b** was most potent as evident by *in-vitro* and *in-vivo* biological assessments. It displayed anti-angiogenic potential by inhibiting endothelial cell proliferation, migration, tube formation and also suppressed new capillary formation in the growing chick chorioallantoic membranes (CAMs). It showed selectivity and potency towards HDAC4 as compared to other HDAC isoforms. Compound **14b** (25 mg/kg, i.p.) also indicated exceptional antitumor efficacy on *in-vivo* animal xenograft model of human colorectal adenocarcinoma (HT-29). The mechanism of action of **14b** was also confirmed by western blot.

## 1. INTRODUCTION

Cancer is the most prevalent disease worldwide which is controlled by both genetic and epigenetic modifications. To combat cancer, it is essential for a molecule to have target specificity as well as potency. However, administration of single targeting agent might not always produce desired pharmacological effects due to target mutation or development of resistance.[1,2] In addition, commencement and progression of cancer rely on multiple receptor or signaling pathway, therefore, alternative strategies to target cancer is either use of combination therapy or development of multi-targeting agents.[3,4] Limitations of using combination therapy are dose-limiting toxicities, drug-drug interactions and cost of two separate agents. A single agent simultaneously targeting multiple pathways may provide therapeutic benefits in cancer treatment due to synergistic potential.[5–7] In dual/multi-target approach, the concept of “magic bullets” exists which is “a single drug with multi-target specificity and high potency”,[8] therefore, dual/multi-targeting approach could be used extensively for the development of potential agents in cancer treatment.

Angiogenesis plays a fundamental role in many physiological processes such as embryonic development, wound healing, growth of endometrium during menstrual cycle and ovulation. However, excessive angiogenesis is often linked with numerous pathologies, including chronic inflammation, arthritis, psoriasis, proliferative blinding retinopathy and cancer.[9,10] There are varieties of molecules involved in regulation of angiogenesis, among which, vascular endothelial growth factors (VEGF) and their kinase receptors remains the most prominent ones. The interaction of VEGF with VEGF receptors (VEGF receptor 2 - VEGFR-2/KDR/Flk1) starts critical downstream signaling pathways that bring about tumor angiogenesis. Thus, VEGF/VEGFR pathway signifies a rational target for therapeutic intervention.[11–14] FDA has approved bevacizumab & ramucizumab antibody that target VEGF and other synthetic agents such as sorafenib, sunitinib, pazopanib, vandetanib, axitinib and regorafenib.[5,15] However, their use as monotherapy is limited due to drug resistance, low efficacy, aggressive relapse and metastasis of tumor post withdrawal of drugs.[16–20] Resistance is the major concern among all, thus, over decades researchers are directing their focus on potential treatment of resistance.[5]

Histone deacetylase (HDAC) is a key enzyme involved in epigenetic alterations thus, it is well known therapeutic target in anticancer drug discovery.[21,22] However, monotherapy of HDAC inhibitors fails to display any significant effectiveness against solid tumors.[23] So far there are various FDA approved non-selective HDAC inhibitors used for hematologic cancer such as vorinostat, panobinostat and belinostat, but they are associated with several side effects such as mutagenicity, thrombocytopenia, leukopenia, diarrhoea and fatigue.[24,25] Hydroxamic acids are under suspicion in being potentially mutagenic besides the intrinsic propensity for unselectivity.[26] Thus, best alternative strategy to circumvent potential mutagenicity and unselectivity issues associated with hydroxamate function would be to develop non-hydroxamate ZBGs. A suitable example would be prodrug romidepsin (FK228) which contain thiol ZBG and has been approved for cutaneous and peripheral T-cell lymphoma.[27] On the similar lines various HDAC inhibitors with non-hydroxamate ZBGs have been reported.[28–30]

Interestingly, HDAC inhibitors are also known to inhibit angiogenesis by downregulation of VEGF and suppression of neovascularization through alteration of other genes directly involved in angiogenesis.[31–34] Literature reports also state that HDAC inhibitors mediate anti-angiogenesis actions by several mechanisms viz. suppression of hypoxia inducible factor-1 $\alpha$  (HIF-1 $\alpha$ ), initiating cell cycle arrest, and inducing apoptosis and autophagy.[35,36] Furthermore, in 2011, cabozantinib was developed using multitarget approach, which was reported as dual inhibitor of VEGFR-2 and c-Met and is successfully used for treatment of renal cell carcinoma.[37–39] Various dual targeting agents are evident, wherein, VEGFR-2 is one of the target along with other potential targets[1,2,40–43] and same remain true in case of HDAC also.[28,44–48] Additionally, multi-target 2-indolinone derivatives were reported as protein kinase and HDAC inhibitors.[49] In clinical studies HDAC inhibitors have also been used in combination with anti-angiogenic agents for the treatment of sarcomas.[50] HDACs are known to involve in VEGF-induced angiogenesis, endothelial cell proliferation and migration; and also several reports support selection of these two as potential druggable targets.[35,51] Thus, by using multitarget approach development of agents simultaneously targeting VEGFR-2 and HDAC would attain anti-tumor effects along with reduced side effects associated to single-target therapy.

Herein, we designed this research project with aim to identify agent/s with inhibition capability of VEGFR-2 and HDAC. After successful synthesis and characterization of all compounds they were comprehensively screened for their biological potency. Synthesized compounds were subjected to *in-vitro* and *in-vivo* assays by which most potent compound **14b** was identified with simultaneous VEGFR-2 and HDAC inhibition potential.

## 2. RESULTS AND DISCUSSION

**2.1 Rationale of Designing.** A few literatures put forward development of VEGFR-2 and HDAC multi-acting candidates by structural hybridization strategy.[6,7,42] Most of this study led to dual inhibitors with micromolar to nanomolar inhibitory concentrations which were in comparative range of the standard drugs. However, most of the reported dual inhibitors incorporated hydroxamate moiety as the ZBG and according to literatures, the physicochemical properties associated with hydroxamic acid ZBG attain some major drawbacks including significant off-target effects, easy metabolism, poor stability, and weak binding to isozymes of class IIa.[26,52–54] For these reasons alternative ZBGs have been explored.

To design dual targeting VEGFR-2 and HDAC inhibitors, it was essential to design such unique structure which will constitute pharmacophoric requirements of both targets. Common features of VEGFR-2 inhibitors are: a hinge-binding group that binds to ATP pocket (by hydrogen bond with the NH backbone of Cys919 residue); a linker that traverses to gatekeeper residue; a hydrogen bonding moiety that interact with DGF motif (with Glu885, Cys1045 and Asp1046), and a hydrophobic tail that occupies allosteric binding pocket formed by DFG-out flip.[55–58] On the other hand, pharmacophoric features of HDAC inhibitors are: CAP portion; a linker, and ZBG[21] (Figure 2). Accordingly, dual targeting agents were designed by considering the structural necessities of both targets. We have previously reported 5-benzylidene-2,4-thiazolidinedione[59] and 5-pyridin-4-yl-2-thioxo-[1,3,4]oxadiazol-3-yl[60] analogs as VEGFR-2 inhibitors

(Figure 2; compound 10 and 11 respectively), with a conclusion that heavy hydrophobic moiety was essential to occupy large DFG motif. Thus, 5-benzylidene-2,4-thiazolidinediones analog was modified by replacing terminal aryl group with bulkier diaryl-substituted pyrazoline (ring A and B) and other structural features were retained. The diaryl-substituted pyrazoline ring was the best choice due to the fact that: they have been identified as appropriate surface recognition motif in designing of HDAC inhibitors (Figure 1; compound 5–9)[61–67]; they exhibit excellent antiproliferative potential[68–74]; and more interestingly, pyrazoline bearing analogs have been reported to show excellent VEGFR-2 inhibition capability (Figure 1; compound 3 and 4)[42,43,75–78] as well as anti-angiogenesis potency (Figure 1; compound 1 and 2).[79–82] Thiazolidinedione (TZD) is a privileged scaffold which has been explored for its antiproliferative potential in the field of anticancer drug discovery.[83,84] We have previously reported HDAC inhibitors (Figure 2; compound 12 and 13)[29,85] where TZD was placed at the zinc binding tail and served as replacement of classical hydroxamate ZBG, led to a novel non-hydroxamate ZBG. Additionally, our previously reported VEGFR-2 inhibitors (Figure 2 compound 10) also hold TZD; hence, keeping the TZD scaffold would ensure retention of VEGFR-2 inhibition along with HDAC inhibitory potential. Thus, while designing the dual inhibitors, TZD scaffold was projected at the tail portion. In particular, many non-classical HDAC inhibitors contain cyclic ring as a linker instead of straight chain with potent HDAC inhibitory activity[21,86,87] and similar was found true with our recently reported selective-HDAC8 inhibitors (Figure 2 compound 13),[29] which contains naphthalene as cyclic linker. Thus, two different cyclic rings (ring C) viz. naphthalene and pyridine were incorporated as linker to give completely novel structure and also to compare their structure activity relationship as VEGFR-2 and HDAC inhibitors.

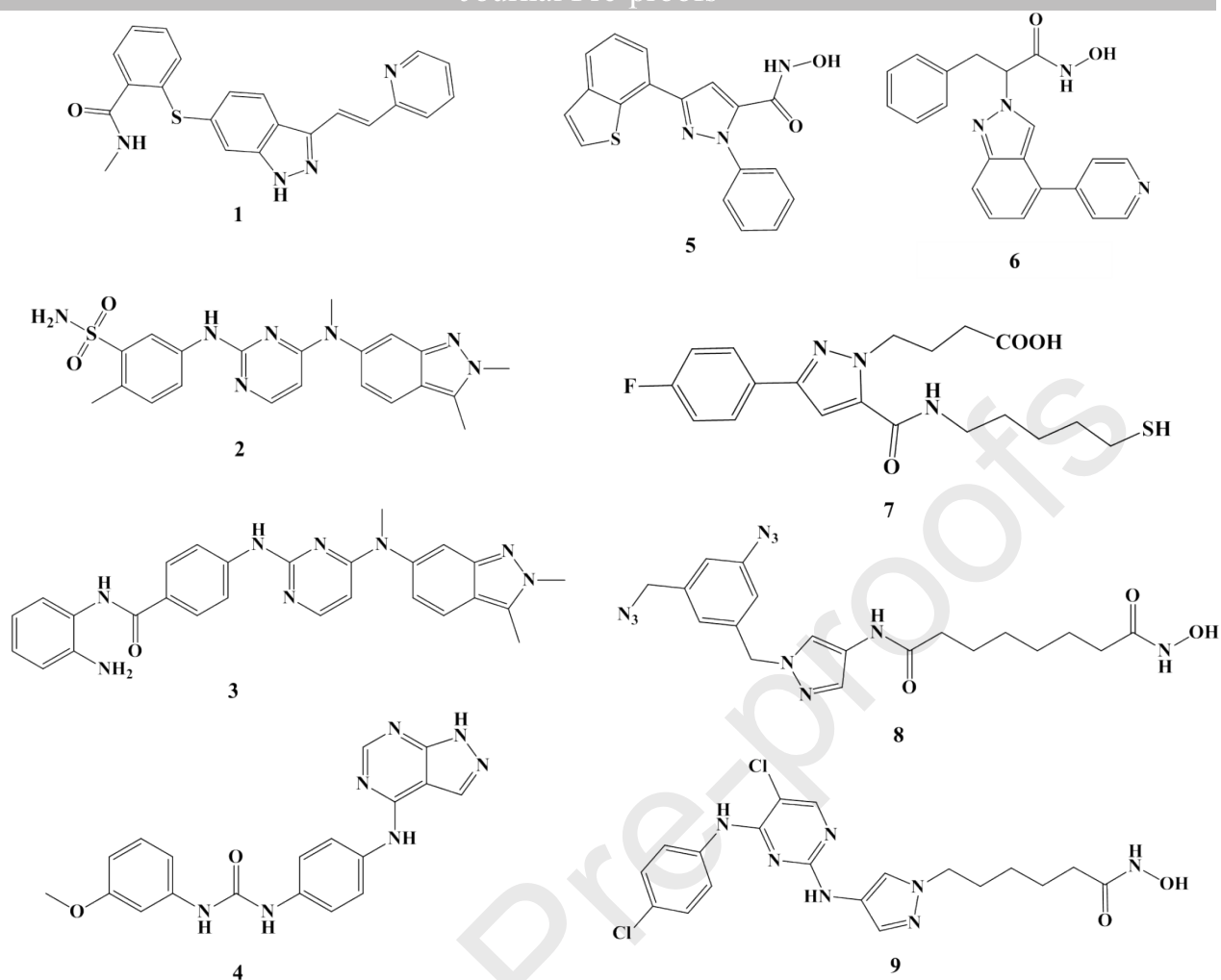


**Figure 1.** Different VEGFR-2 and HDAC inhibitors.

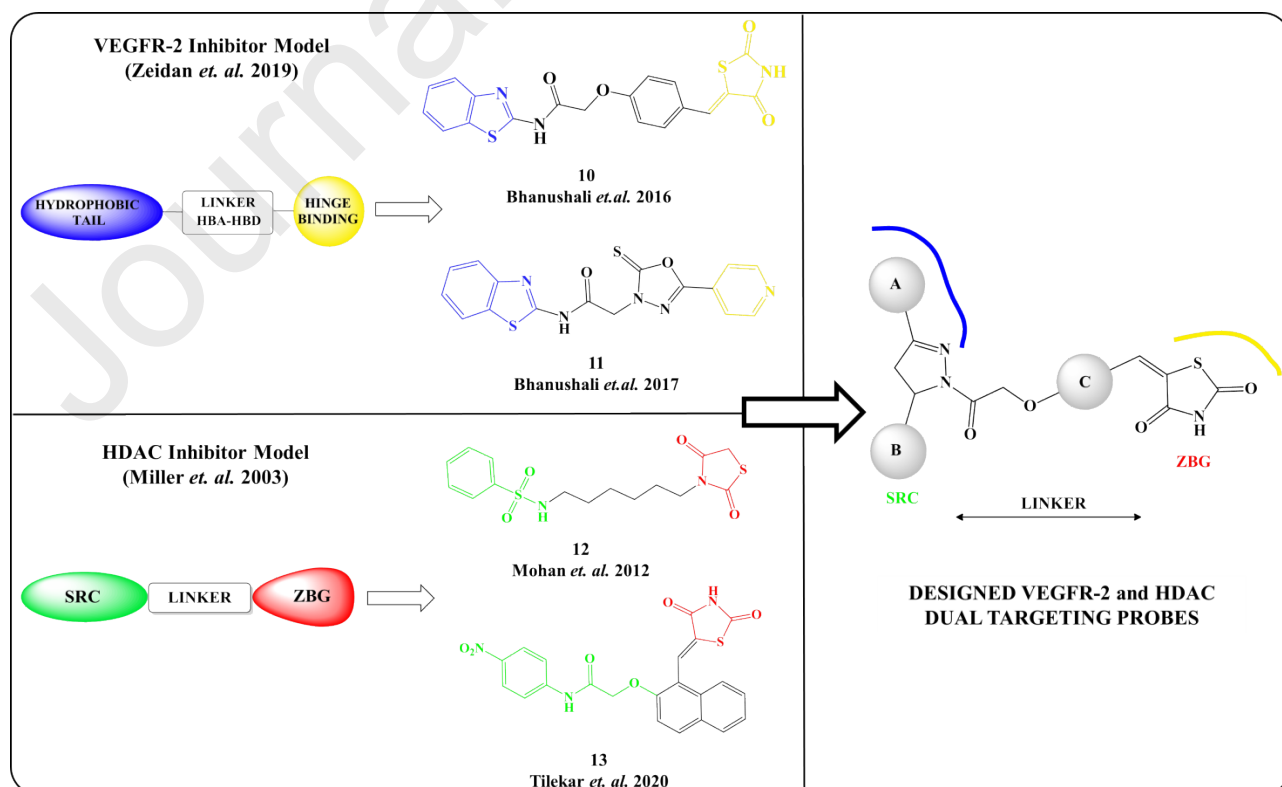


**Figure 2.** Designing strategy of novel VEGFR-2 and HDAC dual inhibitors. HBA – hydrogen bond acceptor; HBD – hydrogen bond donor; SRC – surface recognition cap; ZBG – zinc binding group.

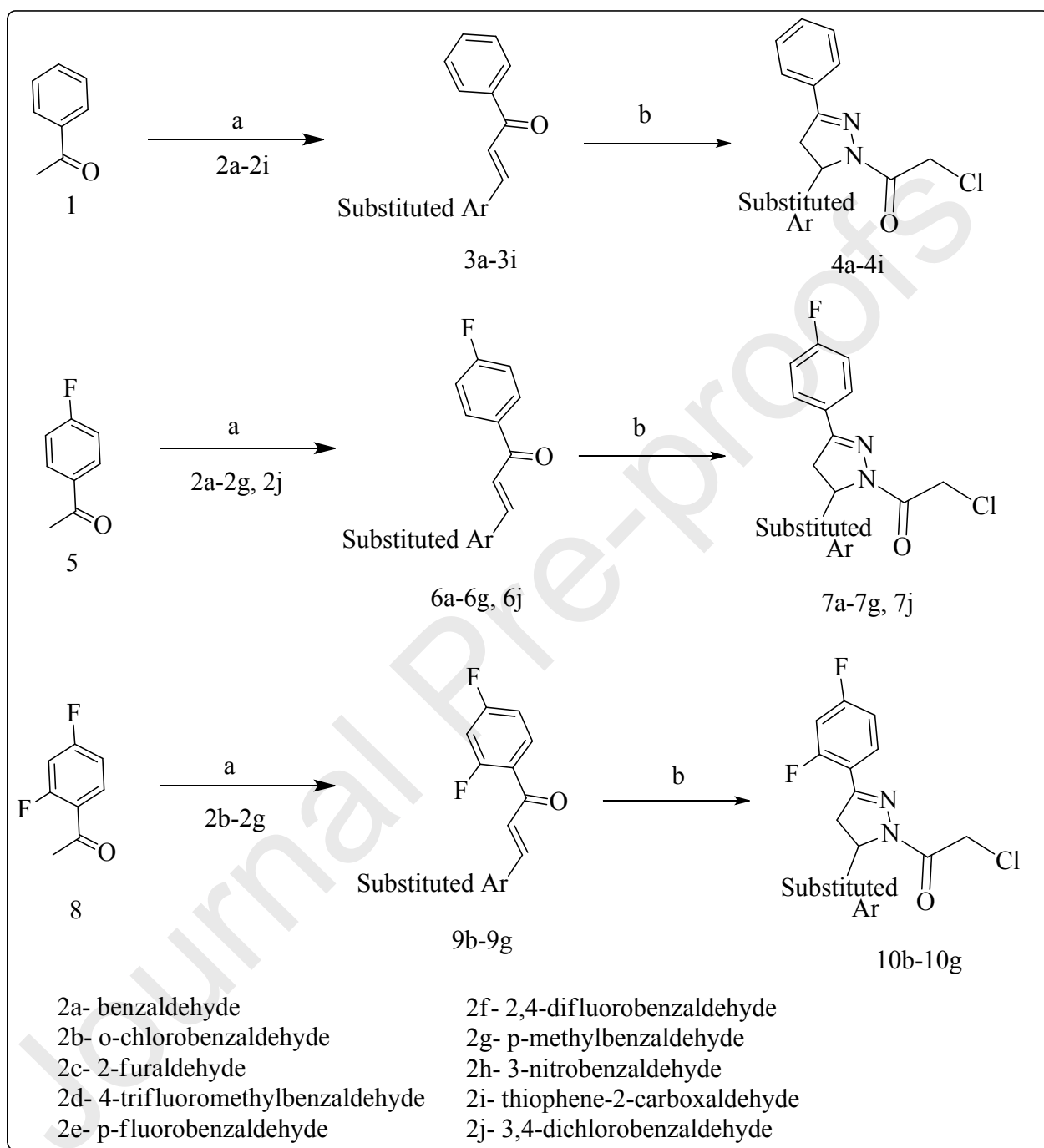
**2.2 Chemistry.** All intermediates and final compounds were synthesized by using 3 different schemes (scheme I, II and III). The detailed procedure of synthesis and other spectral observations have been presented in the experimental section. The purity of all the final compounds were confirmed by HPLC which was >95%. Structures of all the intermediates were confirmed by <sup>1</sup>H-NMR and FTIR and that of all the final compounds by different spectroscopies viz. <sup>1</sup>H-NMR, <sup>13</sup>C-NMR, FTIR and Mass.

Scheme I outline the synthesis of intermediates viz. chalcones and, chloroacetylated pyrazolines. First step was synthesis of different chalcones (**3a-3c**, **3e**, **3g**, **3i**, **6a-6g**, **6j**, and **9b-9g**), which occurred via renowned Claisen-Schmidt condensation reaction. Substituted acetophenone (**1**, **5** and **8**) were reacted with different aromatic aldehydes (**2a-2g**, **2i**, and **2j**) in basic medium to obtain respective chalcone derivatives (**3a-3c**, **3e**, **3g**, **3i**, **6a-6g**, **6j**, and **9b-9g**). Chloroacetylated pyrazoline intermediates (**4a-4c**, **4e**, **4g**, **4i**, **7a-7g**, **7j**, and **10b-10g**) were synthesized by refluxing different chalcones (**3a-3c**, **3e**, **3g**, **3i**, **6a-6g**, **6j**, and **9b-9g**) with hydrazine hydrate and chloroacetyl chloride in chloroform.

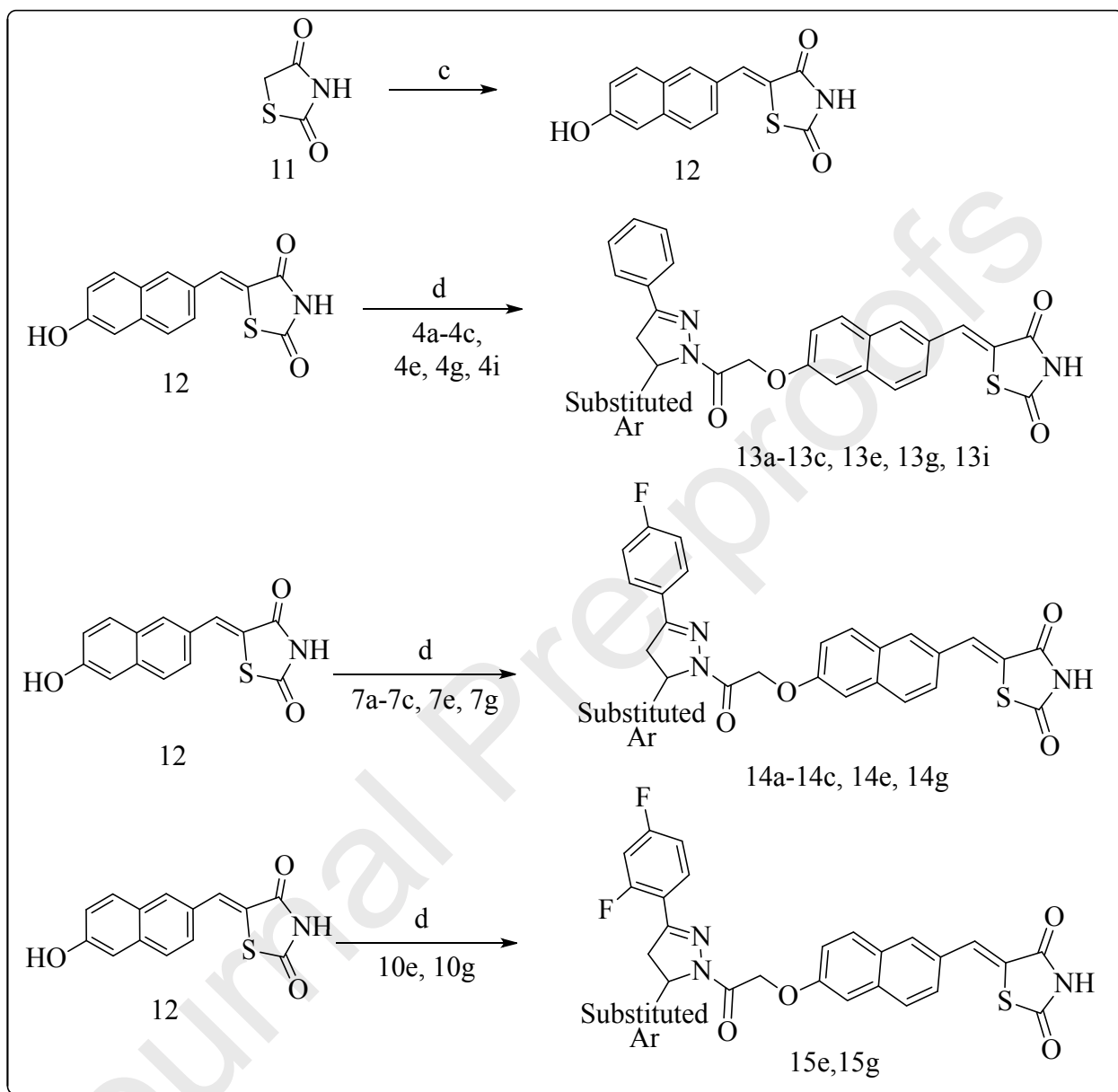
Scheme II outlines the synthesis of final compounds (**13a-13c**, **13e**, **13g**, **13i**, **14a-14c**, **14e**, **14g**, **15e**, and **15g**) which proceed via two steps: 1) Knoevenagel condensation of 2,4-thiazolidinedione (**11**) with 6-hydroxy-2-naphthaldehyde, in the presence of piperidine benzoate in toluene to obtain 5-((6-hydroxynaphthalen-2-yl)methylene)thiazolidine-2,4-dione (**12**); 2) Reaction of **12** with the respective chloroacetylated pyrazolines (**4a-4c**, **4e**, **4g**, **4i**, **7a-7g**, **7j**, and **10b-10g**) in the presence of K<sub>2</sub>CO<sub>3</sub> in DMF to obtain the respective final compounds (**13a-13c**, **13e**, **13g**, **13i**, **14a-14c**, **14e**, **14g**, **15e**, and **15g**).

Scheme III represents the synthesis of final compounds **17a-17b**, **17d-17f**, **17h**, **17i**, **19a-19f**, and **21b-21f**. In this route of synthesis, appropriate changes were made at different steps, as by following the same synthetic routes (Scheme I and II) product was not obtained. Hence, the scheme was reversed by first coupling 6-hydroxynicotinaldehyde with various chloroacetylated intermediates (**4a-4b**, **4d-4f**, **4h**, **4i**, **7a-7f**, and **10b-10f**) in the presence of K<sub>2</sub>CO<sub>3</sub> in DMF to obtain respective aldehyde containing intermediates (**16a-16b**, **16d-16f**, **16h**, **16i**, **18a-18f**, and **20b-20f**). Further, Knoevenagel condensation of 2,4-thiazolidinedione (**11**) in 2-methoxyethanol and catalytic amount of piperidine along with the aldehyde intermediates (**16a-16b**, **16d-16f**, **16h**, **16i**, **18a-18f**, and **20b-20f**) was carried out to give the corresponding target compounds (**17a-17b**, **17d-17f**, **17h**, **17i**, **19a-19f** and **21b-21f**).

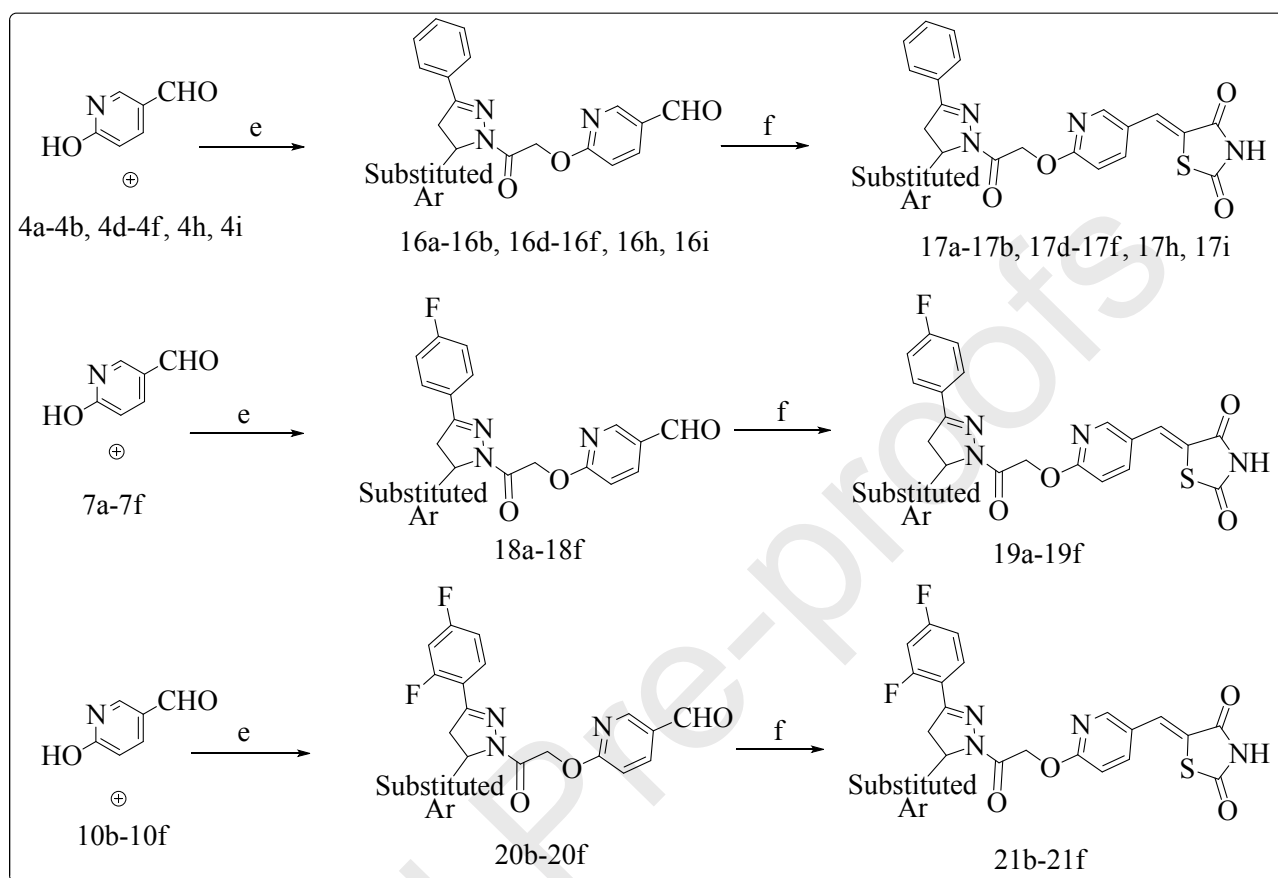
**Scheme I.** Synthesis of intermediates (3a-3i, 6a-6g, 6j, 9b-9g, 4a-4i, 7a-7g, 7j, and 10b-10g). Reagents and conditions: (a) Aq. NaOH, EtOH, RT, 5-6 h, 80-93%; (b)  $\text{NH}_2\text{NH}_2 \cdot \text{H}_2\text{O}$ ,  $\text{CHCl}_3$ ,  $80^\circ\text{C}$ , 12 h, then  $\text{K}_2\text{CO}_3$ ,  $\text{ClCH}_2\text{COCl}$ , RT, 12 h, 50-64%.



**Scheme II.** Synthesis of final compounds (13a-13c, 13e, 13g, 13i, 14a-14c, 14e, 14g, 15e, and 15g). Reagents and conditions: (c) 6-hydroxy-2-naphthaldehyde, piperidine benzoate, toluene, reflux, 4 h, 86%; (d)  $K_2CO_3$ , DMF, RT, 24 h, 52-70%.



**Scheme III.** Synthesis of final compounds (17a-17b, 17d-17f, 17h, 17i, 19a-19f, and 21b-21f). Reagents and conditions: (e)  $K_2CO_3$ , DMF, RT, 48 h, 52-80%; (f) 2,4-thiazolidinedione, 2-methoxyethanol, piperidine, reflux, 3 h, 54-88%.



### 2.3 *In-vitro* HDAC Enzyme Inhibition Assay. Preliminary Screening on Class I and Class II HDAC

**Isoform.** To determine the effects of pyrazoline-based thiazolidinediones (Table 1; compounds **17a-15g**) on the activity of HDACs, all thirty-one compounds were preliminary screened at 50  $\mu$ M concentration on two HDAC isoforms viz. HDAC4 (representative of Class IIa) and HDAC8 (representative of Class I). Test compounds showed excellent inhibitory effects on HDAC4 and significantly lower activity on HDAC8. Based on the results obtained in primary screening, compounds with residual enzyme activity < 50% were taken further to establish a dose-response curve. Many compounds showed considerable selectivity for HDAC4 over HDAC8 with greatest selectivity factors of >100 [ $IC_{50}(\text{HDAC8})/IC_{50}(\text{HDAC4})$ ] for compounds **13b**, **14b** and **15g**. In contrast, compound **13c** and **14c**, both of them containing a furyl group attached to the pyrazoline ring, showed comparable activities against HDAC4 and HDAC8 (supplementary data). All pyrazoline-based thiazolidinediones displayed significant inhibitory activity on HDAC4 (in low to sub-micromolar range). The best activities against HDAC4 were comparable to “Cpd 6” (Table 1).[88] There was visible difference in the HDAC4 activity of compounds containing –pyridyl and –naphthyl linker. Compounds with –pyridyl linker (**17a-17b**, **17d-17f**, **17h**, **17i**, **19a-19f**, and **21b-21f**) offered considerable inhibitory potency,  $IC_{50}$  below 10  $\mu$ M, except for **17a**. Interestingly, all compounds incorporating the naphthyl linker (**13a-13c**, **13e**, **13g**, **13i**, **14a-14c**, **14e**, **14g**, **15e**, and **15g**) demonstrated enhanced potency,  $IC_{50}$  below 1  $\mu$ M, which proved our hypothesis of selecting pyridine and naphthalene ring as linker. For representative

most active compounds **13b** and **14b**, the selectivity profile was determined over a broad panel of zinc-dependent HDAC isoenzymes (Table 2) demonstrating very similar isoenzyme selectivity compared to reference compound “Cpd6”. [88]

Overall HDAC4 and HDAC8 enzyme inhibition assay results suggest that, novel series of pyrazoline-based TZDs are HDAC4-selective inhibitors. Additionally, it was noteworthy that, in compound 13 (Figure 2), the “ortho-position” of the TZD warhead with respect to oxo-linker chain headed to “HDAC8-isoenzyme selectivity” (HDAC8 – 2.7  $\mu\text{M}$  and HDAC4 – 15  $\mu\text{M}$ ), [89] whereas, “para-positioning” shifted the isoenzyme selectivity towards HDAC4. [28] Similar was found true with the proposed pyrazoline-TZDs, wherein, the setting of TZD warhead was at “para-position” to the oxo-linker indicating HDAC4-isoenzyme selectivity (Table 1 and Table 2).

Initially to find the effects of various linkers (bicyclic/heterocyclic/aromatic), the arylidene type Knoevenagel derivatives of TZD containing these rings were synthesized and evaluated for their effects on HDAC4 and HDAC8 isoforms, wherein, Knoevenagel derivatives containing naphthyl and pyridyl ring exhibited relatively weak HDAC inhibitory activity (data not shown here). Comparison of the inhibitory potential of these Knoevenagel derivatives with that of the final compounds demonstrated that attachment to diaryl-pyrazoline ring enhanced the HDAC4 inhibitory capacity several folds as compared to Knoevenagel derivatives.

Precisely, HDACs contribute significantly in the development and growth of tumorigenesis. The, hypoxia-derived transcription factor HIF-1 $\alpha$  regulates the gene expression involved in different cellular signaling pathways of angiogenesis (via expression of VEGF). In multiple malignancies, VEGF-overexpression mediated by stabilization of HIF-1 $\alpha$  has been identified. [35,90] The posttranslational modifications such as acetylation driven by HATs and HDACs are critical for HIF-1 $\alpha$  signaling. More interestingly, class II HDACs (such as HDAC4) are vital for the stability of HIF-1 $\alpha$  protein and its transcriptional activity; and HDAC4 has been shown to regulate the acetylation levels of HIF-1 $\alpha$ . [12] In a nutshell, HDAC4 is directly or indirectly linked to the management of angiogenesis, selective-HDAC4 inhibitors are therefore supposed to be therapeutically effective.

The results demonstrated HDAC4 selectivity of these compounds and to explore their anti-angiogenesis potential, compounds with best inhibitory activity were comprehensively evaluated through various *in-vitro* and *in-vivo* follow-up assays.

**Table 1.** Preliminary screening and IC<sub>50</sub> determination of pyrazoline-based thiazolidinediones on HDAC4 and HDAC8. Residual activities are shown as means  $\pm$  standard deviation, n=3.

Sr. No.	Code	Residual HDAC4 activity (%) at 50 $\mu\text{M}$	Residual HDAC8 activity (%) at 50 $\mu\text{M}$	HDAC4 IC <sub>50</sub> ( $\mu\text{M}$ )	HDAC8 IC <sub>50</sub> ( $\mu\text{M}$ )
1	13a	16 $\pm$ 1	100 $\pm$ 5	3.8 $\pm$ 0.1	>50

2	13b	12 ± 1	59 ± 3	0.34 ± 0.02	31 ± 3
3	13c	14 ± 1	1.3 ± 0.3	1.1 ± 0.2	1.6 ± 0.4
4	13e	10 ± 1	70 ± 2	0.7 ± 0.1	>50
5	13g	12 ± 1	68 ± 2	0.7 ± 0.1	>50
6	13i	6.7 ± 0.6	6.7 ± 1.5	0.35 ± 0.02	14 ± 10
7	14a	5 ± 0.8	27 ± 1	0.8 ± 0.2	>50
8	14b	15 ± 1	75 ± 4	0.36 ± 0.2	>50
9	14c	10 ± 1	1.0 ± 0.5	1.7 ± 0.3	4.7 ± 0.5
10	14e	9.4 ± 1.7	84 ± 7	0.8 ± 0.4	>50
11	14g	8.0 ± 1.3	51 ± 4	0.8 ± 0.4	>50
12	15e	11 ± 1	63 ± 3	0.6 ± 0.1	>50
13	15g	5.6 ± 0.3	40 ± 1	0.4 ± 0.1	>50
14	17a	22 ± 1	100 ± 2	18 ± 4	>50
15	17b	21 ± 1	85 ± 7	3.3 ± 1	>50
16	17d	19 ± 1	100 ± 8	2.7 ± 0.2	>50
17	17e	11 ± 2	100 ± 5	2.5 ± 1.5	>50
18	17f	14 ± 2	100 ± 5	1.9 ± 0.4	>50
19	17h	10 ± 1	97 ± 5	5.2 ± 0.5	>50
20	17i	6.4 ± 0.9	66 ± 3	5.9 ± 0.5	>50
21	19a	10 ± 1	100 ± 8	2.1 ± 0.4	>50
22	19b	7.2 ± 0.7	32 ± 3	2.2 ± 0.3	>50
23	19c	25 ± 1	74 ± 5	>50	>50
24	19d	3.5 ± 0.7	70 ± 5	2.3 ± 0.2	>50
25	19e	11 ± 1	93 ± 3	2.1 ± 0.6	>50
26	19f	5.1 ± 0.6	93 ± 4	2.4 ± 0.2	>50

27	21b	15 ± 1	98 ± 9	4.3 ± 0.3	30.4
28	21c	13 ± 1	96 ± 2	10 ± 2	>50
29	21d	8.2 ± 1.3	98 ± 7	1.9 ± 0.2	>50
30	21e	4.3 ± 0.4	81 ± 4	3.1 ± 0.2	>50
31	21f	4.9 ± 0.3	61 ± 5	0.9 ± 0.6	>50
32	S1[91]	95 ± 1	93 ± 3	>50	>50
33	Cpd 6[88]	-	-	0.22	>50
34	Cpd 31[92]	-	-	0.02	0.36

**2.4 HDAC-Profiling on a Panel of HDACs (HDAC1-HDAC8).** In the primary screening on the two HDAC isoforms (HDAC4 and HDAC8), compounds **13b** and **14b** with naphthyl linker, and compounds **17f** and **21f** with pyridyl linker were found with greatest inhibitory potential; thus, these four compounds were evaluated on a panel of HDAC (HDAC1-HDAC8) to confirm their selectivity towards HDAC4 (Table 2). In particular, these compounds were found to be potent and highly selective towards HDAC4 as compared to other isoforms (Figure 3).

**Table 2** – Selectivity profile of pyrazoline-based thiazolidinediones on HDAC isoenzymes.

Code	IC <sub>50</sub> (μM)						
	HDAC1	HDAC2	HDAC3	HDAC4	HDAC6	HDAC7	HDAC8
13b	24 ± 2	37 ± 2	22 ± 1	0.34 ± 0.02	20 ± 1	>50	31 ± 3
14b	18 ± 1	45 ± 2	16 ± 1	0.36 ± 0.2	15 ± 1	6.3 ± 0.3	>50
17f	34 ± 3	*ND	34 ± 5	1.9 ± 0.4	>50	>50	>50
21f	>50	*ND	29 ± 3	0.9 ± 0.6	>50	>50	>50
Cpd 6[88]	>50	>50	12	0.22	17	>50	>50

\*ND – Not determined.

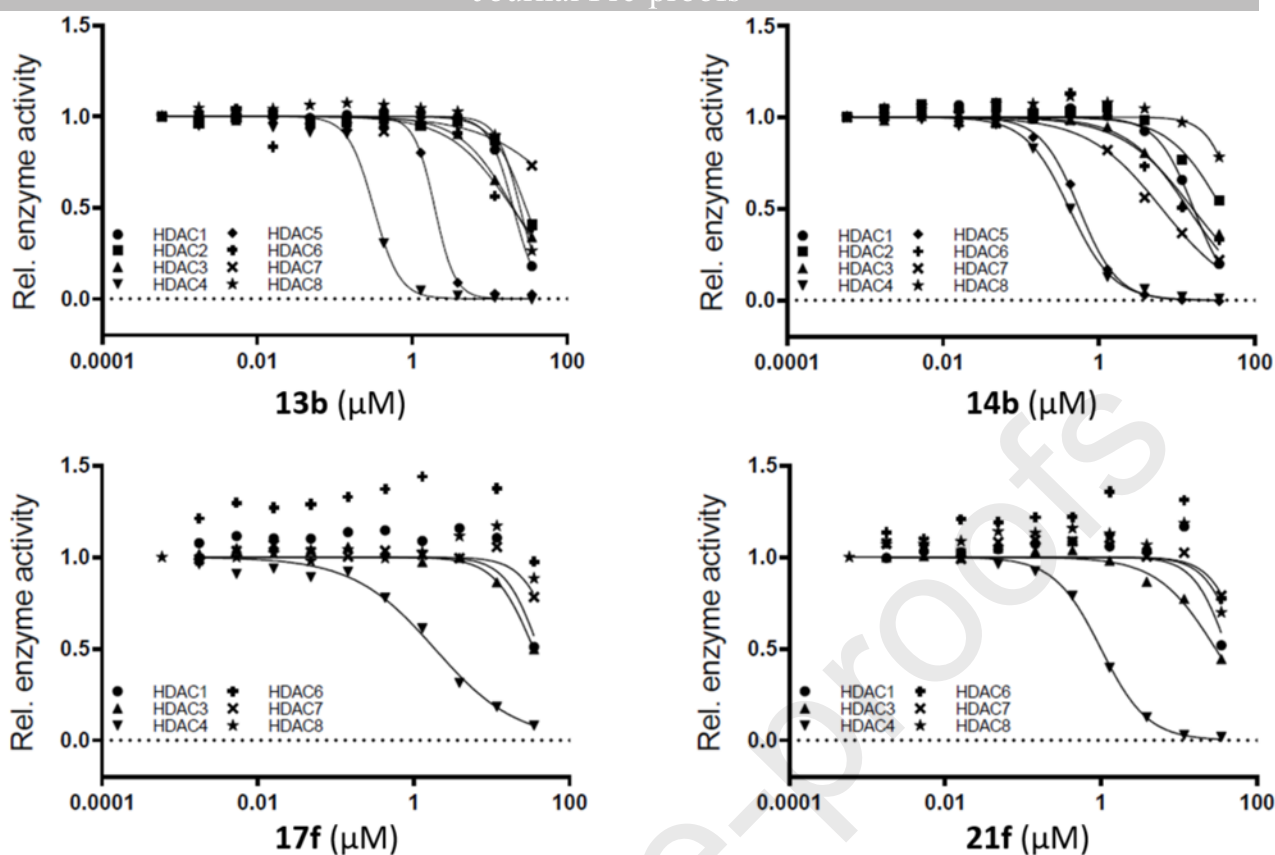


**Figure 3.** Dose response curve of compounds 13b, 14b, 17f, and 21f on different HDAC isoforms.

**2.5 Thermal Shift Assay on HDAC4.** Thermal shift assay is a modern method used to assess the binding of ligands to a target protein. This method is used to demonstrate *in-vitro* target engagement (TE) of ligands. Binding of a ligand to a target protein shifts the melting temperature of the protein producing a thermal shift. Test compounds with HDAC4 inhibitory potential (**13b**, **14b**, **17f**, and **21f**) were subjected to this assay with HDAC4 isoform to examine the thermal stabilization by the ligands. The melting temperature of unbound HDAC4 was 57.3 °C, and those of the protein in the presence of the test compounds were 57.5 °C, 57.9 °C, 60.4 °C, and 58.8 °C, for **13b**, **14b**, **17f**, and **21f**, respectively (Figure 4). In particular, all of the inhibitors were able to stabilize HDAC4, thereby confirming the interaction between HDAC4 and these compounds. Inhibitors **17f** and **21f** with pyridyl linker showed significantly higher stabilizing effects than **13b** and **14b** with naphthyl linker.

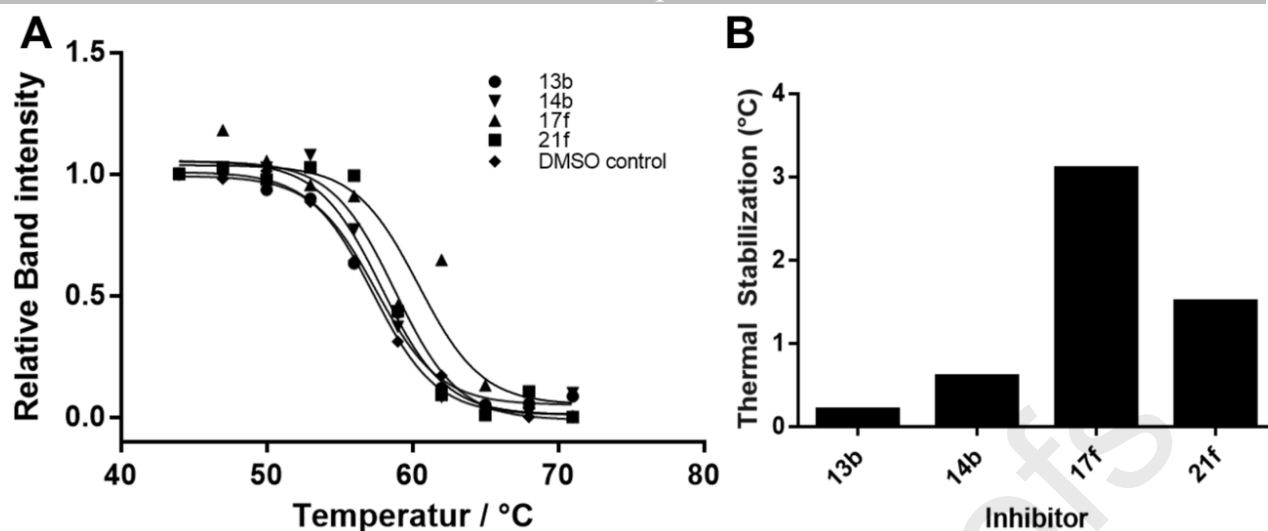


**Figure 4.** Thermal stabilization of HDAC4 upon binding of test compounds **13b**, **14b**, **17f**, and **21f**. A) Residual native HDAC4 in terms of band intensity in protein gel as a function of temperature in the presence of indicated compounds, B) Thermal stabilization of HDAC4 given as difference between the melting point of HDAC4 in the presence of indicated compound minus the melting point of unbound enzyme.

**2.6 HUVECs Cytotoxicity Assay.** Human Umbilical Vein Endothelial Cells (HUVECs) are well known representative of endothelial cells to determine cytotoxicity potential of novel antiangiogenic compounds *in-vitro*. [93,94] Sixteen compounds (Table 3) with highest HDAC4 inhibitory potential were selected to determine their effects on HUVECs proliferation and MTT assay was performed. Staurosporine (STS) was used as positive control. Different concentrations (10, 1, 0.1, 0.01, and 0.001  $\mu\text{M}$ ) of test compounds and STS were used to determine their inhibitory effects. It was noted that **13a**, **13b**, **13e**, **14b**, **14c** and **19c** exhibited good inhibitory effects on HUVEC proliferation with  $\text{IC}_{50} < 10 \mu\text{M}$  (Table 3); while, **13c**, **13g**, **13i**, **15g**, **17e**, **19d**, **19e**, **19f**, **21b**, and **21c** showed poor inhibition  $> 10 \mu\text{M}$ . However, **13a**, **13b**, **14b**, and **14c** showed better inhibitory activity on HUVECs proliferation as compared to other compounds.

**Table 3.** Cytotoxicity of Compounds **13a-13c**, **13e**, **13g**, **13i**, **14b-14c**, **15g**, **17e**, **19c-19f**, **21b**, and **21c** on HUVECs.

Sr. No.	Code	$\text{IC}_{50}$ ( $\mu\text{M}$ ) <sup>a</sup>	Sr. No.	Code	$\text{IC}_{50}$ ( $\mu\text{M}$ ) <sup>a</sup>
1	13a	0.6	10	17e	>10
2	13b	1	11	19c	3
3	13c	>10	12	19d	>10
4	13e	6	13	19e	>10
5	13g	>10	14	19f	>10
6	13i	>10	15	21b	>10

7	14b	2	16	21c	>10
8	14c	0.7	17	STS <sup>b</sup>	0.5
9	15g	>10			

<sup>a</sup>Assays were performed in duplicate (n=2); <sup>b</sup>STS represents staurosporine.

**2.7 VEGFR-2 Inhibition Assay.** Compounds with best inhibitory activity on HUVECs were selected to determine their effects on VEGFR-2 phosphorylation. Phosphorylated VEGFR-2 activates many signaling pathways which leads to endothelial cell proliferation, migration and differentiation.[95,96] *In-vitro* cell-based ELISA method was used to determine the effects of test compounds as well as positive control STS on pVEGFR-2 by primary screening at 10  $\mu$ M concentration. These test compounds with visible structural differences showed poor to good % VEGFR-2 inhibition. Moreover, compounds **13b** and **14b** showed >50% VEGFR-2 inhibition and both structurally comprised of naphthalene at ring C. On the contrary, **19c** with pyridine at ring C showed no significant activity (Table 4). Thus, we assume that compounds with naphthalene as central aryl moiety had more potential for pVEGFR-2 inhibition as compared to pyridine. For more detailed comparison, we compared the IC<sub>50</sub> of 13b and 14b with our previously reported VEGFR-2 inhibitor 3i and sorafenib and found that our current series of compounds showed less potency towards VEGFR-2, even though overall anti-angiogenic effects of 14b were much better than compound 3i.[59] The possible reason could be that the other effects such as inhibition of migration (supplementary data) or tube formation (apart from VEGFR-2 inhibition) are more pronounced leading to overall improved anti-angiogenic effects. Thus, incorporation of the diaryl-pyrazoline moiety led to dual inhibition of HDAC and VEGFR-2, and more structural modification are needed to further improve the VEGFR-2 inhibitory potential of this series of compounds.

**Table 4.** VEGFR-2 Inhibitory Activity of Compounds 13a, 13b, 13e, 14b, 14c, and 19c.

Sr. No.	Code	% Inhibition at 10 $\mu$ M <sup>a</sup>	IC <sub>50</sub> ( $\mu$ M) <sup>a</sup>
1	13a	23.45	ND <sup>b</sup>
2	13b	52.35	5
3	13e	48.17	ND <sup>b</sup>
4	14b	64.12	5
5	14c	35.65	ND <sup>b</sup>
6	19c	18.52	ND <sup>b</sup>
7	STS <sup>c</sup>	87.85	0.5
8	3i[59]	ND <sup>b</sup>	0.5

<sup>a</sup>Assays were performed in duplicate (n=2); <sup>b</sup>Not determined; <sup>c</sup>STS represents staurosporine.

**2.8 Capillary Tube Formation Assay.** The process of capillary-like tube formation of endothelial cells is considered as representative of later stages of angiogenesis. Thus, *in-vitro* tube formation assay could be performed for the test compounds to govern their anti-angiogenesis potency.[93,94,97,100] Compounds **13b** and **14b** displayed substantial inhibitory activity against HUVECs, pVEGFR-2 and endothelial cell migration (supplementary data); so, these two were further evaluated to determine their effects on HUVECs tube formation. STS-treated HUVECs, after 24 h, reduced the number of capillaries to a great extent as compared to control which formed hollow capillary-like networks (Figure 5). However, **14b** exhibited significant decrease in tube formation as compare to **13b** and control [Figure 5 and supplementary data (p=0.1)]. Thus, results indicated that, **14b** exhibited anti-angiogenesis activity by reducing HUVECs tube formation.



**Figure 5.** Graphical representation of intersection counts with different treatments on HUVECs after 48 h of untreated, staurosporine (10  $\mu$ M), 13b (10  $\mu$ M), and 14b (10  $\mu$ M) respectively. Error bar represents SEM, n=3, \*\*\*p $\leq$ 0.0001, \*\*p $\leq$ 0.001 (student's unpaired t-test).

**2.9 MTT Cytotoxicity Assay.** *In-vitro* HDAC inhibitory and anti-angiogenesis assays revealed two best compounds, **13b** and **14b**. These two were further tested for their cytotoxicity potential against 4 cell lines viz. MCF-7 (human breast cancer), K562 (leukaemia), A549 (human lung cancer) and HT-29 (human colorectal adenocarcinoma) along with two positive controls paclitaxel and cis-platin. Results showed that test compounds displayed moderate to good cytotoxicity in mid-micromolar range on the four cell lines (Table 5). Paclitaxel was more potent than test compounds whereas cis-platin showed variation in activity. Compound **13b** presented better inhibitory activity than cis-platin on K562, A549 and HT-29 cell lines, while comparatively poor inhibition on MCF-7, while, **14b** showed significantly better cytotoxicity against K562 and HT-29; specifically, HT-29 appears to be most affected. Thus, cytotoxicity results indicated that **13b** and **14b** had encouraging cytotoxicity on these cell lines.

**Table 5.** Cytotoxicity of Compounds 13b and 14b.

Code	IC <sub>50</sub> (μM) <sup>a</sup>			
	MCF-7	K562	A549	HT-29
13b	24.40±2.42	5.83±1.1	9.63±1.06	8.66±1.30
14b	16.92±3.0	8.92±1.25	17.99±1.51	8.20±0.42
Paclitaxel	0.35	0.29	0.32	0.28
Cis-platin	10.57±1.1	58.4±1.4	16.68±1.74	10.6±1.2

<sup>a</sup>Assays were performed in replicates (n=6). ND – Not determined.

**2.10 *In-vivo* Chick Chorioallontoic Membrane (CAM) Assay.** The CAM of chick offers a reliable system to study the anti-angiogenesis effects of compounds *in-vivo*. Chick CAMs are easy to access outside the embryo and it offers a simple approach to study complex biological systems.[100] Compounds **13b** and **14b** along with positive control STS, were subjected to CAM assay to govern their *in-vivo* anti-angiogenic potency. After 12 days of implanting sponges loaded with VEGFs, STS, and test samples into the CAMs, average number of blood vessels was determined. STS substantially decreased the branching of capillaries (Figure 6) as compared to untreated. Importantly, **14b**-treated CAMs showed a significant reduction in the branching of blood capillaries as compared to untreated and **13b**-treated, further supporting its anti-angiogenesis mechanism.

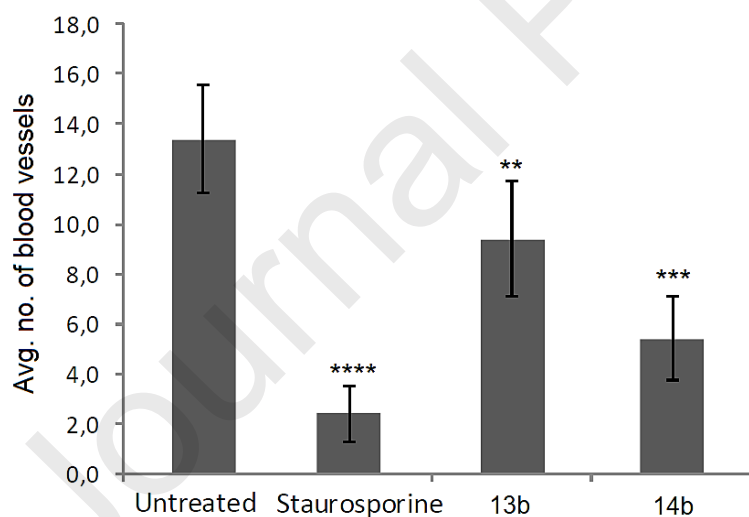


**Figure 6.** Graphical representation of CAM assay. Error bars represent SEM, n=5, \*\*\*\*p≤0.00001, \*\*\*p≤0.0001, \*\*p≤0.01 (student's unpaired t-test). STS represents staurosporine. UT represents untreated.

**2.11 Western Blotting.** With aim to determine effects of **14b** on expression levels of VEGFR-2, western blot was performed on HUVEC cells. STS (10 μM) was used as positive control and TBP as loading control. In proteins, phosphorylation is an essential post-translational modification. Phosphorylated VEGFR-2 (tyrosine residues) transduces the signals to several downstream ligands in order to regulate the angiogenesis events such as endothelial cell proliferation, migration and survival.[101] Upon western blot, phosphorylated

VEGFR-2 expression level was significantly decreased in the presence of **14b** (10  $\mu$ M) as compared to STS at the same concentration (Figure 7).

Tumoral hypoxia is a major factor that regulates tumor angiogenesis which is driven by a key mediator hypoxia inducible factor (HIF)-1 $\alpha$ . It is known to be the chief controller of hypoxia-induced angiogenesis.[102,103] Thus, to analyse whether HIF-1 $\alpha$  was responsible to elicit anti-angiogenesis response, western blot was performed to evaluate the change in the expression levels of HIF-1 $\alpha$  induced by **14b**. Compound **14b** caused slight decrease in expression levels of HIF-1 $\alpha$  as compared to the positive control, which further provided support for anti-angiogenesis potency of **14b** by VEGFR-2 inhibition.

In particular, caspase 3 are key regulators of apoptosis which are produced in inactive-proenzyme form, and they are cleaved further to form smaller subunits which combine together to form active-caspase 3 enzyme. This active-caspase 3 promotes various degradation pathways and DNA fragmentation during apoptosis.[104–106] On western blot of **14b**, the cleaved caspase 3 expression level was enhanced significantly suggesting its potential to increase the production of cleaved caspase 3.

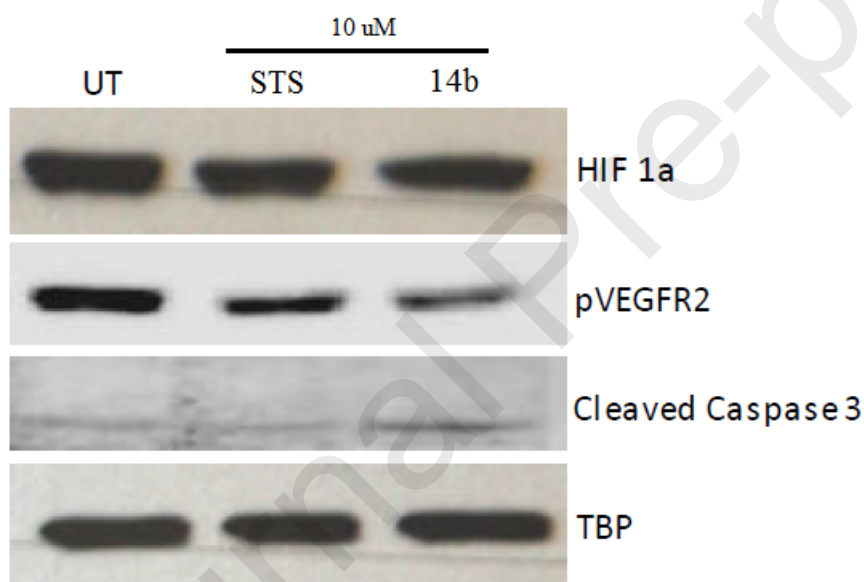


**Figure 7.** Western blotting of VEGFR-2 expression levels on HUVEC treated with staurosporine and compound 14b at 10  $\mu$ M for 5 h. TBP was used as loading control. Expression levels of hypoxia inducible factor (HIF-1 $\alpha$ ), phosphorylated VEGFR-2 (pVEGFR-2), and cleaved caspase 3. STS represents staurosporine. UT represents untreated.

**2.12 Antitumor Activity Studies on Xenograft Models.** To access the *in-vivo* antitumor efficacy of **14b**, HT-29 (human colorectal adenocarcinoma) xenograft model was established. For this assay, 18 SCID mice were used and tumors were generated to a specific size. Then after the tumor bearing mice were separated into three groups each containing six mice, wherein, the untreated or control group received saline; the positive control group were injected with 20 mg/kg of doxorubicin and the test group were introduced with 25 mg/kg of **14b** intraperitoneally on 1-5, 8-12, 15-18 day. The tumor volume of each mouse was measured

every two days and documented. At the end of experiment, mice were sacrificed, and tumors were incised, immediately imaged and volume was measured (supplementary data).

In vehicle-treated group, the tumors developed in exponential manner (Figure 8), whereas, compound **14b** significantly reduced the tumor volumes as presented by tumor size (Figure 8A) as well as tumor growth curve (Figure 8B). Strikingly, **14b**-treated xenograft model produced tumor volume reduction ranging from 30 to 64% and 3 to 44% in comparison to vehicle-treated and doxorubicin-treated respectively, after 18 days of administration in animal. Moreover, **14b** reduced the tumor growth ranging from 30 to 51% as compared to vehicle-treated, additionally, 66% of **14b**-treated animals exhibited greater reduction in tumor growth as compared to doxorubicin whereas, 34% animals showed 15 to 19% reduction.

Thus, it is worth mentioning that the tumor size and volume of **14b** was comparable to doxorubicin, therefore, it will be reasonable to tick on the *in-vivo* antitumor efficacy of pyrazoline-TZD analog **14b**. Furthermore, in the course of experiment, **14b**-treated mice group showed no significant evidence of toxicity or weight loss.

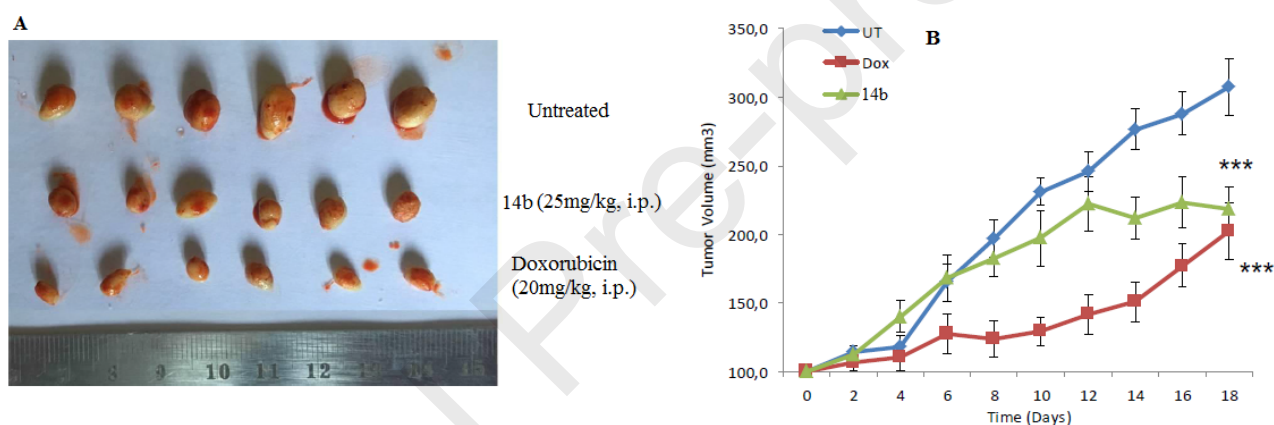


**Figure 8.** *In-vivo* antitumor efficacy of **14b** on human colorectal adenocarcinoma (HT-29) xenograft model. (A) Excised tumors of doxorubicin-treated (Dose – 20 mg/kg i.p.), **14b**-treated (Dose – 25 mg/kg i.p.) and vehicle-treated (saline i.p.). (B) Growth curve of tumor volume (mm<sup>3</sup>) vs. time (days) of vehicle-treated (represented as mean ± SEM, blue line, n=6), **14b**-treated (represented as mean ± SEM, green line, n=6) and doxorubicin-treated (represented as mean ± SEM, red line, n=6). UT represents untreated. Dox represents doxorubicin. i.p. represents intraperitoneally. Error bars represent mean ± SEM n=6; \*\*\*, p < 0.001.

**2.13 Molecular Docking Study.** A comprehensive docking study was performed to rationalize the structure activity data and reveal the molecular determinants of protein-ligand binding. The docking procedure was validated by redocking of the representative ligands in the crystal structure of VEGFR-2 (PDB-ID: 1YWN) and HDAC4 (PDB-ID: 2VQJ and 4CBY).[88] The GBVI/WSA dG docking score of the redocked ligand was -13.6 on HDAC4 (PDB-ID: 4CBY), -13.9 on HDAC4 (PDB-ID 2VQJ) and -11.2 on VEGFR-2 (supplementary data). The ligands of PDB-ID's 1YWN and 4CBY redocked into the protein-receptor yielded an almost perfect overlap between docked and x-ray pose with RMSD-values of less than 0.4 Å (supplementary data). The thiophene linker and trifluoromethyl warhead of the redocked ligand in HDAC4 (PDB ID: 2VQJ) showed a good RMSD value of 0.4 Å with respect to the crystal structure. Since the aromatic head group of the trifluoromethylketone ligand protrudes into free solution, this part of the molecules was

intrinsically flexible and thus not considered for the calculation of RMSD. Consequently, we assumed that all parameters were well configured for docking of pyrazoline TZD-analogs.

Compounds with identical absolute steric configuration at the pyrazole ring as (S)-**14b**, showed better scores on VEGFR-2 than their steric counterparts (supplementary data). Interestingly, all analogs with (S)-14b configuration showed similar binding poses, but the corresponding stereo isomers consistently adopted an inverse binding pose (supplementary data). The reason behind this finding was that the o-chlorophenyl group of (S)-14b and corresponding stereo isomers shows perfect fit into a hydrophobic sub pocket flanked by L1017, I1042, V896, V897, I890, I886 and L887, while the same group of (R)-14b would clash with this sub pocket. (S)-14b as a whole snuggled perfectly in the prolonged binding channel of VEGFR-2. The TZD war head was found to tightly fixed by two hydrogen bonds with L838 and A1048 (Figure 9). The carboxamide-oxygen accepts H-bond with the backbone of Asp1044 which may add to affinity.

Two representatives of TZD analogs with naphthyl-linker and the most potent TZD with pyridyl-linker were docked into the crystal structure of the open (PDB-ID: 2VQJ) and closed (PDB-ID: 4CBY) conformation of HDAC4, HDAC4<sub>o</sub> and HDAC4<sub>c</sub>, respectively. The docking scores for the most potent compounds (S)-**14b** and (S)-**13i** with the same absolute configuration at the pyrazoline ring were better for HDAC4<sub>o</sub> than for HDAC4<sub>c</sub> suggesting preferred binding to the open conformation. It is noteworthy, that the catalytic zinc ion in the complex between TZD-ligands and both, HDAC4<sub>o</sub> and HDAC4<sub>c</sub>, shows tetragonal bipyramidal coordination with similar distances between the electronegative heavy atoms and the central zinc ion (Figure S12, supplementary data).

Interestingly, for all TZD-analogs the enantiomer with the same absolute configuration at the pyrazoline ring as (S)-**14b** shows significantly higher docking scores for binding to HDAC4<sub>o</sub>, than the corresponding enantiomer (supplementary data). In agreement with the activity data, **13i** and **14b** with naphthyl-linker showed higher scores compared with **21d** (pyridyl-linker). If the linker was removed and the TZD-warhead was replaced, as seen with compound **S1**, the activity drops dramatically below an IC<sub>50</sub>-value of 50 μM (Table 1). This correlates well with a lower docking score, when compared with the score of active compounds **13i**, **14b** and **21d** (supplementary data). Looking at the binding pose of (S)-**14b** at the binding groove adjacent to the active site pocket of HDAC4 reveals that the TZD-warhead plays a pivotal role in the molecular recognition of the pyrazoline TZD-analogs by HDAC4<sub>o</sub> (Figure 10). The TZD-group binds to the catalytic zinc ion and forms a hydrogen bond to H159 as well as a Pi-Pi interaction with the sidechain of H198. The naphthyl-linker fits perfectly into the binding groove of HDAC4<sub>o</sub>, which was flanked by hydrophobic amino acids P155, P156, F168, L334 and I38. The linker is optimally oriented to form further Pi-stacking with F871. The naphthyl-linker shows also a two-fold cation-Pi-interaction with R37. In addition, two hydrogen bonds with R37 and R154 contribute to the stabilization of the protein-ligand complex. One ring of the branched pyrazoline capping group occupies a deeper sub-pocket forming Pi-Pi-stacking with H332 and Pi-alkyl interactions with L334 (Figure 10). This was consistent with similar activities of TZD-analogs with the same linker and different smaller substituents at the aromatic rings of the capping group. Altogether, docking results were in agreement with the dual activity of the pyrazoline TZD-analogs against HDAC4 and VEGFR-2.

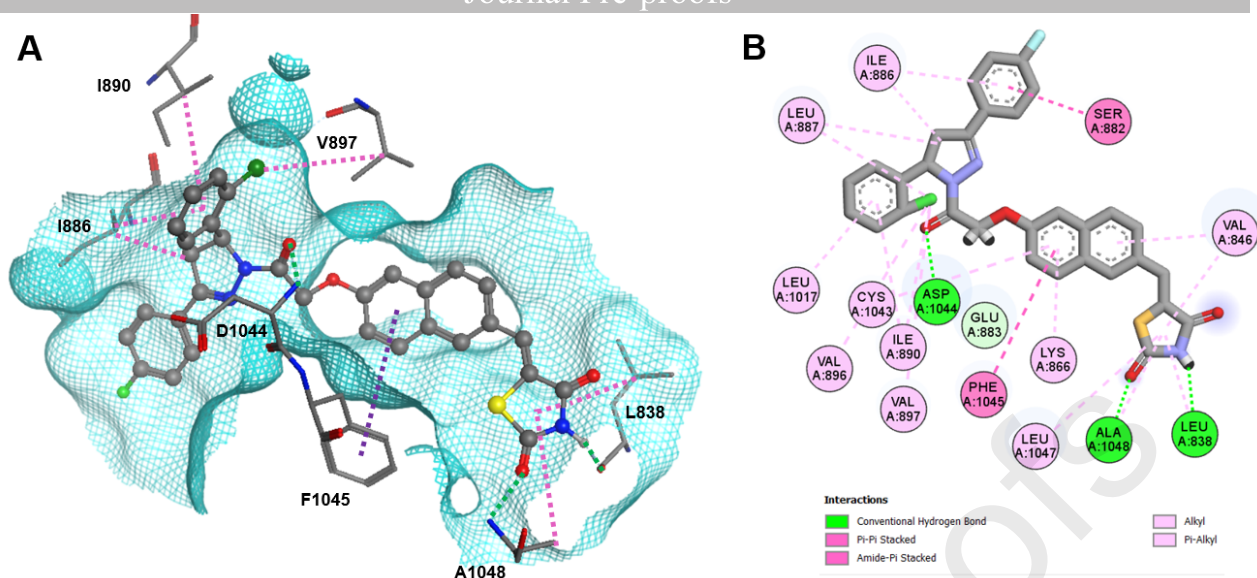


**Figure 9.** (S)-14b docked into the binding pocket of VEGFR-2 (PDB-ID: 1YWN). A) Binding pose with H-bonds to L838, A1048, D1044 (dotted green lines), Pi-Pi-interactions (dotted magenta line) and multiple Pi-alkyl and alkyl-interactions (dotted pink lines). B) 2D diagram of protein-ligand interactions.

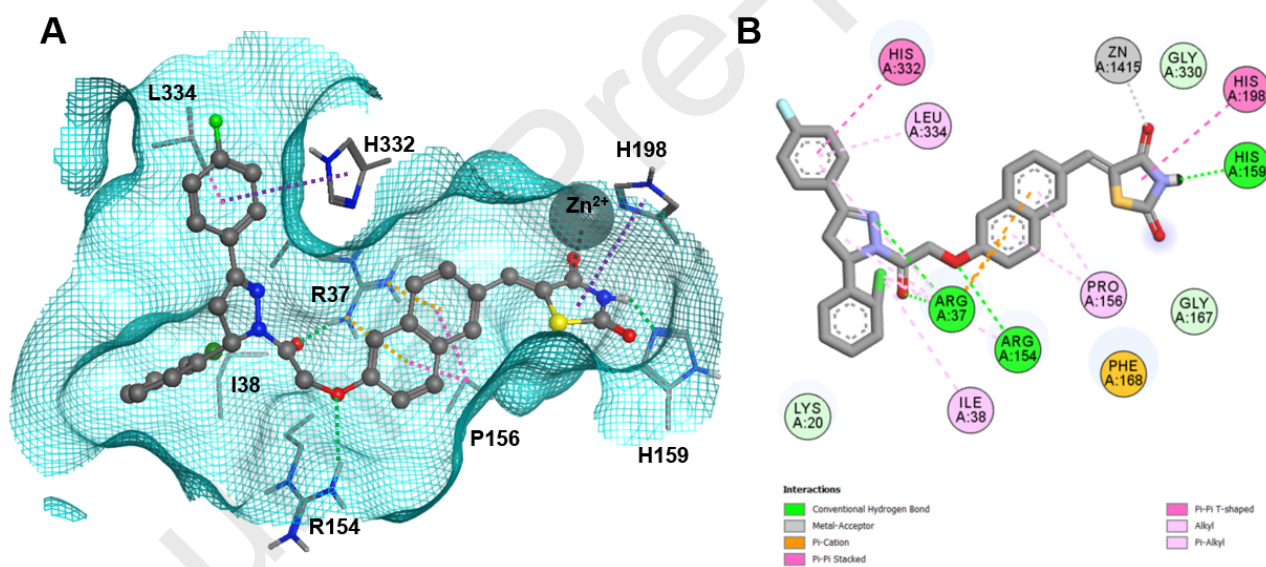


**Figure 10.** A) 3D-docking pose of (S)-14b within HDAC4<sub>o</sub> (PDB-ID: 2VQJ). The ligand forms multiple hydrogen bonds (dotted green lines), Pi-Pi-interactions (dotted magenta lines), Pi-alkyl-interactions (dotted pink lines), Pi-cation interactions (dotted light brown lines) and zinc complexation (dotted gray line) in the binding groove adjacent to the catalytic site pocket. B) 2D diagram of protein-ligand interactions.

### 3. CONCLUSIONS

In this paper, we have rationally designed and developed novel pyrazoline TZD-analogs simultaneously targeting VEGFR-2 and HDAC, wherein, two different series exploring naphthyl and pyridyl linker were constructed. The naphthyl linker demonstrated superior HDAC inhibition with selectivity towards HDAC4 as well as impressive VEGFR-2 inhibition.

Further in depth *in-vitro* assays were performed of the two most active compounds incorporating naphthyl linker, **13b** and **14b**. These structurally different analogs, **13b** and **14b** have exhibited similar inhibitory effects on VEGFR-2 (5  $\mu$ M), whereas they stated pronounced inhibition of HDAC4 with IC<sub>50</sub> of 0.34  $\mu$ M and 0.36  $\mu$ M respectively. Compounds with naphthyl linker (**13b**, **14b**) and pyridyl linker (**17f**, **21f**) were able to stabilize HDAC4 as evident by shift in the melting temperatures confirming its interaction with HDAC4 isoform. Additionally, the anti-angiogenic potential of **13b** and **14b** was evident by different assays such as HUVEC proliferation, migration (supplementary data), and tube formation. Compound **13b** (1  $\mu$ M) was found to have better inhibitory concentration on HUVECs proliferation than that of **14b** (2  $\mu$ M), whereas they both had similar effects on cell mobility of HUVECs. In capillary tube formation, compound **14b** strikingly reduced the number of capillaries as compared to **13b**. The *in-vivo* assay displayed higher potency of **14b** to attenuate the neovascularization in the growing CAMs in comparison to **13b**. These two non-hydroxamate analogs were examined for their effects on cancer cell viability and they significantly reduced it.

In addition, western blot analysis revealed that **14b** considerably decreased phosphorylated VEGFR-2 and HDAC4 expression levels while increased the same of cleaved caspase 3, a key regulator of apoptosis. Additionally, it must be emphasized that **14b** (25 mg/kg, i.p.) showed uncompromised *in-vivo* efficacy (tumor growth and volume reduction) on HT-29 tumor xenograft model comparable to doxorubicin (20 mg/kg, i.p.).

Since, the present results highlight the effects of subtle change of linker on the inhibitory potency and selectivity against these targets, intense efforts are being directed towards optimization of **14b** by linker modification.

## 4. EXPERIMENTAL

### 4.1 Chemistry

The final compounds were synthesized using 3 different schemes (scheme I, II and III). In scheme I, synthesis of intermediates is mentioned, while scheme II and scheme III comprised of synthesis of final compounds.

All the required reagents, solvents and chemicals were procured from commercial sources viz. Sigma Aldrich, S.D. Fine Chem. Ltd., Himedia and were utilized without any further purification. The reactions were monitored at each step by Thin Layer Chromatography (TLC) using Merck precoated silica gel 60 F-254 plates under short wave UV-light (254 nm) to identify the UV absorbing spots for completion of reaction and also to trace presence of any impurities. All intermediates were purified by recrystallization using suitable solvents such as chloroform, methanol, ethanol etc. All the final molecules were purified by column chromatography technique on silica gel 60 (60 to 120 mesh) using combination of different solvents. Melting point of all the intermediates were obtained by using VEEGO, MODEL: VMP-DS Melting Point apparatus and that of the final compounds were obtained using a DSC1 STAR system differential scanning calorimeter from Mettler Toledo. Purity of all final compounds was determined using an Agilent 1200 high-performance liquid chromatography (HPLC) system; software- EZ chrome Elite. The chromatographic column used was HemochromIntsil A31 C18 5U 150 mm × 4.6 mm Sn-B180127, detection at 300 nm. UV-visible detector was used with the flow rate of 1 mL/min. Oven temperature maintained was 30 °C; gradient elution with a run time of 10 min using Methanol: Formic Acid (1%) (Formic acid: in 1000 mL double distilled water 1 mL formic acid was added) in 80:20/90:10 ratio.

The structures of all the compounds were confirmed by different spectroscopic techniques such as: FTIR, <sup>1</sup>H-NMR, <sup>13</sup>C-NMR, Mass. All the intermediates were structurally characterized by FTIR and <sup>1</sup>H-NMR and final compounds by FTIR, <sup>1</sup>H-NMR, <sup>13</sup>C-NMR and Mass spectrometry. IR was recorded using JASCO FT/IR-4100 typeA spectrometer using manual sampling method. <sup>1</sup>H-NMR spectra were recorded using Bruker Avance 400 MHz spectrometer using different solvents. All shifts of <sup>1</sup>H-NMR are reported in δ (ppm) units relative to the signals for the solvent DMSO (δ- 2.50 ppm). All coupling constants (J values) are reported in hertz (Hz). NMR abbreviations are as: bs, broad singlet; s, singlet; d, doublet; t, triplet; q, quartet; m, multiplet; and dd, doublet of doublets. <sup>13</sup>C-NMR was recorded on Bruker Avance Spectrometer at 100 MHz using solvent DMSO-d<sub>6</sub>. Mass spectrum was documented on LC-MS Agilent Technologies 1260 Infinity instrument.

Different chalcones were synthesized by procedure previously reported with minor modifications [91,107]. To ethanolic solution of NaOH (10%, 20 mL), substituted acetophenones (0.04 mol) and different aldehydes (0.04 mol) was added dropwise under ice bath and stirred for 5 h at RT. Reaction mixture was kept in refrigerator overnight, filtered and washed with cold water. Crude obtained was recrystallized using ethanol to obtain appropriate chalcones (**3a-3i**, **6a-6g**, **6j**, and **9b-9g**) (Scheme I). Following are the unpublished chalcone intermediates, others have been reported elsewhere.[91,107]

**3-(3-nitrophenyl)-1-phenylprop-2-en-1-one (3h).** Yellow crystalline solid. 81% yield (6.7 g). M.P. 127-129°C. FTIR (cm<sup>-1</sup>) 3068, 1660, 1577, 1523. <sup>1</sup>H NMR (400 MHz, CDCl<sub>3</sub>) δ ppm 7.44 – 7.56 (m, 2H), 7.60 – 7.64 (m, 2H), 7.67 (s, 1H), 7.82 (s, 1H), 7.91 – 7.93 (m, 1H), 8.03 – 8.06 (m, 2H), 8.25 – 8.27 (m, 1H), 8.51 – 8.52 (m, 1H).

**3-(2-chlorophenyl)-1-(2,4-difluorophenyl)prop-2-en-1-one (9b).** Yellow crystals. 87% yield (9.8 g). M.P. 110-111°C. FTIR (cm<sup>-1</sup>) 3074, 1685, 1599, 1261, 1232, 752. <sup>1</sup>H NMR (400 MHz, CDCl<sub>3</sub>) δ ppm 6.88–6.93 (m, 1H), 6.97–7.02 (m, 1H), 7.26–7.38 (m, 3H), 7.42–7.44 (m, 1H), 7.71–7.74 (m, 1H), 7.87–7.93 (m, 1H), 8.16 (d, J= 15.9 Hz, 1H).

**1-(2,4-difluorophenyl)-3-(4-(trifluoromethyl)phenyl)prop-2-en-1-one (9d).** Yellow crystals. 90% yield (8.5 g). M.P. 108-109°C. FTIR (cm<sup>-1</sup>) 3124, 3076, 1664, 1543, 1519, 1288, 1265, 1230. <sup>1</sup>H NMR (400 MHz, CDCl<sub>3</sub>) δ ppm 6.89 – 6.95 (m, 2H), 6.99 – 7.03 (m, 1H), 7.43 – 7.47 (m, 1H), 7.65 – 7.73 (m, 4H), 7.89 – 7.95 (m, 1H).

**1-(2,4-difluorophenyl)-3-(4-fluorophenyl)prop-2-en-1-one (9e).** Yellow crystals. 90% yield (8.5 g). M.P. 64-65°C. FTIR (cm<sup>-1</sup>) 3101, 3076, 1660, 1587, 1506, 1263, 1222. <sup>1</sup>H NMR (400 MHz, CDCl<sub>3</sub>) δ ppm 6.89 – 6.93 (m, 1H), 6.94 – 7.02 (m, 4H), 7.44 – 7.45 (m, 2H), 7.61 – 7.66 (m, 1H), 7.88 – 7.94 (m, 1H).

**1,3-bis(2,4-difluorophenyl)prop-2-en-1-one (9f).** Yellow crystals. 89% yield (8 g). M.P. 63-65°C. FTIR (cm<sup>-1</sup>) 3086, 1664, 1595, 1265, 1234. <sup>1</sup>H NMR (400 MHz, CDCl<sub>3</sub>) δ ppm 6.69 – 6.81 (m, 1H), 6.86 – 7.05 (m, 4H), 7.40 – 7.45 (m, 1H), 7.60 – 7.66 (m, 1H), 7.87 – 7.93 (m, 1H).

Various pyrazoline derivatives were synthesized by previously reported procedure with suitable modifications [91,107]. To solution of different chalcones (3a-3i, 6a-6g, 6j, and 9b-9g) (0.02 mol) in chloroform, hydrazine hydrate (0.04 mol) was added and refluxed for 12 h. The reaction mixture was cooled under ice-bath and K<sub>2</sub>CO<sub>3</sub> (0.05 mol) was added to this mixture and stirred for 15 min. Chloroacetyl chloride (0.03 mol) was added dropwise with stirring under ice-bath and further stirred at RT. After 12 h, reaction was stopped and chloroform layer was washed several times with water to remove excess of K<sub>2</sub>CO<sub>3</sub> and evaporated to obtain solid. Crude was purified by extracting with diethylether to get appropriate chloroacetylated pyrazolines (**4a-4i**, **7a-7g**, **7j**, and **10b-10g**) (Scheme I). Following are the unpublished chloroacetylated intermediates, others have been reported elsewhere.[91,107]

**2-chloro-1-(5-(3-nitrophenyl)-3-phenyl-4,5-dihydro-1H-pyrazol-1-yl)ethanone (4h).** White colour solid. 59% yield (5.6 g). M.P. 146-148°C. FTIR (cm<sup>-1</sup>) 1670, 1600, 1572, 1588, 1523, 1500, 688. <sup>1</sup>H NMR (400 MHz, CDCl<sub>3</sub>) δ ppm 3.23 (d, J= 18.0 Hz, 1H), 3.85-3.92 (m, 1H), 4.54-4.64 (m, 2H), 5.68 (d, J= 12.0 Hz, 1H), 7.43-7.55 (m, 4H), 7.60-7.62 (m, 1H), 7.74-7.77 (m, 2H), 8.11-8.16 (m, 1H), 8.76 (s, 1H).

**2-chloro-1-(5-(2-chlorophenyl)-3-(2,4-difluorophenyl)-4,5-dihydro-1H-pyrazol-1-yl)ethanone (10b).** White colour solid. 70% yield (4.7 g). M.P. 114-115°C. FTIR (cm<sup>-1</sup>) 1668, 1600, 1504, 1263, 1211, 858, 752. <sup>1</sup>H NMR (400 MHz, CDCl<sub>3</sub>) δ ppm 3.16–3.23 (m, 1H), 3.90–3.99 (m, 1H), 4.52 (d, J= 13.28 Hz, 1H), 4.65 (d, J= 13.28 Hz, 1H), 5.90 (d, J= 11.9 Hz, 1H), 6.83–6.89 (m, 1H), 6.94–6.99 (m, 1H), 7.08–7.10 (m, 1H), 7.20–7.26 (m, 2H), 7.39–7.41 (m, 1H), 7.94–8.00 (m, 1H).

**2-chloro-1-(3-(2,4-difluorophenyl)-5-(4-(trifluoromethyl)phenyl)-4,5-dihydro-1H-pyrazol-1-yl)**

**ethanone (10d).** Cream colour solid. 57% yield (4.8 g); M.P. 123-124°C. FTIR (cm<sup>-1</sup>) 1676, 1600, 1512, 1274, 1246, 839. <sup>1</sup>H NMR (400 MHz, CDCl<sub>3</sub>) δ ppm 3.23 – 3.25 (m, 1H), 3.86 – 3.95 (m, 1H), 4.48 – 4.95 (m, 2H), 4.60 (d, J = 11.8 Hz, 1H), 6.85 – 6.91 (m, 1H), 6.96 – 7.01 (m, 1H), 7.36 (d, J = 8.4 Hz, 2H), 7.60 (d, J = 8.0 Hz, 2H), 7.97 – 8.03 (m, 1H).

**2-chloro-1-(3-(2,4-difluorophenyl)-5-(4-fluorophenyl)-4,5-dihydro-1H-pyrazol-1-yl)ethanone (10e).**

Pale yellow solid. 60% yield (4 g). M.P. 97-98°C. FTIR (cm<sup>-1</sup>) 1672, 1602, 1504, 1417, 1259, 1219, 815. <sup>1</sup>H NMR (400 MHz, CDCl<sub>3</sub>) δ ppm 3.17 (d, J = 17.6 Hz, 1H), 3.74 – 3.82 (m, 1H), 4.50 – 4.61 (m, 2H), 5.73 (d, J = 11.8 Hz, 1H), 6.68 – 6.79 (m, 2H), 7.10 – 7.20 (m, 3H), 7.71 – 7.76 (m, 2H).

**1-(3,5-bis(2,4-difluorophenyl)-4,5-dihydro-1H-pyrazol-1-yl)-2-chloroethanone (10f).**

Off white colour solid. 63% yield (5.3 g). M.P. 112-114°C. FTIR (cm<sup>-1</sup>) 1678, 1602, 1500, 1444, 1259, 1219, 844. <sup>1</sup>H NMR (400 MHz, CDCl<sub>3</sub>) δ ppm 3.25 – 3.21 (m, 1H), 3.82 – 3.91 (m, 1H), 4.48 – 4.59 (m, 2H), 5.70 (d, J = 12.0 Hz, 1H), 6.79 – 6.90 (m, 3H), 6.95 – 7.00 (m, 1H), 7.15 – 7.20 (m, 1H), 7.95 – 8.01 (m, 1H).

**5-((6-hydroxynaphthalen-2-yl)methylene)thiazolidine-2,4-dione (12).**

This intermediate was synthesized by previously reported procedure[29]. In brief, toluene (10 mL), 2,4-thiazolidinedione (11) (4.68 g, 0.04 mmol) and 6-hydroxy-2-naphthaldehyde (6.88 g, 0.04 mmol) was taken together in RBF. To this mixture, catalytic amount of piperidinium benzoate was dispersed and refluxed in Dean Stark apparatus. The reaction was continuously monitored by TLC, after 4 h reaction was stopped and mixture was cooled to RT. Solid precipitated was collected by filtering under vacuum and washed with water to obtained intermediate **12** (Scheme II). Yellow shiny crystals. 86% yield (10 g). M.P. charred at 300 °C. FTIR (cm<sup>-1</sup>) 3390, 3119, 1672, 1662, 1587. <sup>1</sup>H-NMR (400 MHz, DMSO-d<sub>6</sub>) δ ppm 7.16-7.19 (m, 2H), 7.55 (dd, J = 1.8, 8.68 Hz, 1H), 7.80 (d, J = 8.68 Hz, 1H), 7.88-7.90 (m, 2H), 8.04 (d, J = 0.96 Hz, 1H), 10.21 (s, 1H), 12.59 (bs, 1H).

To the solution of K<sub>2</sub>CO<sub>3</sub> (0.007 mol) in dimethylformamide (10 mL), 6-hydroxynicotinaldehyde (0.008 mol) was added with stirring. In this mixture, appropriate chloroacetylated intermediate (0.004 mol) (4a-4b, 4d-4f, 4h, 4i, 7a-7f, and 10b-10f) was added and stirred for 48 h at RT. Reaction was immobilized by adding water (40 mL), precipitated residue was collected by filtering under vacuum and washed several times with water. Residue collected was purified by recrystallization technique with methanol (25 mL) to give respective intermediates (**16a-16b**, **16d-16f**, **16h**, **16i**, **18a-18f**, and **20b-20f**) (Scheme III).

**6-(2-(3,5-diphenyl-4,5-dihydro-1H-pyrazol-1-yl)-2-oxoethoxy)nicotinaldehyde (16a).**

Grey colour solid. 55% yield (1 g). M.P. charred at 130 °C. FTIR (cm<sup>-1</sup>) 2868, 1656, 1606, 1543, 1502, 1265. <sup>1</sup>H-NMR (400 MHz, DMSO-d<sub>6</sub>) δ ppm 3.23 (dd, J = 4.8, 18.4 Hz, 1H), 3.92-3.99 (m, 1H), 5.27 (d, J = 16.4 Hz, 1H), 5.36 (d, J = 16.4 Hz, 1H), 5.59 (dd, J = 4.8, 11.6 Hz, 1H), 6.51 (d, J = 9.6 Hz, 1H), 7.24-7.32 (m, 3H), 7.32 – 7.35 (m, 2H), 7.47-7.51 (m, 3H), 7.80 (dd, J = 2.4, 9.6 Hz, 1H), 7.84-7.86 (m, 2H), 8.55 (d, J = 2.4 Hz, 1H), 9.58 (s, 1H).

**6-(2-(5-(2-chlorophenyl)-3-phenyl-4,5-dihydro-1H-pyrazol-1-yl)-2-oxoethoxy)nicotinaldehyde (16b).**

Grey colour solid. 59% yield (0.9 g). M.P. charred at 250 °C. FTIR (cm<sup>-1</sup>) 2862, 1654, 1602, 1541, 1502, 1267, 846. <sup>1</sup>H-NMR (400 MHz, DMSO-d<sub>6</sub>) δ ppm 3.11 (dd, J = 5.16, 18.24 Hz, 1H), 4.02-4.09 (m, 1H), 5.27

(d, J = 16.6 Hz, 1H), 5.45 (d, J=16.6 Hz, 1H), 5.80 (dd, J = 5.0, 11.8 Hz, 1H), 6.42-6.54 (m, 1H), 7.22-7.33 (m, 4H), 7.48-7.50 (m, 3H), 7.80–7.95 (m, 3H), 8.57 (d, J = 2.2 Hz, 1H), 9.60 (s, 1H).

**6-(2-oxo-2-(3-phenyl-5-(4-(trifluoromethyl)phenyl)-4,5-dihydro-1H-pyrazol-1-yl)ethoxy)**

**nicotinaldehyde (16d).** Grey colour solid. 58% yield (1.1 g). M.P. charred at 270 °C. FTIR (cm<sup>-1</sup>) 2848, 1651, 1600, 1539, 1500, 1325, 1267. <sup>1</sup>H-NMR (400 MHz, DMSO-d<sub>6</sub>) δ ppm 3.27 (d, J = 4.8 Hz, 1H), 3.95-4.03 (m, 1H), 5.27 (d, J = 16.4 Hz, 1H), 5.37 (d, J = 16.4 Hz, 1H), 5.70 (dd, J = 5.2, 12.0 Hz, 1H), 6.49-6.54 (m, 2H), 7.48-7.52 (m, 3H), 7.70 (d, J = 8.0 Hz, 2H), 7.79-7.84 (m, 4H), 8.54-8.6 (m, 1H), 9.58 (s, 1H).

**6-(2-(5-(4-fluorophenyl)-3-phenyl-4,5-dihydro-1H-pyrazol-1-yl)-2-oxoethoxy)nicotinaldehyde (16e).**

Grey colour solid. 60% yield (0.95 g). M.P. 130-132 °C. FTIR (cm<sup>-1</sup>) 3064, 1658, 1600, 1545, 1512, 1383, 1269. <sup>1</sup>H-NMR (400 MHz, DMSO-d<sub>6</sub>) δ ppm 3.24 (dd, J = 4.8, 18.4 Hz, 1H), 3.91-3.96 (m, 1H), 5.24 (d, J = 16.4 Hz, 1H), 5.34 (d, J = 16.4 Hz, 1H), 5.60-5.61 (m, 1H), 6.50 (d, J = 9.2 Hz, 1H), 7.15 (t, J = 8.8 Hz, 2H), 7.28-7.32 (m, 2H), 7.50-7.52 (m, 3H), 7.79-7.86 (m, 3H), 8.54 (d, J = 2.4 Hz, 1H), 9.58 (s, 1H).

**6-(2-(5-(2,4-difluorophenyl)-3-phenyl-4,5-dihydro-1H-pyrazol-1-yl)-2-oxoethoxy) nicotinaldehyde (16f).**

Grey colour solid. 59% yield (1.2 g). M.P. 137-139 °C. FTIR (cm<sup>-1</sup>) 3049, 1656, 1649, 1546, 1502, 1352, 1269. <sup>1</sup>H-NMR (400 MHz, DMSO-d<sub>6</sub>) δ ppm 3.19 (dd, J = 5.2, 18.4 Hz, 1H), 4.01-4.08 (m, 1H), 5.26 (d, J = 16.4 Hz, 1H), 5.43 (d, J = 16.4 Hz, 1H), 5.80 (dd, J = 5.2, 12.0 Hz, 1H), 6.51 (d, J = 9.6 Hz, 1H), 7.21-7.24 (m, 1H), 7.29-7.36 (m, 4H), 7.47-7.50 (m, 1H), 7.80 (dd, J = 2.4, 9.6 Hz, 1H), 7.89-7.92 (m, 2H), 8.56 (d, J = 2.4 Hz, 1H), 9.59 (s, 1H).

**6-(2-(5-(3-nitrophenyl)-3-phenyl-4,5-dihydro-1H-pyrazol-1-yl)-2-oxoethoxy)nicotinaldehyde (16h).**

Brown colour powder. 56% yield (1.1 g). M.P. charred at 240 °C. FTIR (cm<sup>-1</sup>) 3068, 1654, 1602, 1527, 1502, 1348, 1269. <sup>1</sup>H-NMR (400 MHz, DMSO-d<sub>6</sub>) δ ppm 3.36 (dd, J = 5.2, 18.4 Hz, 1H), 3.97-4.04 (m, 1H), 5.26 (d, J = 16.4 Hz, 1H), 5.37 (d, J = 16.4 Hz, 1H), 5.78 (dd, J = 5.2, 12.0 Hz, 1H), 6.50 (d, J = 9.6 Hz, 1H), 7.51-7.52 (m, 3H), 7.65 (t, J = 8.4 Hz, 1H), 7.73 (d, J = 8.0 Hz, 1H), 7.78-7.81 (m, 1H), 7.82-7.87 (m, 2H), 8.13-8.14 (m, 2H), 8.54 (d, J = 2.4 Hz, 1H), 9.59 (s, 1H).

**6-(2-oxo-2-(3-phenyl-5-(thiophen-2-yl)-4,5-dihydro-1H-pyrazol-1-yl)ethoxy)nicotinaldehyde (16i).**

Grey colour powder. 52% yield (0.8 g). M.P. charred at 210 °C. FTIR (cm<sup>-1</sup>) 3061, 1651, 1604, 1547, 1500, 1386, 1267. <sup>1</sup>H-NMR (400 MHz, DMSO-d<sub>6</sub>) δ ppm 3.44 (dd, J = 4.4, 18.4 Hz, 1H), 3.90-3.98 (m, 1H), 5.21 – 5.30 (m, 2H), 5.90 (dd, J = 4.4, 11.6 Hz, 1H), 6.49-6.51 (m, 1H), 6.95-6.96 (m, 1H), 7.06-7.07 (m, 2H), 7.42-7.44 (m, 2H), 7.50-7.53 (m, 2H), 7.79-7.89 (m, 2H), 8.54-8.59 (m, 1H), 9.59 (s, 1H).

**6-(2-(3-(4-fluorophenyl)-5-phenyl-4,5-dihydro-1H-pyrazol-1-yl)-2-oxoethoxy)nicotinaldehyde (18a).**

Grey colour solid. 52% yield (1.3 g). M.P. 139-141 °C. FTIR (cm<sup>-1</sup>) 3028, 1658, 1600, 1543, 1504, 1398, 1327, 1263. <sup>1</sup>H-NMR (400 MHz, DMSO-d<sub>6</sub>) δ ppm 3.17 (dd, J = 5.2, 18.4 Hz, 1H), 4.02-4.12 (m, 1H), 5.26 (d, J = 16.4 Hz, 1H), 5.43 (d, J = 16.4 Hz, 1H), 5.80 (dd, J = 5.2, 12.0 Hz, 1H), 7.21-7.23 (m, 1H), 7.29-7.33 (m, 2H), 7.46-7.52 (m, 4H), 7.79-7.87 (m, 4H), 8.54-8.58 (m, 1H), 9.59 (s, 1H).

**6-(2-(5-(2-chlorophenyl)-3-(4-fluorophenyl)-4,5-dihydro-1H-pyrazol-1-yl)-2-oxoethoxy)**

**nicotinaldehyde (18b).** Grey colour solid. 53% yield (1 g). M.P. charred at 150 °C. FTIR (cm<sup>-1</sup>) 3076, 1658, 1600, 1545, 1514, 1269, 1200, 752. <sup>1</sup>H-NMR (400 MHz, DMSO-d<sub>6</sub>) δ ppm 3.11 (dd, J = 5.2, 17.92 Hz, 1H), 3.85-3.92 (m, 1H), 5.19 (d, J = 16.6 Hz, 1H), 5.23 (d, J = 16.6 Hz, 1H), 5.92 (dd, J = 5.16, 11.8 Hz, 1H), 6.59

(d,  $J = 9.52$  Hz, 1H), 7.16 (t,  $J = 8.6$  Hz, 2H), 7.19-7.27 (m, 3H), 7.37 (t,  $J = 6.4$  Hz, 1H), 7.74–7.81 (m, 3H), 7.91 (d,  $J = 2.16$  Hz, 1H), 9.56 (s, 1H).

**6-(2-(3-(4-fluorophenyl)-5-(furan-2-yl)-4,5-dihydro-1H-pyrazol-1-yl)-2-oxoethoxy) nicotinaldehyde (18c).** Grey colour solid. 49% yield (0.9 g). M.P. charred at 173 °C. FTIR ( $\text{cm}^{-1}$ ) 3282, 1664, 1606, 1546, 1510, 1274, 1220.  $^1\text{H-NMR}$  (400 MHz,  $\text{DMSO-d}_6$ )  $\delta$  ppm 3.48 (dd,  $J = 5.08, 17.68$  Hz, 1H), 3.59-3.66 (m, 1H), 5.03 (d,  $J = 16.72$  Hz, 1H), 5.39 (d,  $J = 16.72$  Hz, 1H), 5.67 (dd,  $J = 5.04, 11.56$  Hz, 1H), 6.30-6.37 (m, 2H), 6.57 (d,  $J = 9.48$  Hz, 1H), 7.14 (t,  $J = 8.6$  Hz, 2H), 7.28-7.30 (m, 1H), 7.76–7.80 (m, 3H), 7.90 (d,  $J = 2.2$  Hz, 1H), 9.55 (s, 1H).

**6-(2-(3-(4-fluorophenyl)-5-(4-(trifluoromethyl)phenyl)-4,5-dihydro-1H-pyrazol-1-yl)-2-oxoethoxy) nicotinaldehyde (18d).** Grey colour solid. 56% yield (1.1 g). M.P. charred at 215 °C. FTIR ( $\text{cm}^{-1}$ ) 3205, 1656, 1602, 1545, 1514, 1323, 1224, 1269.  $^1\text{H-NMR}$  (400 MHz,  $\text{DMSO-d}_6$ )  $\delta$  ppm 3.30 (dd,  $J = 5.2, 18.4$  Hz, 1H), 3.95-4.02 (m, 1H), 5.27 (d,  $J = 16.4$  Hz, 1H), 5.36 (d,  $J = 16.4$  Hz, 1H), 5.70 (dd,  $J = 5.2, 12.0$  Hz, 1H), 6.51 (d,  $J = 9.6$  Hz, 1H), 7.33-7.37 (m, 2H), 7.49 (d,  $J = 8.0$  Hz, 2H), 7.70 (d,  $J = 8.4$  Hz, 2H), 7.78-7.82 (m, 1H), 7.89-7.92 (m, 2H), 8.54 (d,  $J = 2.4$  Hz, 1H), 9.58 (s, 1H).

**6-(2-(3,5-bis(4-fluorophenyl)-4,5-dihydro-1H-pyrazol-1-yl)-2-oxoethoxy)nicotinaldehyde (18e).** Grey colour solid. 51% yield (0.85 g). M.P. 135-137 °C. FTIR ( $\text{cm}^{-1}$ ) 3064, 1656, 1602, 1546, 1510, 1384, 1220, 1269.  $^1\text{H-NMR}$  (400 MHz,  $\text{DMSO-d}_6$ )  $\delta$  ppm 3.28 (dd,  $J = 4.8, 18.4$  Hz, 1H), 3.90-3.97 (m, 1H), 5.24 (d,  $J = 16.4$  Hz, 1H), 5.33 (d,  $J = 16.4$  Hz, 1H), 5.60 (dd,  $J = 4.8, 11.6$  Hz, 1H), 6.50 (d,  $J = 9.6$  Hz, 1H), 7.15 (t,  $J = 8.8$  Hz, 2H), 7.28-7.37 (m, 4H), 7.80 (dd,  $J = 2.4, 9.6$  Hz, 1H), 7.89-7.93 (m, 2H), 8.53 (d,  $J = 2.4$  Hz, 1H), 9.58 (s, 1H).

**6-(2-(5-(2,4-difluorophenyl)-3-(4-fluorophenyl)-4,5-dihydro-1H-pyrazol-1-yl)-2-oxoethoxy) nicotinaldehyde (18f).** Grey colour solid. 54% yield (0.9 g). M.P. 150-152 °C. FTIR ( $\text{cm}^{-1}$ ) 3064, 1656, 1602, 1543, 1502, 1386, 1330, 1309, 1267.  $^1\text{H-NMR}$  (400 MHz,  $\text{DMSO-d}_6$ )  $\delta$  ppm 3.13-3.18 (m, 1H), 4.07-4.14 (m, 1H), 5.24 (d,  $J = 16.8$  Hz, 1H), 5.41 (d,  $J = 16.4$  Hz, 1H), 5.77 (dd,  $J = 5.2, 12.0$  Hz, 1H), 6.50-6.53 (m, 1H), 7.22-7.27 (m, 2H), 7.29-7.34 (m, 2H), 7.39-7.45 (m, 1H), 7.47-7.50 (m, 1H), 7.79-7.82 (m, 1H), 7.97-8.04 (m, 1H), 8.54-8.56 (m, 1H), 9.58-9.59 (m, 1H).

**6-(2-(5-(2-chlorophenyl)-3-(2,4-difluorophenyl)-4,5-dihydro-1H-pyrazol-1-yl)-2-oxoethoxy) nicotinaldehyde (20b).** Grey solid. 80% yield (2 g). M.P. 200-202 °C. FTIR ( $\text{cm}^{-1}$ ) 3190, 1662, 1604, 1545, 1444, 1307, 1226, 1269, 756.  $^1\text{H-NMR}$  (400 MHz,  $\text{CDCl}_3$ )  $\delta$  ppm 3.12–3.19 (m, 1H), 4.07–4.14 (m, 1H), 5.24 (d,  $J = 16.52$  Hz, 1H), 5.41 (d,  $J = 16.52$  Hz, 1H), 5.78 (dd,  $J = 5.2, 12.0$  Hz, 1H), 6.49-6.53 (m, 1H), 7.22–7.30 (m, 2H), 7.30–7.34 (m, 2H), 7.40–7.50 (m, 2H), 7.78–7.82 (m, 1H), 7.98–8.04 (m, 1H), 8.54–8.57 (m, 1H), 9.59 (s, 1H).

**6-(2-(3-(2,4-difluorophenyl)-5-(furan-2-yl)-4,5-dihydro-1H-pyrazol-1-yl)-2-oxoethoxy)nicotinaldehyde (20c).** Grey colour solid. 69% yield (0.94 g). M.P. 167-169 °C. FTIR ( $\text{cm}^{-1}$ ) 3091, 1658, 1600, 1543, 1504, 1398, 1379, 1263.  $^1\text{H-NMR}$  (400 MHz,  $\text{CDCl}_3$ )  $\delta$  ppm 3.55–3.62 (m, 1H), 3.68–3.76 (m, 1H), 5.03 (d,  $J = 16.76$  Hz, 1H), 5.38 (d,  $J = 16.72$  Hz, 1H), 5.66 (dd,  $J = 5.16, 11.6$  Hz, 1H), 6.30-6.31 (m, 1H), 6.37 (d,  $J = 3.2$  Hz, 1H), 6.59 (d,  $J = 9.48$  Hz, 1H), 6.88–6.94 (m, 1H), 6.97–7.01 (m, 1H), 7.28-7.32 (m, 1H), 7.80 (dd,  $J = 2.4, 9.48$  Hz, 1H), 7.90 (d,  $J = 2.32$  Hz, 1H), 7.97–8.03 (m, 1H), 9.6 (s, 1H).

**6-(2-(3-(2,4-difluorophenyl)-5-(4-(trifluoromethyl)phenyl)-4,5-dihydro-1H-pyrazol-1-yl)-2-oxoethoxy)nicotinaldehyde (20d).** Grey colour solid. 63% yield (1.5 g). M.P. charred at 260 °C. FTIR (cm<sup>-1</sup>) 3064, 1658, 1602, 1543, 1514, 1384, 1352, 1327, 1269. <sup>1</sup>H-NMR (400 MHz, DMSO-d<sub>6</sub>) δ ppm 3.23-3.30 (m, 1H), 4.00-4.08 (m, 1H), 5.24 (d, J = 16.4 Hz, 1H), 5.34 (d, J = 16.4 Hz, 1H), 5.67 (dd, J = 5.2, 12 Hz, 1H), 6.50 (d, J = 9.6 Hz, 1H), 7.23-7.28 (m, 1H), 7.40-7.46 (m, 1H), 7.50 (d, J = 8.0 Hz, 2H), 7.70 (d, J = 8.0 Hz, 2H), 7.78-7.82 (m, 1H), 7.98-8.04 (m, 1H), 8.53-8.54 (m, 1H), 9.57-9.59 (m, 1H).

**6-(2-(3-(2,4-difluorophenyl)-5-(4-fluorophenyl)-4,5-dihydro-1H-pyrazol-1-yl)-2-oxoethoxy)nicotinaldehyde (20e).** Grey colour solid. 61% yield (1.4 g). M.P. charred at 250 °C. FTIR (cm<sup>-1</sup>) 3047, 1654, 1602, 1541, 1504, 1386, 1354, 1330, 1267. <sup>1</sup>H-NMR (400 MHz, DMSO-d<sub>6</sub>) δ ppm 3.20-3.32 (m, 1H), 3.96-4.04 (m, 1H), 5.22 (d, J = 16.4 Hz, 1H), 5.31 (d, J = 16.4 Hz, 1H), 5.57 (dd, J = 5.2, 12.0 Hz, 1H), 6.47-6.51 (m, 1H), 7.13-7.17 (m, 2H), 7.23-7.33 (m, 2H), 7.40-7.43 (m, 1H), 7.75-7.81 (m, 2H), 7.98-8.04 (m, 1H), 8.50-8.55 (m, 1H), 9.56-9.59 (m, 1H).

**6-(2-(3,5-bis(2,4-difluorophenyl)-4,5-dihydro-1H-pyrazol-1-yl)-2-oxoethoxy)nicotinaldehyde (20f).** Grey colour solid. 67% yield (1.6 g). M.P. 179-181 °C. FTIR (cm<sup>-1</sup>) 3066, 1658, 1600, 1541, 1504, 1398, 1379, 1350, 1327, 1263. <sup>1</sup>H-NMR (400 MHz, DMSO-d<sub>6</sub>) δ ppm 3.26-3.30 (m, 1H), 3.98-4.05 (m, 1H), 5.24 (d, J = 16.8 Hz, 1H), 5.29 (d, J = 16.8 Hz, 1H), 5.66 (dd, J = 5.6, 12.0 Hz, 1H), 6.50 (d, J = 9.6 Hz, 1H), 7.05-7.07 (m, 1H), 7.22-7.28 (m, 2H), 7.32-7.38 (m, 1H), 7.41-7.47 (m, 1H), 7.80 (dd, J = 2.4, 9.6 Hz, 1H), 7.97-8.03 (m, 1H), 8.53-8.54 (m, 1H), 9.58 (s, 1H).

The final product was synthesized by similar route mentioned previously[29,84]. 5-((6-hydroxynaphthalen-2-yl)methylene)thiazolidine-2,4-dione (12) (1 mol) and potassium carbonate (1.5 mol) was added in dimethyl formamide (10 mL) and stirred for 5 min at RT. To this solution chloroacetylated pyrazolines (4a-4c, 4e, 4g, 4i, 7a-7c, 7e, 7g, 10e, and 10g) (1.5 mol) were added with stirring. The reaction mixture was allowed to stir for 24 h at RT, and water was added (50 mL) to stop the reaction. Precipitated solid was collected by filtering and washed thoroughly with water. Crude obtained were purified by column chromatography (hexane: ethylacetate, 1:1 to 0.5:1.5) get respective final compounds (**13a-13c**, **13e**, **13g**, **13i**, **14a-14c**, **14e**, **14g**, **15e**, and **15g**) (Scheme II).

**5-((6-(2-(3,5-diphenyl)-4,5-dihydro-1H-pyrazol-1-yl)-2-oxoethoxy)naphthalen-2-yl)methylene)thiazolidine-2,4-dione (13a).** Yellow colour powder. 70% yield (0.7 g). M.P. 260.3 °C. FTIR (cm<sup>-1</sup>) 3389, 1739, 1680, 1622, 1579, 1494, 1475, 1427, 1267, 817. <sup>1</sup>H-NMR (400 MHz, DMSO-d<sub>6</sub>) δ ppm 3.20 (dd, J = 4.8, 18.4 Hz, 1H), 3.89-3.97 (m, 1H), 5.31 (d, J = 16.4 Hz, 1H), 5.47 (d, J = 16.0 Hz, 1H), 5.62 (dd, J = 4.4, 11.6 Hz, 1H), 7.23-7.24 (m, 1H), 7.27-7.29 (m, 2H), 7.29-7.32 (m, 2H), 7.34-7.36 (m, 2H), 7.50-7.51 (m, 3H), 7.63 (d, J = 8.4 Hz, 1H), 7.87-7.91 (m, 4H), 7.95 (d, J = 8.8 Hz, 1H), 8.10 (s, 1H), 12.60 (bs, 1H). <sup>13</sup>C-NMR (100 MHz, DMSO-d<sub>6</sub>) δ 41.86, 59.92, 65.58, 107.19, 119.70, 122.31, 125.47, 126.51, 126.93, 127.35, 127.77, 128.25, 128.31, 128.68, 128.79, 130.39, 130.64, 130.74, 130.84, 132.10, 134.72, 141.83, 155.48, 157.67, 164.50, 167.32, 167.93. Theoretical mass: 533.60, LC-MS (m/z, I %): 532.1 [(M-H)<sup>+</sup>, 100%]. HPLC Purity: % Area 95.82, Retention Time 5.65 mins.

**5-((6-(2-(5-(2-chlorophenyl)-3-phenyl)-4,5-dihydro-1H-pyrazol-1-yl)-2-oxoethoxy)naphthalen-2-yl)methylene)thiazolidine-2,4-dione (13b).** Pale yellow colour powder. 69% yield (0.72 g). M.P. 281.5 °C.

FTIR (cm<sup>-1</sup>) 3379, 1737, 1676, 1626, 1587, 1498, 1475, 1440, 1257, 837, 750. <sup>1</sup>H-NMR (400 MHz, DMSO-d<sub>6</sub>) δ ppm 3.15 (dd, J = 5.2, 18.0 Hz, 1H), 3.97-4.05 (m, 1H), 5.33 (d, J = 16.4 Hz, 1H), 5.54 (d, J = 16.4 Hz, 1H), 5.83 (dd, J = 4.8, 12.0 Hz, 1H), 7.29-7.31 (m, 4H), 7.37 (s, 1H), 7.49-7.51 (m, 4H), 7.64 (d, J = 8.8 Hz, 1H), 7.86-7.88 (m, 2H), 7.89-7.91 (m, 1H), 7.94-7.95 (m, 1H), 7.95-7.97 (m, 1H), 8.10 (s, 1H), 12.59 (bs, 1H). <sup>13</sup>C-NMR (100 MHz, DMSO-d<sub>6</sub>) δ 40.64, 57.72, 65.52, 107.21, 119.70, 122.29, 126.52, 126.95, 127.64, 127.76, 128.26, 128.31, 128.79, 129.15, 129.67, 130.40, 130.58, 130.71, 130.78, 130.86, 132.12, 134.74, 138.40, 146.50, 155.61, 157.65, 164.63, 167.93. Theoretical mass: 568.04, LC-MS (m/z, I %): 566.0 [(M-2H)<sup>+</sup>, 100%]. HPLC Purity: % Area 97.42, Retention Time 4.12 mins.

**5-(((6-(2-(5-(furan-2-yl)-3-phenyl-4,5-dihydro-1H-pyrazol-1-yl)-2-oxoethoxy)naphthalen-2-yl)**

**methylene)thiazolidine-2,4-dione (13c).** Yellow colour powder. 66% yield (0.75 g). M.P. 269.7 °C. FTIR (cm<sup>-1</sup>) 3302, 1737, 1669, 1643, 1595, 1572, 1535, 1500, 1462, 1444, 1269, 815. <sup>1</sup>H-NMR (400 MHz, DMSO-d<sub>6</sub>) δ ppm 3.45 (dd, J = 3.2, 8.4 Hz, 1H), 3.76-3.84 (m, 1H), 5.27 (d, J = 16.0 Hz, 1H), 5.35 (d, J = 16.0 Hz, 1H), 5.72 (dd, J = 4.8, 12.0 Hz, 1H), 6.39 (s, 2H), 7.28-7.30 (m, 2H), 7.51-7.52 (m, 3H), 7.58-7.60 (m, 1H), 7.60-7.62 (m, 1H), 7.86-7.89 (m, 4H), 7.96 (d, J = 8.8 Hz, 1H), 8.10 (s, 1H), 12.60 (bs, 1H). <sup>13</sup>C-NMR (100 MHz, DMSO-d<sub>6</sub>) δ 38.12, 53.55, 65.59, 107.24, 107.28, 110.51, 119.64, 122.37, 126.50, 126.89, 127.76, 128.26, 128.33, 128.82, 130.39, 130.60, 130.70, 130.86, 132.06, 134.71, 142.50, 152.18, 155.66, 164.62, 167.38, 167.97. Theoretical mass: 523.56, LC-MS (m/z, I %): 522.0 [(M-H)<sup>+</sup>, 100%]. HPLC Purity: % Area 96.34, Retention Time 5.01 mins.

**5-(((6-(2-(5-(4-fluorophenyl)-3-phenyl-4,5-dihydro-1H-pyrazol-1-yl)-2-oxoethoxy)naphthalen-2-yl)**

**methylene)thiazolidine-2,4-dione (13e).** Yellow colour powder. 68% yield (0.7 g). M.P. 283.3 °C. FTIR (cm<sup>-1</sup>) 3371, 1722, 1672, 1627, 1589, 1477, 1438, 1274, 1193, 862. <sup>1</sup>H-NMR (400 MHz, DMSO-d<sub>6</sub>) δ ppm 3.20 (dd, J = 4.8, 18.4 Hz, 1H), 3.87-3.95 (m, 1H), 5.30 (d, J = 16.0 Hz, 1H), 5.46 (d, J = 16.4 Hz, 1H), 5.62 (dd, J = 4.8, 11.6 Hz, 1H), 7.14 (t, J = 8.8 Hz, 2H), 7.27-7.29 (m, 2H), 7.30-7.36 (m, 2H), 7.51 (s, 3H), 7.62 (d, J = 8.4 Hz, 1H), 7.88-7.90 (m, 4H), 7.94 (d, J = 8.8 Hz, 1H), 8.08 (s, 1H), 12.59 (bs, 1H). <sup>13</sup>C-NMR (100 MHz, DMSO-d<sub>6</sub>) δ 41.72, 59.28, 65.57, 107.18, 115.27, 115.48, 119.66, 122.32, 126.49, 126.94, 127.67, 127.76, 128.24, 128.32, 128.78, 130.38, 130.66, 130.69, 130.84, 132.09, 134.71, 138.01, 155.47, 157.66, 160.12, 162.54, 164.55, 167.32, 167.94. Theoretical mass: 551.59, LC-MS (m/z, I %): 550.1 [(M-H)<sup>+</sup>, 100%]. HPLC Purity: % Area 95.49, Retention Time 5.09 mins.

**5-(((6-(2-oxo-2-(3-phenyl-5-(p-tolyl)-4,5-dihydro-1H-pyrazol-1-yl)ethoxy)naphthalen-2-yl)methylene)**

**thiazolidine-2,4-dione (13g).** Pale yellow colour powder. 65% yield (0.66 g). M.P. 261.8 °C. FTIR (cm<sup>-1</sup>) 3381, 3111, 1728, 1672, 1627, 1587, 1475, 1440, 1273, 862. <sup>1</sup>H-NMR (400 MHz, DMSO-d<sub>6</sub>) δ ppm 2.24 (s, 3H), 3.17 (dd, J = 4.68, 18.2 Hz, 1H), 3.85-3.92 (m, 1H), 5.30 (d, J = 16.04 Hz, 1H), 5.45 (d, J = 16.04 Hz, 1H), 5.57 (dd, J = 4.6, 11.64 Hz, 1H), 7.12-7.18 (m, 4H), 7.26-7.29 (m, 2H), 7.47-7.51 (m, 3H), 7.61 (dd, J = 1.64, 8.68 Hz, 1H), 7.85-7.88 (m, 4H), 7.94 (d, J = 8.88 Hz, 1H), 8.08 (s, 1H), 12.61 (bs, 1H). <sup>13</sup>C-NMR (100 MHz, DMSO-d<sub>6</sub>) δ 20.57, 27.98, 42.01, 59.98, 115.78, 116.00, 120.83, 124.50, 125.55, 129.18, 129.35, 134.31, 134.91, 138.60, 140.10, 155.06, 161.79, 162.76, 177.13. Theoretical mass: 547.62, LC-MS (m/z, I %): 546.2 [(M-H)<sup>+</sup>, 100%]. HPLC Purity: % Area 97.15, Retention Time 4.17 mins.

**5-((6-(2-oxo-2-(3-phenyl-5-(thiophen-2-yl)-4,5-dihydro-1H-pyrazol-1-yl)ethoxy)naphthalen-2-yl)**

**methylene)thiazolidine-2,4-dione (13i).** Yellow colour powder. 68% yield (0.58 g). M.P. 263.1 °C. FTIR (cm<sup>-1</sup>) 3394, 1743, 1681, 1620, 1585, 1500, 1475, 1431, 1267, 848. <sup>1</sup>H-NMR (400 MHz, DMSO-d<sub>6</sub>) δ ppm 3.88-3.95 (m, 2H), 5.28 (d, J = 16.0 Hz, 1H), 5.38 (d, J = 16.4 Hz, 1H), 5.94 (dd, J = 4.0, 11.2 Hz, 1H), 6.96 (dd, J = 3.6, 4.8 Hz, 1H), 7.10 (d, J = 3.2 Hz, 1H), 7.29-7.31 (m, 2H), 7.43 (d, J = 4.4 Hz, 1H), 7.51-7.53 (m, 3H), 7.62 (dd, J = 1.6, 8.8 Hz, 1H), 7.85-7.90 (m, 4H), 7.95-7.98 (m, 1H), 8.10 (s, 1H), 12.56 (bs, 1H). <sup>13</sup>C-NMR (100 MHz, DMSO-d<sub>6</sub>) δ 41.48, 55.52, 65.61, 107.23, 119.67, 122.39, 124.84, 125.17, 126.51, 126.82, 126.96, 127.75, 128.27, 128.34, 128.85, 130.41, 130.58, 130.77, 130.88, 132.06, 134.69, 144.24, 155.73, 157.65, 164.65, 167.43, 168.02 Theoretical mass: 539.62, LC-MS (m/z, I %): 538.1 [(M-H)<sup>+</sup>, 100%]. HPLC Purity: % Area 98.15, Retention Time 3.98 mins.

**5-((6-(2-(3-(4-fluorophenyl)-5-phenyl-4,5-dihydro-1H-pyrazol-1-yl)-2-oxoethoxy)naphthalen-2-yl)**

**methylene)thiazolidine-2,4-dione (14a).** Yellow solid. 61% yield (0.62 g). M.P. 286.7 °C. FTIR (cm<sup>-1</sup>) 3292, 1737, 1681, 1585, 1514, 1496, 1446, 1267, 1188, 833. <sup>1</sup>H-NMR (400 MHz, DMSO-d<sub>6</sub>) δ ppm 3.20 (dd, J = 4.4, 18.0 Hz, 1H), 3.87-3.95 (m, 1H), 5.31 (d, J = 16.0 Hz, 1H), 5.46 (d, J = 16.4 Hz, 1H), 5.62 (dd, J = 4.4, 11.6 Hz, 1H), 7.24-7.27 (m, 1H), 7.27-7.29 (m, 1H), 7.29-7.32 (m, 3H), 7.32-7.34 (m, 3H), 7.34-7.36 (m, 1H), 7.62 (d, J = 8.8 Hz, 1H), 7.89-7.90 (m, 1H), 7.90-7.91 (m, 1H), 7.91-7.93 (m, 1H), 7.93-7.95 (m, 1H), 7.95-7.96 (m, 1H), 8.09 (s, 1H), 12.60 (bs, 1H). <sup>13</sup>C-NMR (100 MHz, DMSO-d<sub>6</sub>) δ 41.91, 60.03, 65.56, 107.19, 115.76, 115.98, 119.68, 122.31, 125.48, 126.50, 127.36, 127.41, 127.76, 128.24, 128.30, 128.67, 129.31, 129.40, 130.38, 130.84, 132.09, 134.71, 141.77, 154.57, 157.66, 162.18, 164.50, 164.65, 167.31, 167.94. Theoretical mass: 551.59, LC-MS (m/z, I %): 550.3 [(M-H)<sup>+</sup>, 100%]. HPLC Purity: % Area 96.14, Retention Time 4.81 mins.

**5-((6-(2-(5-(2-chlorophenyl)-3-(4-fluorophenyl)-4,5-dihydro-1H-pyrazol-1-yl)-2-oxoethoxy)**

**naphthalene-2-yl)methylene)thiazolidine-2,4-dione (14b).** Yellow colour powder. 60% yield (0.58 g). M.P. 288.8 °C. FTIR (cm<sup>-1</sup>) 3321, 1741, 1701, 1668, 1626, 1602, 1516, 1475, 1440, 1271, 1180, 837, 690. <sup>1</sup>H-NMR (400 MHz, DMSO-d<sub>6</sub>) δ ppm 3.16 (dd, J = 5.2, 18.0 Hz, 1H), 3.96-4.03 (m, 1H), 5.33 (d, J = 16.0 Hz, 1H), 5.53 (d, J = 16.4 Hz, 1H), 5.82 (dd, J = 5.2, 12.0 Hz, 1H), 7.31-7.33 (m, 4H), 7.33-7.36 (m, 2H), 7.47-7.49 (m, 2H), 7.63 (d, J = 8.4 Hz, 1H), 7.89-7.93 (m, 2H), 7.93-7.97 (m, 3H), 8.10 (s, 1H), 12.60 (bs, 1H). <sup>13</sup>C-NMR (100 MHz, DMSO-d<sub>6</sub>) δ 40.70, 57.83, 65.50, 107.21, 115.76, 115.98, 119.69, 122.30, 126.53, 126.75, 127.23, 127.26, 127.64, 127.75, 128.26, 128.31, 129.16, 129.35, 129.44, 129.67, 130.39, 130.78, 130.86, 132.10, 134.73, 138.35, 154.70, 157.64, 162.21, 164.62, 167.29, 167.92. Theoretical mass: 586.03, LC-MS (m/z, I %): 584.1 [(M-2H)<sup>+</sup>, 100%]. HPLC Purity: % Area 95.66, Retention Time 3.74 mins.

**5-((6-(2-(3-(4-fluorophenyl)-5-(furan-2-yl)-4,5-dihydro-1H-pyrazol-1-yl)-2-oxoethoxy)**

**naphthalen-2-yl)methylene)thiazolidine-2,4-dione (14c).** Yellow solid. 69% yield (0.78 g). M.P. 276.6 °C. FTIR (cm<sup>-1</sup>) 3389, 1741, 1697, 1643, 1626, 1595, 1460, 1269, 1184, 813. <sup>1</sup>H-NMR (400 MHz, DMSO-d<sub>6</sub>) δ ppm 3.44 (dd, J = 4.8, 14.4 Hz, 1H), 3.75-3.83 (m, 1H), 5.26 (d, J = 16.0 Hz, 1H), 5.34 (d, J = 16.0 Hz, 1H), 5.72 (dd, J = 4.4, 11.6 Hz, 1H), 6.39 (s, 2H), 7.28-7.30 (m, 2H), 7.35 (t, J = 8.8 Hz, 2H), 7.59 (s, 1H), 7.62 (d, J = 8.8 Hz, 1H), 7.86-7.89 (m, 2H), 7.92-7.97 (m, 3H), 8.10 (s, 1H), 12.59 (bs, 1H). <sup>13</sup>C-NMR (100 MHz, DMSO-d<sub>6</sub>) δ 38.21, 53.66, 65.57, 107.27, 110.51, 115.81, 116.03, 119.64, 122.32, 126.51, 127.28, 127.77, 128.26, 128.32,

129.29, 129.37, 130.40, 130.88, 132.10, 134.71, 142.52, 152.13, 154.74, 157.69, 164.62, 167.31, 167.93. Theoretical mass: 541.55, LC-MS (m/z, I %): 540.1 [(M-H)<sup>+</sup>, 100%]. HPLC Purity: % Area 96.00, Retention Time 3.61 mins.

**5-((6-(2-(3,5-bis(4-fluorophenyl)-4,5-dihydro-1H-pyrazol-1-yl)-2-oxoethoxy)naphthalen-2-yl)**

**methylene)thiazolidine-2,4-dione (14e).** Yellow colour powder. 65% yield (0.72 g). M.P. 286.6 °C. FTIR (cm<sup>-1</sup>) 3321, 1728, 1676, 1627, 1587, 1508, 1477, 1446, 1274, 1192, 1151, 831. <sup>1</sup>H-NMR (400 MHz, DMSO-d<sub>6</sub>) δ ppm 3.21 (dd, J = 4.8, 18.4 Hz, 1H), 3.86-3.94 (m, 1H), 5.30 (d, J = 16.0 Hz, 1H), 5.44 (d, J = 16.4 Hz, 1H), 5.62 (dd, J = 4.8, 11.6 Hz, 1H), 7.14 (t, J = 8.8 Hz, 2H), 7.26-7.30 (m, 2H), 7.32-7.36 (m, 4H), 7.62 (d, J = 8.4 Hz, 1H), 7.88-7.90 (m, 2H), 7.90-7.91 (m, 1H), 7.91-7.93 (m, 1H), 7.94-7.96 (m, 1H), 8.09 (s, 1H), 12.60 (bs, 1H). <sup>13</sup>C-NMR (100 MHz, DMSO-d<sub>6</sub>) δ 41.78, 59.39, 65.56, 107.18, 115.26, 115.48, 115.76, 115.98, 119.65, 122.44, 126.50, 127.35, 127.37, 127.69, 127.77, 128.24, 128.34, 129.32, 129.41, 130.38, 130.82, 132.00, 134.69, 137.95, 154.56, 157.63, 162.19, 164.55, 164.67, 167.45, 168.01. Theoretical mass: 569.58, LC-MS (m/z, I %): 568.1 [(M-H)<sup>+</sup>, 100%]. HPLC Purity: % Area 95.78, Retention Time 3.61 mins.

**5-((6-(2-(3-(4-fluorophenyl)-5-(p-tolyl)-4,5-dihydro-1H-pyrazol-1-yl)-2-oxoethoxy)naphthalen-2-yl)**

**methylene)thiazolidine-2,4-dione (14g).** Yellow colour solid. 63% yield (0.7 g). M.P. 256.8 °C. FTIR (cm<sup>-1</sup>) 3389, 3045, 1728, 1676, 1627, 1587, 1514, 1475, 1446, 1273, 1188, 837. <sup>1</sup>H-NMR (400 MHz, DMSO-d<sub>6</sub>) δ ppm 2.26 (s, 3H), 3.16 (dd, J = 4.8, 18.4 Hz, 1H), 3.82-3.90 (m, 1H), 5.28 (d, J = 16.0 Hz, 1H), 5.43 (d, J = 16.0 Hz, 1H), 5.56 (dd, J = 4.8, 12.0 Hz, 1H), 7.11-7.17 (m, 4H), 7.25-7.27 (m, 2H), 7.33 (t, J = 8.8 Hz, 2H), 7.60 (d, J = 8.4 Hz, 1H), 7.84 (s, 1H), 7.86-7.87 (m, 1H), 7.89-7.91 (m, 1H), 7.91-7.92 (m, 1H), 7.92-7.93 (m, 1H), 8.06 (s, 1H), 12.60 (bs, 1H). <sup>13</sup>C-NMR (100 MHz, DMSO-d<sub>6</sub>) δ 20.57, 41.83, 59.82, 65.58, 107.18, 115.74, 115.96, 119.65, 122.26, 125.46, 126.42, 127.40, 127.43, 127.73, 128.23, 128.28, 129.17, 129.25, 129.33, 130.35, 130.85, 132.10, 134.69, 136.53, 138.83, 154.53, 157.65, 162.16, 164.41, 164.63, 167.28, 167.91. Theoretical mass: 565.61, LC-MS (m/z, I %): 564.1 [(M-H)<sup>+</sup>, 100%]. HPLC Purity: % Area 96.58, Retention Time 3.65 mins.

**5-((6-(2-(3-(2,4-difluorophenyl)-5-(4-fluorophenyl)-4,5-dihydro-1H-pyrazol-1-yl)-2-oxoethoxy)**

**naphthalen-2-yl)methylene)thiazolidine-2,4-dione (15e).** Yellow solid. 65% yield (0.73 g). M.P. 253.2 °C. FTIR (cm<sup>-1</sup>) 3390, 1726, 1674, 1624, 1587, 1504, 1477, 1444, 1415, 1273, 1219, 1190, 1143, 852. <sup>1</sup>H-NMR (400 MHz, DMSO-d<sub>6</sub>) δ ppm 3.17 (dd, J = 3.2, 18.8 Hz, 1H), 3.92-3.99 (m, 1H), 5.27 (d, J = 16.0 Hz, 1H), 5.42 (d, J = 16.0 Hz, 1H), 5.60 (dd, J = 4.4, 11.6 Hz, 1H), 7.14 (t, J = 8.8 Hz, 2H), 7.22-7.28 (m, 3H), 7.33-7.38 (m, 2H), 7.41-7.43 (m, 1H), 7.61 (d, J = 8.4 Hz, 1H), 7.86-7.89 (m, 2H), 7.93 (d, J = 8.8 Hz, 1H), 8.03-8.07 (m, 2H), 12.60 (bs, 1H). <sup>13</sup>C-NMR (100 MHz, DMSO-d<sub>6</sub>) δ 30.74, 35.74, 43.65, 59.04, 65.52, 79.11, 104.79, 105.06, 105.32, 107.16, 112.29, 112.53, 115.27, 115.48, 115.55, 115.59, 115.67, 115.71, 119.58, 122.85, 126.49, 127.70, 127.79, 128.26, 128.44, 130.35, 130.73, 130.91, 130.95, 131.00, 131.05, 131.68, 134.62, 137.77, 137.79, 150.96, 157.56, 159.56, 160.15, 161.98, 162.11, 162.31, 162.57, 164.77, 167.94, 168.24. Theoretical mass: 587.57, LC-MS (m/z, I %): 586.0 [(M-H)<sup>+</sup>, 100%]. HPLC Purity: % Area 98.09, Retention Time 4.46 mins.

**5-((6-(2-(3-(2,4-difluorophenyl)-5-(p-tolyl)-4,5-dihydro-1H-pyrazol-1-yl)-2-oxoethoxy) naphthalen-2-yl)methylene)thiazolidine-2,4-dione (15g).** Yellow solid. 67% yield (0.69 g). M.P. 245.0 °C. FTIR (cm<sup>-1</sup>)

3389, 2928, 1737, 1685, 1624, 1564, 1504, 1477, 1438, 1411, 1265, 1184, 1141, 852. <sup>1</sup>H-NMR (400 MHz, DMSO-d<sub>6</sub>) δ ppm 2.24 (s, 3H), 3.13 (dd, J = 2.4, 18.4 Hz, 1H), 3.89-3.97 (m, 1H), 5.26 (d, J = 16.0 Hz, 1H), 5.42 (d, J = 16.0 Hz, 1H), 5.52 (dd, J = 4.8, 11.6 Hz, 1H), 7.12-7.18 (m, 4H), 7.21-7.24 (m, 1H), 7.24-7.26 (m, 2H), 7.37-7.42 (m, 1H), 7.60 (d, J = 8.4 Hz, 1H), 7.84-7.86 (m, 1H), 7.86-7.87 (m, 1H), 7.92-7.94 (m, 1H), 8.02-8.04 (m, 1H), 8.07 (s, 1H), 12.60 (bs, 1H). <sup>13</sup>C-NMR (100 MHz, DMSO-d<sub>6</sub>) δ 20.57, 43.74, 43.80, 59.45, 65.54, 104.80, 105.07, 105.33, 107.16, 112.32, 112.52, 115.62, 115.73, 119.64, 122.28, 125.46, 126.44, 127.73, 128.24, 128.30, 129.19, 130.37, 130.84, 132.10, 134.67, 136.58, 138.69, 150.91, 150.94, 157.62, 164.62, 167.27, 167.90. Theoretical mass: 583.60, LC-MS (m/z, I %): 581.9 [(M-H)<sup>+</sup>, 100%]. HPLC Purity: % Area 95.28, Retention Time 4.23 mins.

Final compounds were synthesized by following scheme III, where, 2,4-thiazolidinedione (0.005 mol) was swirled in 2-methoxyethanol (10 mL). To this solution, piperidine (0.4 mL) was added dropwise followed by addition of nicotinaldehyde intermediates (0.002 mol) (16a-16b, 16d-16f, 16h, 16i, 18a-18f, and 20b-20f). The reaction mixture was refluxed and monitored constantly by TLC, after 3 h reaction was stopped; reaction mixture was cooled and treated with acetic acid (30%, 3 mL). Precipitated residue was collected by filtration and washed with water followed by methanol (50 mL). The residue obtained was purified by column chromatography by using hexane: ethylacetate (1:1 to 0.5:1.5) to give the respective final products (**17a-17b**, **17d-17f**, **17h**, **17i**, **19a-19f**, and **21b-21f**).

**5-(((2-(3,5-diphenyl-4,5-dihydro-1H-pyrazol-1-yl)-2-oxoethoxy)pyridin-3-yl)methylene)thiazolidine-2,4-dione (17a)**. Creamish solid. 54% yield (0.5 g). M.P. 311.7 °C. FTIR (cm<sup>-1</sup>) 3383, 1745, 1697, 1668, 1647, 1593, 1527, 1448, 1265, 844. <sup>1</sup>H-NMR (400 MHz, DMSO-d<sub>6</sub>) δ ppm 3.20-3.26 (m, 1H), 3.92-3.99 (m, 1H), 5.21 (d, J = 16.52 Hz, 1H), 5.29-5.35 (m, 1H), 5.60 (dd, J = 4.68, 11.68 Hz, 1H), 6.56 (d, J = 9.6 Hz, 1H), 7.24-7.38 (m, 3H), 7.32-7.36 (m, 2H), 7.47-7.51 (m, 4H), 7.65 (dd, J = 2.68, 9.64 Hz, 1H), 7.84-7.86 (m, 2H), 8.20 (d, J = 2.6 Hz, 1H), 12.61 (bs, 1H). <sup>13</sup>C-NMR (100 MHz, DMSO-d<sub>6</sub>) δ 40.62, 50.92, 54.74, 65.42, 104.14, 112.02, 119.24, 119.83, 126.87, 128.34, 128.84, 130.47, 130.74, 138.43, 145.69, 156.13, 160.24, 163.79, 167.12, 167.44. Theoretical mass: 484.52, LC-MS (m/z, I %): 483.0 [(M-H)<sup>+</sup>, 100%]. HPLC Purity: % Area 97.11, Retention Time 5.96 mins.

**5-(((2-(5-(2-chlorophenyl)-3-phenyl-4,5-dihydro-1H-pyrazol-1-yl)-2-oxoethoxy)pyridin-3-yl)methylene)thiazolidine-2,4-dione (17b)**. Cream colour solid. 60% yield (0.58 g). M.P. 313.5 °C. FTIR (cm<sup>-1</sup>) 3398, 1747, 1697, 1662, 1649, 1635, 1595, 1508, 1456, 1271, 835, 759. <sup>1</sup>H-NMR (400 MHz, DMSO-d<sub>6</sub>) δ ppm 3.20-3.26 (m, 1H), 4.05 (m, 1H), 5.21 (d, J = 16.44 Hz, 1H), 5.41 (d, J = 16.52 Hz, 1H), 5.80 (dd, J = 5.2, 11.88 Hz, 1H), 6.57 (d, J = 1.6 Hz, 1H), 7.29-7.33 (m, 2H), 7.48-7.53 (m, 6H), 7.66 (dd, J = 2.64, 9.6 Hz, 1H), 7.84-7.86 (m, 2H), 8.22 (s, 1H), 12.49 (bs, 1H). <sup>13</sup>C-NMR (100 MHz, DMSO-d<sub>6</sub>) δ 41.99, 50.97, 59.53, 112.00, 115.25, 115.47, 115.80, 116.02, 119.21, 119.83, 127.79, 127.87, 128.33, 129.28, 129.47, 137.62, 138.42, 145.68, 155.00, 160.16, 160.22, 163.75, 167.22, 167.46. Theoretical mass: 518.97, LC-MS (m/z, I %): 517.1 [(M-H)<sup>+</sup>, 100%]. HPLC Purity: % Area 96.93, Retention Time 7.35 mins.

**5-(((2-oxo-2-(3-phenyl-5-(4-(trifluoromethyl)phenyl)-4,5-dihydro-1H-pyrazol-1-yl)ethoxy)pyridin-3-yl)methylene)thiazolidine-2,4-dione (17d)**. Off white solid. 67% yield (0.66 g). M.P. 327.3 °C. FTIR (cm<sup>-1</sup>) 3365, 1749, 1689, 1654, 1602, 1541, 1441, 1406, 1269, 1145, 846. <sup>1</sup>H-NMR (400 MHz, DMSO-d<sub>6</sub>) δ ppm

3.28 (dd,  $J = 5.2, 18.4$  Hz, 1H), 3.95-4.03 (m, 1H), 5.21 (d,  $J = 16.4$  Hz, 1H), 5.35 (d,  $J = 16.4$  Hz, 1H), 5.70 (dd,  $J = 4.8, 11.6$  Hz, 1H), 6.57 (d,  $J = 9.6$  Hz, 1H), 7.48-7.51 (m, 6H), 7.65-7.72 (m, 3H), 7.84-7.86 (m, 2H), 8.19 (s, 1H), 12.49 (bs, 1H).  $^{13}\text{C-NMR}$  (100 MHz,  $\text{DMSO-d}_6$ )  $\delta$  41.72, 50.96, 59.64, 112.01, 119.42, 119.76, 125.57, 126.52, 126.87, 128.10, 128.78, 130.37, 130.75, 145.54, 145.94, 155.88, 160.20, 163.83, 167.54. Theoretical mass: 551.52, LC-MS ( $m/z$ , I %): 551.1 [(M-H)<sup>+</sup>, 100%]. HPLC Purity: % Area 95.67, Retention Time 7.25 mins.

**5-((6-(2-(5-(4-fluorophenyl)-3-phenyl-4,5-dihydro-1H-pyrazol-1-yl)-2-oxoethoxy)pyridin-3-yl)**

**methylene)thiazolidine-2,4-dione (17e).** Creamish solid. 65% yield (0.68 g). M.P. 318.2 °C. FTIR ( $\text{cm}^{-1}$ ) 3381, 1747, 1697, 1666, 1599, 1508, 1437, 1265, 1155, 835.  $^1\text{H-NMR}$  (400 MHz,  $\text{DMSO-d}_6$ )  $\delta$  ppm 3.21-3.27 (m, 1H), 3.89-3.97 (m, 1H), 5.20 (d,  $J = 13.4$  Hz, 1H), 5.31 (d,  $J = 13.2$  Hz, 1H), 5.56-5.62 (m, 1H), 6.41-6.57 (m, 1H), 7.14-7.17 (m, 2H), 7.29-7.31 (m, 2H), 7.50-7.51 (m, 4H), 7.58-7.60 (m, 1H), 7.77-7.85 (m, 2H), 8.20 (d,  $J = 1.6$  Hz, 1H), 12.48 (s, 1H).  $^{13}\text{C-NMR}$  (100 MHz,  $\text{DMSO-d}_6$ )  $\delta$ . 41.85, 50.92, 59.34, 111.89, 115.21, 115.38, 119.14, 119.76, 126.82, 127.72, 127.78, 128.23, 128.75, 130.50, 130.65, 130.66, 137.59, 137.61, 138.33, 145.65, 155.82, 160.14, 160.33, 160.59, 162.26, 163.67, 164.02, 167.14, 167.44. Theoretical mass: 502.52, LC-MS ( $m/z$ , I %): 501.0 [(M-H)<sup>+</sup>, 100%]. HPLC Purity: % Area 95.05, Retention Time 5.77 mins.

**5-((6-(2-(5-(2,4-difluorophenyl)-3-phenyl-4,5-dihydro-1H-pyrazol-1-yl)-2-oxoethoxy)pyridin-3-yl)**

**methylene)thiazolidine-2,4-dione (17f).** Cream colour solid. 68% yield (0.7 g). M.P. 340.5 °C. FTIR ( $\text{cm}^{-1}$ ) 3383, 1714, 1697, 1653, 1593, 1541, 1506, 1456, 1269, 1138, 842.  $^1\text{H-NMR}$  (400 MHz,  $\text{DMSO-d}_6$ )  $\delta$  ppm 3.30 (dd,  $J = 5.2, 18.4$  Hz, 1H), 3.93-4.00 (m, 1H), 5.19 (d,  $J = 16.4$  Hz, 1H), 5.31 (d,  $J = 16.4$  Hz, 1H), 5.69 (dd,  $J = 5.2, 12.0$  Hz, 1H), 6.56 (d,  $J = 9.6$  Hz, 1H), 7.04 (t,  $J = 8.0$  Hz, 1H), 7.25 (t,  $J = 9.2$  Hz, 1H), 7.30-7.36 (m, 1H), 7.52 (s, 3H), 7.65 (d,  $J = 9.6$  Hz, 2H), 7.84-7.85 (m, 2H), 8.19 (s, 1H), 12.50 (bs, 1H).  $^{13}\text{C-NMR}$  (100 MHz,  $\text{DMSO-d}_6$ )  $\delta$  40.68, 50.97, 54.74, 65.32, 104.17, 112.02, 119.22, 119.83, 126.87, 128.34, 128.84, 130.47, 130.77, 138.43, 145.69, 156.10, 160.24, 163.79, 167.12, 167.46. Theoretical mass: 520.51, LC-MS ( $m/z$ , I %): 519.1 [(M-H)<sup>+</sup>, 100%]. HPLC Purity: % Area 97.69, Retention Time 7.19 mins.

**5-((6-(2-(5-(3-nitrophenyl)-3-phenyl-4,5-dihydro-1H-pyrazol-1-yl)-2-oxoethoxy)pyridin-3-yl)**

**methylene)thiazolidine-2,4-dione (17h).** Yellow solid. 68% yield (0.7 g). M.P. 283.6 °C. FTIR ( $\text{cm}^{-1}$ ) 3383, 1749, 1697, 1670, 1654, 1604, 1523, 1498, 1438, 1350, 1271, 847.  $^1\text{H-NMR}$  (400 MHz,  $\text{DMSO-d}_6$ )  $\delta$  ppm 3.27-3.33 (m, 1H), 3.97-4.04 (m, 1H), 5.20 (d,  $J = 16.8$  Hz, 1H), 5.36 (d,  $J = 16.4$  Hz, 1H), 5.78 (d,  $J = 4.8, 11.6$  Hz, 1H), 6.55 (d,  $J = 9.6$  Hz, 1H), 7.51 (s, 4H), 7.64-7.66 (m, 2H), 7.72-7.74 (m, 1H), 7.85-7.86 (m, 2H), 8.14 (s, 2H), 8.19 (s, 1H), 12.50 (bs, 1H).  $^{13}\text{C-NMR}$  (100 MHz,  $\text{DMSO-d}_6$ )  $\delta$  41.69, 51.08, 59.47, 112.02, 119.30, 119.84, 120.98, 122.45, 126.98, 128.85, 130.33, 130.41, 132.48, 138.49, 143.52, 145.63, 147.93, 156.05, 160.24, 164.05, 167.48. Theoretical mass: 529.52, LC-MS ( $m/z$ , I %): 528.1 [(M-H)<sup>+</sup>, 100%]. HPLC Purity: % Area 95.62, Retention Time 5.66 mins.

**5-((6-(2-oxo-2-(3-phenyl-5-(thiophen-2-yl)-4,5-dihydro-1H-pyrazol-1-yl)ethoxy)pyridin-3-yl)**

**methylene)thiazolidine-2,4-dione (17i).** Off white colour solid. 54% yield (0.66 g). M.P. 290.9 °C. FTIR ( $\text{cm}^{-1}$ ) 3385, 1747, 1697, 1666, 1593, 1527, 1456, 1438, 1269, 844.  $^1\text{H-NMR}$  (400 MHz,  $\text{DMSO-d}_6$ )  $\delta$  ppm 3.45-3.47 (m, 1H), 3.89-3.97 (m, 1H), 5.17 (d,  $J = 16.8$  Hz, 1H), 5.26 (d,  $J = 16.8$  Hz, 1H), 5.90 (dd,  $J = 3.6,$

11.2 Hz, 1H), 6.57 (d, J = 9.6 Hz, 1H), 6.95-6.76 (m, 1H), 7.06 (s, 1H), 7.42-7.43 (m, 1H), 7.52 (s, 4H), 7.67 (d, J = 9.6 Hz, 1H) 7.87 (d, J = 4.8 Hz, 2H), 8.19 (s, 1H), 12.50 (bs, 1H). <sup>13</sup>C-NMR (100 MHz, DMSO-d<sub>6</sub>) δ 41.64, 50.92, 55.62, 112.02, 119.23, 119.86, 124.97, 125.38, 126.73, 126.90, 128.37, 128.88, 130.46, 130.83, 138.45, 143.79, 145.71, 156.03, 160.25, 163.73, 167.15, 167.49. Theoretical mass: 490.55, LC-MS (m/z, I %): 489.0 [(M-H)<sup>+</sup>, 100%]. HPLC Purity: % Area 95.25, Retention Time 5.56 mins.

**5-((6-(2-(3-(4-fluorophenyl)-5-phenyl-4,5-dihydro-1H-pyrazol-1-yl)-2-oxoethoxy)pyridin-3-yl)**

**methylene)thiazolidine-2,4-dione (19a).** Pale yellow colour solid. 57% yield (0.67 g). M.P. 297.1 °C. FTIR (cm<sup>-1</sup>) 3385, 1745, 1699, 1664, 1597, 1527, 1448, 1267, 1155, 844. <sup>1</sup>H-NMR (400 MHz, DMSO-d<sub>6</sub>) δ ppm 3.21-3.26 (m, 1H), 3.90-3.97 (m, 1H), 5.20 (d, J = 16.52 Hz, 1H), 5.32 (d, J=16.48 Hz, 1H), 6.59 (dd, J = 11.72 Hz, 1H), 6.55 (d, J = 9.6 Hz, 1H), 7.24-7.28 (m, 3H), 7.32-7.36 (m, 4H), 7.50 (s, 1H), 7.63 (dd, J = 2.6, 9.62 Hz, 1H), 7.89-7.92 (m, 2H), 8.19 (d, J = 2.6 Hz, 1H), 12.53 (bs, 1H). <sup>13</sup>C-NMR (100 MHz, DMSO-d<sub>6</sub>) δ 41.45, 50.99, 59.81, 112.12, 115.84, 116.04, 119.84, 125.62, 126.61, 128.34, 129.34, 129.42, 138.45, 145.64, 155.05, 160.24, 162.17, 153.89, 167.41. Theoretical mass: 502.52, LC-MS (m/z, I %): 501.1 [(M-H)<sup>+</sup>, 100%]. HPLC Purity: % Area 96.17, Retention Time 5.97 mins.

**5-((6-(2-(5-(2-chlorophenyl)-3-(4-fluorophenyl)-4,5-dihydro-1H-pyrazol-1-yl)-2-oxoethoxy)pyridin-3-yl)**

**methylene)thiazolidine-2,4-dione (19b).** Creamish solid. 88% yield (0.96 g). M.P. 325.3 °C. FTIR (cm<sup>-1</sup>) 3298, 1741, 1662, 1593, 1521, 1450, 1271, 1151, 837, 758. <sup>1</sup>H-NMR (400 MHz, DMSO-d<sub>6</sub>) δ ppm 3.36-3.47 (m, 2H), 3.79-3.86 (m, 1H), 5.18 (d, J = 16.28 Hz, 1H), 5.26 (d, J = 16.28 Hz, 1H), 5.68 (dd, J = 4.8, 11.8 Hz, 1H), 6.38-6.42 (m, 2H), 7.05 (d, J = 8.84 Hz, 2H), 7.23-7.28 (m, 1H), 7.41-7.47 (m, 1H), 7.52 (d, J = 8.88 Hz, 2H), 7.60 (d, J = 0.88 Hz, 1H), 7.72 (s, 1H), 8.01-8.07 (m, 1H), 12.55 (bs, 1H). <sup>13</sup>C-NMR (100 MHz, DMSO-d<sub>6</sub>) δ 53.28, 65.42, 105.15, 107.46, 110.54, 112.38, 112.62, 115.37, 115.55, 121.03, 125.89, 130.90, 131.26, 131.80, 142.59, 151.17, 151.90, 159.64, 164.74, 168.12, 168.31. Theoretical mass: 536.96, LC-MS (m/z, I %): 535.0 [(M-H)<sup>+</sup>, 100%]. HPLC Purity: % Area 98.17, Retention Time 7.22 mins.

**5-((6-(2-(3-(4-fluorophenyl)-5-(furan-2-yl)-4,5-dihydro-1H-pyrazol-1-yl)-2-oxoethoxy)pyridin-3-yl)**

**methylene)thiazolidine-2,4-dione (19c).** Pale yellow solid. 64% yield (0.6 g). M.P. 312.5 °C. FTIR (cm<sup>-1</sup>) 3302, 1743, 1695, 1670, 1599, 1531, 1450, 1269, 1139, 831. <sup>1</sup>H-NMR (400 MHz, DMSO-d<sub>6</sub>) δ ppm 3.46 (dd, J = 4.84, 18.16 Hz, 1H), 3.76-3.83 (m, 1H), 5.17 (d, J = 16.6 Hz, 1H), 5.22 (d, J = 16.6 Hz, 1H), 5.70 (dd, J = 4.68, 11.64 Hz, 1H), 6.36-3.40 (m, 2H), 6.56 (d, J = 9.64 Hz, 1H), 7.34 (t, J = 8.8 Hz, 2H), 7.50 (s, 1H), 7.58 (d, J = 0.68 Hz, 1H), 7.64 (dd, J = 2.5, 9.6 Hz, 1H), 7.90-7.95 (m, 2H), 8.19 (d, J = 2.44 Hz, 1H), 12.52 (bs, 1H). <sup>13</sup>C-NMR (100 MHz, DMSO-d<sub>6</sub>) δ 42.08, 59.32, 65.50, 107.38, 115.26, 115.48, 115.76, 115.93, 119.65, 122.44, 126.53, 127.35, 127.57, 127.69, 127.77, 128.24, 128.54, 129.32, 129.41, 130.38, 130.82, 132.10, 134.69, 137.95, 154.56, 157.63, 162.19, 164.65, 164.67, 167.45, 168.01. Theoretical mass: 492.48, LC-MS (m/z, I %): 490.0 [(M-2H)<sup>+</sup>, 100%]. HPLC Purity: % Area 95.67, Retention Time 5.92 mins.

**5-((6-(2-(3-(4-fluorophenyl)-5-(4-(trifluoromethyl)phenyl)-4,5-dihydro-1H-pyrazol-1-yl)-2-oxoethoxy)**

**pyridin-3-yl)methylene)thiazolidine-2,4-dione (19d).** Creamish solid. 62% yield (0.65 g). M.P. 338.3 °C. FTIR (cm<sup>-1</sup>) 3381, 1712, 1672, 1600, 1529, 1514, 1452, 1269, 1161, 1134, 846. <sup>1</sup>H-NMR (400 MHz, DMSO-d<sub>6</sub>) δ ppm 3.29 (dd, J = 5.2, 18.4 Hz, 1H), 3.94-4.01 (m, 1H), 5.21 (d, J = 16.4 Hz, 1H), 5.34 (d, J = 16.8 Hz, 1H), 5.70 (dd, J = 4.8, 11.2 Hz, 1H), 6.57 (d, J = 9.6 Hz, 1H), 7.35 (t, J = 8.8 Hz, 2H), 7.48-7.50 (m, 2H),

7.50-7.52 (m, 2H), 7.71 (d,  $J = 8.0$  Hz, 2H), 7.89-7.92 (m, 2H), 8.19 (s, 1H), 12.50 (bs, 1H).  $^{13}\text{C}$ -NMR (100 MHz, DMSO- $d_6$ )  $\delta$  41.85, 50.99, 59.81, 112.02, 115.82, 116.04, 119.84, 125.62, 126.61, 128.33, 129.34, 129.42, 138.45, 145.64, 155.05, 160.24, 162.27, 163.89, 167.44. Theoretical mass: 570.51, LC-MS ( $m/z$ , I %): 569.0 [(M-H) $^+$ , 100%]. HPLC Purity: % Area 97.73, Retention Time 7.23 mins.

**5-((6-(2-(3,5-bis(4-fluorophenyl)-4,5-dihydro-1H-pyrazol-1-yl)-2-oxoethoxy)pyridin-3-yl)methylene)thiazolidine-2,4-dione (19e)**. Off white solid. 66% yield (0.78 g). M.P. 292.8 °C. FTIR ( $\text{cm}^{-1}$ ) 3381, 1749, 1699, 1666, 1599, 1529, 1508, 1437, 1404, 1269, 1197, 1138, 842.  $^1\text{H}$ -NMR (400 MHz, DMSO- $d_6$ )  $\delta$  ppm 3.25 (dd,  $J = 4.8, 18.4$  Hz, 1H), 3.89-3.97 (m, 1H), 5.17-5.21 (m, 1H), 5.31 (d,  $J = 16.4$  Hz, 1H), 5.60 (dd,  $J = 4.8, 11.6$  Hz, 1H), 6.56 (d,  $J = 9.6$  Hz, 1H), 7.15 (t,  $J = 8.4$  Hz, 2H), 7.28-7.32 (m, 2H), 7.34-7.36 (m, 2H), 7.51 (s, 1H), 7.65 (d,  $J = 9.6$  Hz, 1H), 7.89-7.92 (m, 2H), 8.18 (s, 1H), 12.48 (bs, 1H).  $^{13}\text{C}$ -NMR (100 MHz, DMSO- $d_6$ )  $\delta$  41.99, 50.97, 59.53, 112.00, 115.25, 115.47, 115.80, 116.02, 119.21, 119.83, 127.79, 127.87, 128.33, 129.28, 129.37, 137.61, 138.41, 145.68, 155.00, 160.16, 160.24, 163.75, 167.12, 167.46. Theoretical mass: 520.51, LC-MS ( $m/z$ , I %): 519.1 [(M-H) $^+$ , 100%]. HPLC Purity: % Area 98.58, Retention Time 6.92 mins.

**5-((6-(2-(5-(2,4-difluorophenyl)-3-(4-fluorophenyl)-4,5-dihydro-1H-pyrazol-1-yl)-2-oxoethoxy)pyridin-3-yl)methylene)thiazolidine-2,4-dione (19f)**. Off white solid. 58% yield (0.65 g). M.P. 319.3 °C. FTIR ( $\text{cm}^{-1}$ ) 3302, 1745, 1695, 1664, 1595, 1529, 1506, 1454, 1425, 1269, 1199, 1157, 1139, 842.  $^1\text{H}$ -NMR (400 MHz, DMSO- $d_6$ )  $\delta$  ppm 3.28-3.34 (m, 1H), 3.92-3.99 (m, 1H), 5.18 (d,  $J = 16.4$  Hz, 1H), 5.29 (d,  $J = 16.4$  Hz, 1H), 5.69 (dd,  $J = 5.2, 12.0$  Hz, 1H), 6.56 (d,  $J = 9.6$  Hz, 1H), 7.04 (t,  $J = 7.6$  Hz, 1H), 7.25 (t,  $J = 9.6$  Hz, 1H), 7.30-7.33 (m, 1H), 7.35-7.37 (m, 2H), 7.51 (s, 1H), 7.65 (d,  $J = 9.6$  Hz, 1H), 7.89-7.92 (m, 2H), 8.18 (s, 1H), 12.49 (bs, 1H).  $^{13}\text{C}$ -NMR (100 MHz, DMSO- $d_6$ )  $\delta$  40.76, 50.95, 54.85, 112.02, 115.82, 116.03, 119.22, 119.83, 128.33, 129.35, 138.47, 145.67, 155.20, 160.23, 163.79, 167.14, 167.45. Theoretical mass: 538.50, LC-MS ( $m/z$ , I %): 537.0 [(M-H) $^+$ , 100%]. HPLC Purity: % Area 95.73, Retention Time 5.61 mins.

**5-((6-(2-(5-(2-chlorophenyl)-3-(2,4-difluorophenyl)-4,5-dihydro-1H-pyrazol-1-yl)-2-oxoethoxy)pyridin-3-yl)methylene)thiazolidine-2,4-dione (21b)**. Pale yellow solid. 60% yield (0.57 g). M.P. 276.9 °C. FTIR ( $\text{cm}^{-1}$ ) 3383, 1747, 1697, 1668, 1647, 1616, 1595, 1533, 1456, 1425, 1269, 1143, 1099, 844, 746.  $^1\text{H}$ -NMR (400 MHz, DMSO- $d_6$ )  $\delta$  ppm 3.14 (dd,  $J = 4.0, 18.0$  Hz, 1H), 4.07-4.14 (m, 1H), 5.18 (d,  $J = 16.4$  Hz, 1H), 5.39 (d,  $J = 16.8$  Hz, 1H), 5.78 (dd,  $J = 5.2, 12.0$  Hz, 1H), 6.58 (d,  $J = 9.6$  Hz, 1H), 7.23-7.25 (m, 2H), 7.30-7.33 (m, 2H), 7.39-7.45 (m, 2H), 7.48-7.50 (m, 1H), 7.66 (dd,  $J = 2.4, 9.6$  Hz, 1H), 7.98-8.04 (m, 1H), 8.20 (d,  $J = 2.4$  Hz, 1H), 12.53 (bs, 1H).  $^{13}\text{C}$ -NMR (100 MHz, DMSO- $d_6$ )  $\delta$  41.64, 57.72, 65.43, 115.48, 120.41, 125.76, 126.69, 126.93, 127.66, 128.73, 129.15, 129.67, 130.53, 130.76, 130.79, 131.76, 131.87, 138.35, 155.66, 159.80, 164.53, 167.32, 167.81. Theoretical mass: 554.95, LC-MS ( $m/z$ , I %): 552.8 [(M-2H) $^+$ , 100%]. HPLC Purity: % Area 96.85, Retention Time 8.23 mins.

**5-((6-(2-(3-(2,4-difluorophenyl)-5-(furan-2-yl)-4,5-dihydro-1H-pyrazol-1-yl)-2-oxoethoxy)pyridin-3-yl)methylene)thiazolidine-2,4-dione (21c)**. Pale yellow solid. 65% yield (0.77 g). M.P. 311.2 °C. FTIR ( $\text{cm}^{-1}$ ) 3383, 1749, 1699, 1668, 1597, 1525, 1506, 1448, 1417, 1265, 1141, 1095, 846.  $^1\text{H}$ -NMR (400 MHz, DMSO- $d_6$ )  $\delta$  ppm 3.37-3.46 (m, 1H), 3.83-3.91 (m, 1H), 5.15 (d,  $J = 16.64$  Hz, 1H), 5.21 (d,  $J = 16.64$  Hz, 1H), 5.67 (dd,  $J = 4.8, 11.8$  Hz, 1H), 6.37-6.41 (m, 2H), 6.57 (d,  $J = 9.56$  Hz, 1H), 7.23-7.28 (m, 1H), 7.42-

7.48 (m, 1H), 7.51 (s, 1H), 7.591-7.597 (m, 1H), 7.65 (dd,  $J = 2.64, 9.6$  Hz, 1H), 7.98–8.04 (m, 1H), 8.19 (d,  $J = 2.46$  Hz, 1H), 12.57 (bs, 1H).  $^{13}\text{C-NMR}$  (100 MHz, DMSO- $d_6$ )  $\delta$  43.49, 50.84, 59.00, 65.26, 105.05, 109.85, 111.95, 115.20, 115.47, 119.76, 127.76, 127.85, 128.28, 137.42, 138.38, 145.60, 151.37, 160.01, 160.63, 163.91, 164.23, 167.39. Theoretical mass: 510.47, LC-MS ( $m/z$ , I %): 508.8 [(M-H) $^+$ , 100%]. HPLC Purity: % Area 96.23, Retention Time 5.96 mins.

**5-((6-(2-(3-(2,4-difluorophenyl)-5-(4-(trifluoromethyl)phenyl)-4,5-dihydro-1H-pyrazol-1-yl)-2-oxoethoxy)pyridin-3-yl)methylene)thiazolidine-2,4-dione (21d).** Pale yellow solid. 60% yield (0.67 g). M.P. 327.3 °C. FTIR ( $\text{cm}^{-1}$ ) 3383, 1712, 1670, 1602, 1506, 1456, 1421, 1269, 1165, 1138, 1111, 854.  $^1\text{H-NMR}$  (400 MHz, DMSO- $d_6$ )  $\delta$  ppm 3.25 (dd,  $J = 4.8, 18.4$  Hz, 1H), 4.00-4.08 (m, 1H), 5.19 (d,  $J = 16.8$  Hz, 1H), 5.33 (d,  $J = 16.8$  Hz, 1H), 5.67 (dd,  $J = 5.2, 11.6$  Hz, 1H), 6.56 (d,  $J = 9.6$  Hz, 1H), 7.23-7.27 (m, 1H), 7.40-7.45 (m, 1H), 7.50 (d,  $J = 8.8$  Hz, 3H), 7.66 (dd,  $J = 2.4, 9.6$  Hz, 1H), 7.71 (d,  $J = 8.0$  Hz, 2H), 7.98-8.04 (m, 1H), 8.18 (d,  $J = 2.0$  Hz, 1H), 12.50 (bs, 1H).  $^{13}\text{C-NMR}$  (100 MHz, DMSO- $d_6$ )  $\delta$  43.684, 50.97, 59.37, 112.04, 119.29, 119.83, 125.57, 126.65, 128.30, 138.49, 145.61, 145.79, 160.24, 164.11, 167.14, 167.47. Theoretical mass: 588.51, LC-MS ( $m/z$ , I %): 587.0 [(M-H) $^+$ , 100%]. HPLC Purity: % Area 96.63, Retention Time 8.57 mins.

**5-((6-(2-(3-(2,4-difluorophenyl)-5-(4-fluorophenyl)-4,5-dihydro-1H-pyrazol-1-yl)-2-oxoethoxy)pyridin-3-yl)methylene)thiazolidine-2,4-dione (21e).** Creamish solid. 59% yield (0.65 g). M.P. 288.7 °C. FTIR ( $\text{cm}^{-1}$ ) 3383, 1749, 1699, 1668, 1600, 1533, 1506, 1456, 1419, 1267, 1141, 1097, 1037, 827.  $^1\text{H-NMR}$  (400 MHz, DMSO- $d_6$ )  $\delta$  ppm 3.15 (d,  $J = 13.96$  Hz, 1H), 4.06-4.14 (m, 1H), 5.18 (d,  $J = 16.48$  Hz, 1H), 5.39 (d,  $J = 16.44$  Hz, 1H), 5.77 (dd,  $J = 5.16, 11.76$  Hz, 1H), 6.57 (d,  $J = 9.76$  Hz, 1H), 7.25-7.33 (m, 5H), 7.41-7.51 (m, 2H), 7.66 (d,  $J = 9.4$  Hz, 1H), 7.98-8.02 (m, 1H), 8.20 (s, 1H), 12.53 (bs, 1H).  $^{13}\text{C-NMR}$  (100 MHz, DMSO- $d_6$ )  $\delta$  43.79, 50.88, 59.04, 65.26, 105.07, 109.89, 111.95, 115.20, 115.41, 119.76, 127.76, 127.85, 128.28, 137.42, 138.38, 145.60, 151.37, 160.17, 160.63, 163.91, 164.23, 167.39. Theoretical mass: 538.50, LC-MS ( $m/z$ , I %): 537.1 [(M-H) $^+$ , 100%]. HPLC Purity: % Area 97.55, Retention Time 6.32 mins.

**5-((6-(2-(3,5-bis(2,4-difluorophenyl)-4,5-dihydro-1H-pyrazol-1-yl)-2-oxoethoxy)pyridin-3-yl)methylene)thiazolidine-2,4-dione (21f).** Cream colour solid. 60% yield (0.63 g). M.P. 295.3 °C. FTIR ( $\text{cm}^{-1}$ ) 3363, 1749, 1699, 1666, 1597, 1533, 1504, 1456, 1419, 1265, 1139, 1139, 1093, 1039, 846.  $^1\text{H-NMR}$  (400 MHz, DMSO- $d_6$ )  $\delta$  ppm 3.27 (dd,  $J = 5.2, 18.4$  Hz, 1H), 3.98-4.05 (m, 1H), 5.16 (d,  $J = 16.8$  Hz, 1H), 5.27 (d,  $J = 16.4$  Hz, 1H), 5.67 (dd,  $J = 5.6, 12.0$  Hz, 1H), 6.56 (d,  $J = 9.6$  Hz, 1H), 7.04 (t,  $J = 8.4$  Hz, 1H), 7.25-7.27 (m, 2H), 7.32-7.38 (m, 1H), 7.43 (t,  $J = 11.6$  Hz, 1H), 7.51 (s, 1H), 7.65 (d,  $J = 9.6$  Hz, 1H), 7.98-8.04 (m, 1H), 8.18 (s, 1H), 12.49 (bs, 1H).  $^{13}\text{C-NMR}$  (100 MHz, DMSO- $d_6$ )  $\delta$  42.45, 50.83, 54.37, 103.86, 104.11, 104.37, 104.77, 105.11, 105.39, 111.59, 111.96, 112.31, 112.50, 119.19, 119.76, 128.25, 138.40, 145.57, 160.16, 163.92, 167.06, 167.40. Theoretical mass: 556.49, LC-MS ( $m/z$ , I %): 555.1 [(M-H) $^+$ , 100%]. HPLC Purity: % Area 98.58, Retention Time 6.92 mins.

**4.2 In-vitro HDAC Enzyme Inhibition Assay.** Recombinant HDACs 1, 2, 3, 6 and 7 were purchased at BPS Bioscience. Recombinant HDAC8 was produced as described recently [108]. In short, HDAC8 was produced in *E. coli* (BL21) DE3 pLysS cells using a pET14b vector containing codon-optimized human HDAC8. The expression of recombinant cHDAC4 was performed according to another recently published procedure [109].

Recombinant cHDAC4 was expressed in *E. coli* (BL21) DE3 pLysS using a pET14b vector (Novagen, EMD Millipore) containing the codon-optimized catalytic domain of human HDAC4, fused to a N-terminal His6-SUMO tag and a C-terminal SII tag and autoinduction media. Enzyme activity assays were performed in a two-step procedure as described in detail previously procedure [109]. The fluorogenic activity assay relies on the transformation of Boc-Lys(trifluoroacetyl)-AMC (Bachem) as substrate for HDAC4, 7 and 8 and Boc-Lys(acetyl)-AMC as substrate for HDAC1, 2, 3 and 6. Afterwards, the deacetylated substrates are converted into a fluorescent product by trypsin.

**4.3 Thermal Shift Assay of HDAC4.** HDAC4 was tested in the absence (DMSO control) and in the presence of compounds. For thermal shift assay 3  $\mu\text{M}$  HDAC4 was mixed with 100  $\mu\text{M}$  of compound (dissolved in DMSO) and incubated for 15 min at 30  $^{\circ}\text{C}$ . Ten aliquots of this mix were transferred into PCR strips (25  $\mu\text{l}$ /well) and further incubated for 60 min at 30  $^{\circ}\text{C}$  in a PCR cycler (T Gradient, Biometra). Each indicated temperature was held for 10 min followed by a temperature increase of 2  $^{\circ}\text{C}$ . After 9.5 min a sample from the respective well was stored on ice. After the sample collection for all indicated temperatures the samples were centrifuged at 4  $^{\circ}\text{C}$  and 18000 g for 15 min. After centrifugation the supernatant was treated with Laemmli Buffer and denatured via heat followed by a SDS-PAGE. By using ImageJ program, the relative band intensity at each indicated temperature was calculated and GraphPad Prism program was used for plotting intensities against respective temperatures and fitting the data to a logistic function [110]. The melting point of the protein is the x-value of the point of inflection, which is the IC<sub>50</sub>-value of the logistic function.

**4.4 Antiproliferative Assay on HUVECs.** HUVECs were procured from Vinod Nursing Home, Bhopal, India; and umbilical cord cells were isolated by collagenase treatment of the umbilical cord and HUVECs were further cultured and maintained for all the further experiments. [(3-(4,5-dimethylthiazol-2-yl)-2,5-diphenyl tetrazolium bromide)] or MTT, a pale-yellow substrate is known to be cleaved by living cells to form a dark blue formazan product. The process involves active mitochondria, and freshly dead cells do not cleave significant amount of MTT. Hence, the amount of MTT cleaved is in directly proportion with the number of viable cells, this is quantified by colorimetric methods. Test compounds and STS were solubilized in DMSO and diluted with complete medium to get 5 different ranges of test concentrations (10, 1, 0.1, 0.01, and 0.001  $\mu\text{M}$ ). DMSO concentration was retained to < 0.1% in all the samples. HUVEC maintained in suitable environments were seeded in 96 well plates and treated with different concentrations of all the test compounds and incubated at 37  $^{\circ}\text{C}$  in 5% CO<sub>2</sub>, for 96 h. MTT reagents were added to the well plates and kept for incubation for 4 h. The formazan products (dark blue colored) formed by the living cells were dissolved in DMSO under a safety cabinet and read at 550 nm. The % inhibitions were calculated and IC<sub>50</sub> for all test compounds were determined by plotting with the different concentrations used.

**4.5 In-vitro VEGFR-2 Inhibition Assay.** HUVEC cells were seeded at 4000-5000 cells/well by using DMEM medium and 10% FCS for 12 h. Post-incubation the cells were incubated in serum for 24 h. Synthesized compounds/STS (10  $\mu\text{M}$ ) and serum were added together and incubated for 30 minutes at 37  $^{\circ}\text{C}$ . The medium was removed and cells were fixed with 4% formaldehyde in PBS. The cells were washed thrice with PBS. The cells were incubated with anti-phospho VEGF Tyr 1175 antibody (1:1000) for 1 h. The cells

were washed thrice with PBS T and incubated with second antibody labelled with HRP (1:5000) for 1 h. The cells were washed and incubated with TMB. The reaction was immobilized with 2N H<sub>2</sub>SO<sub>4</sub> and read at 450 nM. The % inhibition was calculated by normalizing with the control.

**4.6 MTT Cytotoxicity Assay.** *In-vitro* antiproliferative assay were conducted by procedure previously described[29,111]. To summarize, the cells were seeded in 96-well flat-bottom micro plate and maintained at 37 °C in 95% humidity and 5% CO<sub>2</sub> overnight. Different concentration (100, 75, 50, 25, 10, 2.5 µm/ml) of test samples (13b and 14b) and positive control (Paclitaxel and Cis-platin) were treated. The cells were incubated for 48 h. The wells were washed twice with PBS and 20 µL of MTT staining solution was added to each well and plate was incubated at 37 °C. After 4 h, 100 µL of DMSO was added to each well to dissolve the formazan crystals, and absorbance was recorded at 570 nm using micro plate reader. The IC<sub>50</sub> of compounds were calculated by using Graph Pad Prism Version 5.1.

Formula: Surviving cells (%) = Mean OD of test compound / Mean OD of Negative control × 100

**4.7 Capillary Tube Formation Assay.** In order to perform capillary-like tube formation assay, human umbilical vein endothelial cells (HUVECs) were trypsinized at 80% confluency and seeded in a 6-well plate 50,000 cells, DMEM + 10% FCS per well coated with collagen gel. Test compounds (13b and 14b) and STS 10 µM were added into it 3 h post seeding and PBS with 0.001% DMSO was used as control. The plates were incubated at 37 °C in 5% CO<sub>2</sub> for 48 h. The intersections of the tubes were measured in a given field and recorded.

**4.8 Western Blotting.** Immunoblotting assay was performed using previously prescribed procedure[112]. To brief, cells were grown in multi-well dishes on HUVEC cells and washed with cold PBS twice, lysed in Laemmli buffer (62.5 mM Tris-HCl, pH 6.8, 2% SDS, 10% glycerol) supplemented complete® protease inhibitors (Roche), sonication was performed before protein quantification (DC BioRad Protein Assay Cat No. 500-0114). Test compound and STS with equal quantity of proteins were accompanied with 5% β-mercaptoethanol, mixture was heated (95 °C; 12 min); size was fractionated on 9% SDS-PAGE gel and was shifted to nitrocellulose membranes. All Blue Precision Plus Protein Standard (Bio-Rad Cat. No. 161-0373) was used as protein size marker. Membranes were blocked in PBS-T-milk (0.05% Tween, 5% dried fat-free milk) for 45 mins, incubated with primary antibody (3 h; RT; diluted in PBS-T milk), washed (PBS-T) and it was incubated with secondary antibodies (1 h; RT; diluted in PBS-T milk). After removal of unbound secondary antibodies, signals were exposed using super signal west femto maximum sensitivity substrate (Pierce).

**4.9 Chick chorioallontoic membrane (CAM) Assay. Test Substance Preparation:** Test samples were putted in airtight glass vials and stored at 4 °C under light-controlled environment. 10 or 1 µg/µl solution of test samples were prepared in PBS and sterilized by passing through a syringe filter (0.22µm). 1 µg/µl STS solution was prepared in PBS containing 0.1% DMSO. hVEGF (SIGMA) 50 ng/µl was prepared in sterile PBS. **Grafting:** Gelatin sponges (Abogel) was cut in approximately 2 mm\*3 pieces and loaded with 2ul of 1:1 mixture of test solution and VEGF solution. The graft was placed on the CAM. **Eggs:** Fertile Hen eggs

were procured from hatchery and cleaned; they were decontaminated by using alcohol. 1ml of albumin was removed using a syringe and incubated for 8 days. Grafts were placed on developing CAMs and further incubated to day 12. On day 12 CAMs were fixed with formaldehyde and dissected. **Imaging:** Fixed CAMs were observed and scored under constant illumination and magnification under a stereo microscope by two independent experts. **Statistical Analysis:** Data was analysed on MS Excel 2007.

**4.10 In-vivo Antitumor Evaluation on Xenograft Model. Experimental dose determination** – SCID mice were housed in separately ventilated cage for 12 h light dark cycle and that area was controlled for noise and humidity. Animals were fed autoclaved commercial pellets and water ad libitum and were handled in laminar air flow. Mice aged 8-10 weeks were used to carry out experiment. 5 animals were administered 500 mg/kg and 1000 mg/kg single dose of 14b i.p. The animals receiving 1000 mg/kg dose showed symptoms of distress and mortality in 2 animals, whereas animals receiving 500 mg/kg did not show mortality. Clinical distress symptoms were recovered within 6 h. 1/10 of this dose was selected for experimental work. **Antitumor activity** – To brief, HT29 (ATCC – colon carcinoma) cells ( $1 \times 10^5$ ) were injected on back of the mice and allowed to form palpable tumors. Tumors were minced and re-grafted in experimental animals. Test sample were administered after tumor reached a physical size. Doxorubicin (20 mg/kg) and 14b (25 mg/kg) were given by i.p. on 1-5, 8-12, 15-18 day. Tumor volumes were measured using digital vernier callipers (Mitutoyo JAPAN). Tumor volume was calculated by  $\text{Volume} = (\text{width})^2 \times \text{length} / 2$ . At the end of experiment, animals were sacrificed by cervical dislocation. The animals were dissected, and tumors were excised. The excised tumors were immediately imaged.

**4.11 Molecular docking.** Preparation, visualization of structural data and molecular docking was performed using MOE 2019 software (Chemical Computing Group ULC, Canada). The crystal structures of VEGFR-2 (PDB-ID: 1YWN) and HDAC4 (PDB-ID: 4CBY) were obtained from RCSB Protein Data Bank. The structure files were loaded into the program and subjected to structure preparation including 3D-protonation for subsequent docking. The partial charges of all protein and ligand atoms were calculated using the implemented Amber14 force field. Molecular docking was performed choosing the triangle matcher for placement of the ligand in the binding site and ranked with the London dG scoring function. The best 50 poses were passed to the refinement and energy minimization in the pocket using the induced fit method and then rescored with the GBVI/WSA dG scoring function. The protein-ligand complexes were subsequently energy minimized within a radius of 10 Å around the ligand using Amber14 force field.

## ACKNOWLEDGEMENTS

This research work was supported by, “Indo-ASEAN Collaborative Research Project Grant” from ASEAN-India S&T Development Fund (AISTDF), Department of Science and Technology (DST), Government of India, Project Reference Number IMRC/AISTDF/CRD/2018/000001 (to CSR); National Medical Research Council of Singapore (to APK); and National Medical Research Council of Singapore and the Singapore Ministry of Education under its Research Centres of Excellence initiative to Cancer Science Institute of

Singapore, National University of Singapore (to APK). We also acknowledge funding through the LOEWE priority program TRABITA, State of Hesse, Germany (to FJMA).

#### **ABBREVIATIONS USED**

TZD, Thiazolidinediones; VEGFR-2, Vascular endothelial growth factor receptor-2; HDAC, Histone deacetylase; FDA, Food and drug administration; ZBG, Zinc binding group; HIF-1 $\alpha$ , Hypoxia inducible factor-1 $\alpha$ ; <sup>1</sup>H-NMR, Proton Nuclear Magnetic Resonance; Hz, Hertz; J, Coupling Constant; <sup>13</sup>C-NMR, Carbon Nuclear Magnetic Resonance; FTIR, Fourier-transform infrared spectroscopy; UV, Ultraviolet Spectroscopy; HPLC, High Performance Liquid Chromatography; M.P., Melting Point; DMSO, Dimethyl sulfoxide; DMF, Dimethylformamide; K<sub>2</sub>CO<sub>3</sub>, Potassium carbonate; MTT – 3-(4,5-dimethylthiazol-2-yl)-2,5-diphenyl tetrazolium bromide; STS, Staurosporine; IC<sub>50</sub>, Inhibitory concentration; HUVECs, Human umbilical vein endothelial cells; CAM, Chick chorioallantoic membrane.

## REFERENCES

- [1] N.M. Raghavendra, D. Pingili, S. Kadasi, A. Mettu, S.V.U.M. Prasad, Dual or multi-targeting inhibitors: The next generation anticancer agents, *European Journal of Medicinal Chemistry*. 143 (2018) 1277–1300. <https://doi.org/10.1016/j.ejmech.2017.10.021>.
- [2] R. Fu, Y. Sun, W. Sheng, D. Liao, Designing multi-targeted agents: An emerging anticancer drug discovery paradigm, *European Journal of Medicinal Chemistry*. 136 (2017) 195–211. <https://doi.org/10.1016/j.ejmech.2017.05.016>.
- [3] P. Csermely, V. Agoston, S. Pongor, The efficiency of multi-target drugs: the network approach might help drug design, *Trends Pharmacol. Sci.* 26 (2005) 178–182. <https://doi.org/10.1016/j.tips.2005.02.007>.
- [4] L. Huang, Z. Huang, Z. Bai, R. Xie, L. Sun, K. Lin, Development and strategies of VEGFR-2/KDR inhibitors, *Future Medicinal Chemistry*. 4 (2012) 1839–1852. <https://doi.org/10.4155/fmc.12.121>.
- [5] F.-W. Peng, D.-K. Liu, Q.-W. Zhang, Y.-G. Xu, L. Shi, VEGFR-2 inhibitors and the therapeutic applications thereof: a patent review (2012-2016), *Expert Opinion on Therapeutic Patents*. 27 (2017) 987–1004. <https://doi.org/10.1080/13543776.2017.1344215>.
- [6] F.-W. Peng, J. Xuan, T.-T. Wu, J.-Y. Xue, Z.-W. Ren, D.-K. Liu, X.-Q. Wang, X.-H. Chen, J.-W. Zhang, Y.-G. Xu, L. Shi, Design, synthesis and biological evaluation of N-phenylquinazolin-4-amine hybrids as dual inhibitors of VEGFR-2 and HDAC, *European Journal of Medicinal Chemistry*. 109 (2016) 1–12. <https://doi.org/10.1016/j.ejmech.2015.12.033>.
- [7] F.-W. Peng, T.-T. Wu, Z.-W. Ren, J.-Y. Xue, L. Shi, Hybrids from 4-anilinoquinazoline and hydroxamic acid as dual inhibitors of vascular endothelial growth factor receptor-2 and histone deacetylase, *Bioorganic & Medicinal Chemistry Letters*. 25 (2015) 5137–5141. <https://doi.org/10.1016/j.bmcl.2015.10.006>.
- [8] A. Anighoro, J. Bajorath, G. Rastelli, Polypharmacology: Challenges and Opportunities in Drug Discovery: Miniperspective, *J. Med. Chem.* 57 (2014) 7874–7887. <https://doi.org/10.1021/jm5006463>.
- [9] P. Carmeliet, R.K. Jain, Molecular mechanisms and clinical applications of angiogenesis, *Nature*. 473 (2011) 298.
- [10] R.S. Kerbel, Tumor angiogenesis, *N. Engl. J. Med.* 358 (2008) 2039–2049. <https://doi.org/10.1056/NEJMra0706596>.
- [11] N. Ferrara, VEGF as a therapeutic target in cancer, *Oncology*. 69 Suppl 3 (2005) 11–16. <https://doi.org/10.1159/000088479>.
- [12] D.Z. Qian, Targeting Tumor Angiogenesis with Histone Deacetylase Inhibitors: the Hydroxamic Acid Derivative LBH589, *Clinical Cancer Research*. 12 (2006) 634–642. <https://doi.org/10.1158/1078-0432.CCR-05-1132>.
- [13] G.L. Semenza, Targeting HIF-1 for cancer therapy, *Nature Reviews Cancer*. 3 (2003) 721.
- [14] G.D. Yancopoulos, S. Davis, N.W. Gale, J.S. Rudge, S.J. Wiegand, J. Holash, Vascular-specific growth factors and blood vessel formation, *Nature*. 407 (2000) 242.
- [15] S.J. Modi, V.M. Kulkarni, Vascular Endothelial Growth Factor Receptor (VEGFR-2)/KDR Inhibitors: Medicinal Chemistry Perspective, *Medicine in Drug Discovery*. 2 (2019) 100009. <https://doi.org/10.1016/j.medidd.2019.100009>.
- [16] G. Bergers, D. Hanahan, Modes of resistance to anti-angiogenic therapy, *Nature Reviews Cancer*. 8 (2008) 592.
- [17] R.N. Gacche, R.J. Meshram, Angiogenic factors as potential drug target: Efficacy and limitations of anti-angiogenic therapy, *Biochimica et Biophysica Acta (BBA) - Reviews on Cancer*. 1846 (2014) 161–179. <https://doi.org/10.1016/j.bbcan.2014.05.002>.
- [18] S. Giordano, A. Petrelli, From Single- to Multi-Target Drugs in Cancer Therapy: When Aspecificity Becomes an Advantage, *CMC*. 15 (2008) 422–432. <https://doi.org/10.2174/092986708783503212>.
- [19] A. Petrelli, G. Valabrega, Multitarget drugs: the present and the future of cancer therapy, *Expert Opinion on Pharmacotherapy*. 10 (2009) 589–600. <https://doi.org/10.1517/14656560902781907>.
- [20] L. Xie, P.E. Bourne, Developing multi-target therapeutics to fine-tune the evolutionary dynamics of the cancer ecosystem, *Front. Pharmacol.* 6 (2015). <https://doi.org/10.3389/fphar.2015.00209>.
- [21] T.A. Miller, D.J. Witter, S. Belvedere, Histone Deacetylase Inhibitors, *J. Med. Chem.* 46 (2003) 5097–5116. <https://doi.org/10.1021/jm0303094>.

- [22] M. Mottamal, S. Zheng, T.L. Huang, G. Wang, Histone deacetylase inhibitors in clinical studies as templates for new anticancer agents, *Molecules*. 20 (2015) 3898–3941.
- [23] F. Yang, N. Zhao, D. Ge, Y. Chen, Next-generation of selective histone deacetylase inhibitors, *RSC Adv*. 9 (2019) 19571–19583. <https://doi.org/10.1039/C9RA02985K>.
- [24] T. Eckschlager, J. Plch, M. Stiborova, J. Hrabeta, Histone Deacetylase Inhibitors as Anticancer Drugs, *Int J Mol Sci*. 18 (2017). <https://doi.org/10.3390/ijms18071414>.
- [25] S. Subramanian, S.E. Bates, J.J. Wright, I. Espinoza-Delgado, R.L. Piekarz, Clinical Toxicities of Histone Deacetylase Inhibitors, *Pharmaceuticals (Basel)*. 3 (2010) 2751–2767. <https://doi.org/10.3390/ph3092751>.
- [26] S. Shen, A.P. Kozikowski, Why Hydroxamates May Not Be the Best Histone Deacetylase Inhibitors-What Some May Have Forgotten or Would Rather Forget?, *ChemMedChem*. 11 (2016) 15–21. <https://doi.org/10.1002/cmdc.201500486>.
- [27] K.M. VanderMolen, W. McCulloch, C.J. Pearce, N.H. Oberlies, Romidepsin (Istodax, NSC 630176, FR901228, FK228, depsipeptide): a natural product recently approved for cutaneous T-cell lymphoma, *J Antibiot*. 64 (2011) 525–531. <https://doi.org/10.1038/ja.2011.35>.
- [28] K. Tilekar, J.D. Hess, N. Upadhyay, A.L. Bianco, M. Schweipert, A. Laghezza, F. Loiodice, F.-J. Meyer-Almes, R.J. Aguilera, A. Lavecchia, R. C S, Thiazolidinedione “Magic Bullets” Simultaneously Targeting PPAR $\gamma$  and HDACs: Design, Synthesis, and Investigations of their In Vitro and In Vivo Antitumor Effects, *J. Med. Chem.* (2021). <https://doi.org/10.1021/acs.jmedchem.1c00491>.
- [29] K. Tilekar, N. Upadhyay, N. Jansch, M. Schweipert, P. Mrowka, F.J. Meyer-Almes, C.S. Ramaa, Discovery of 5-naphthylidene-2,4-thiazolidinedione derivatives as selective HDAC8 inhibitors and evaluation of their cytotoxic effects in leukemic cell lines, *Bioorganic Chemistry*. 95 (2020) 103522. <https://doi.org/10.1016/j.bioorg.2019.103522>.
- [30] N. Upadhyay, K. Tilekar, N. Jansch, M. Schweipert, J.D. Hess, L. Henze Macias, P. Mrowka, R.J. Aguilera, J. Choe, F.-J. Meyer-Almes, C.S. Rama, Discovery of novel N-substituted thiazolidinediones (TZDs) as HDAC8 inhibitors: in-silico studies, synthesis, and biological evaluation, *Bioorganic Chemistry*. (2020) 103934. <https://doi.org/10.1016/j.bioorg.2020.103934>.
- [31] M.S. Kim, H.J. Kwon, Y.M. Lee, J.H. Baek, J.-E. Jang, S.-W. Lee, E.-J. Moon, H.-S. Kim, S.-K. Lee, H.Y. Chung, Histone deacetylases induce angiogenesis by negative regulation of tumor suppressor genes, *Nature Medicine*. 7 (2001) 437.
- [32] H.J. Kwon, M.S. Kim, M.J. Kim, H. Nakajima, K.-W. Kim, Histone deacetylase inhibitor FK228 inhibits tumor angiogenesis, *International Journal of Cancer*. 97 (2002) 290–296.
- [33] M. Michaelis, U.R. Michaelis, I. Fleming, T. Suhan, J. Cinatl, R.A. Blaheta, K. Hoffmann, R. Kotchetkov, R. Busse, H. Nau, Valproic acid inhibits angiogenesis in vitro and in vivo, *Molecular Pharmacology*. 65 (2004) 520–527.
- [34] D.Z. Qian, X. Wang, S.K. Kachhap, Y. Kato, Y. Wei, L. Zhang, P. Atadja, R. Pili, The histone deacetylase inhibitor NVP-LAQ824 inhibits angiogenesis and has a greater antitumor effect in combination with the vascular endothelial growth factor receptor tyrosine kinase inhibitor PTK787/ZK222584, *Cancer Research*. 64 (2004) 6626–6634.
- [35] B. Deng, Q. Luo, A. Halim, Q. Liu, B. Zhang, G. Song, The Antiangiogenesis Role of Histone Deacetylase Inhibitors: Their Potential Application to Tumor Therapy and Tissue Repair, *DNA and Cell Biology*. 39 (2020) 167–176. <https://doi.org/10.1089/dna.2019.4877>.
- [36] I. Hrgovic, M. Doll, A. Pinter, R. Kaufmann, S. Kippenberger, M. Meissner, Histone deacetylase inhibitors interfere with angiogenesis by decreasing endothelial VEGFR-2 protein half-life in part via a VE-cadherin-dependent mechanism, *Exp Dermatol*. 26 (2017) 194–201. <https://doi.org/10.1111/exd.13159>.
- [37] R. Kurzrock, S.I. Sherman, D.W. Ball, A.A. Forastiere, R.B. Cohen, R. Mehra, D.G. Pfister, E.E.W. Cohen, L. Janisch, F. Nauling, D.S. Hong, C.S. Ng, L. Ye, R.F. Gagel, J. Frye, T. Müller, M.J. Ratain, R. Salgia, Activity of XL184 (Cabozantinib), an Oral Tyrosine Kinase Inhibitor, in Patients With Medullary Thyroid Cancer, *J Clin Oncol*. 29 (2011) 2660–2666. <https://doi.org/10.1200/JCO.2010.32.4145>.
- [38] K.A. Lyseng-Williamson, Cabozantinib as first-line treatment in advanced renal cell carcinoma: a profile of its use, *Drugs Ther Perspect*. 34 (2018) 457–465. <https://doi.org/10.1007/s40267-018-0547-6>.

- [39] S. Yu, D. Quinn, T. Dorff, Clinical use of cabozantinib in the treatment of advanced kidney cancer: efficacy, safety, and patient selection, *OTT*. Volume 9 (2016) 5825–5837. <https://doi.org/10.2147/OTT.S97397>.
- [40] Y. Li, C. Tan, C. Gao, C. Zhang, X. Luan, X. Chen, H. Liu, Y. Chen, Y. Jiang, Discovery of benzimidazole derivatives as novel multi-target EGFR, VEGFR-2 and PDGFR kinase inhibitors, *Bioorganic & Medicinal Chemistry*. 19 (2011) 4529–4535.
- [41] B.D. Smith, M.D. Kaufman, C.B. Leary, B.A. Turner, S.C. Wise, Y.M. Ahn, R.J. Booth, T.M. Caldwell, C.L. Ensinger, M.M. Hood, Altiratinib inhibits tumor growth, invasion, angiogenesis, and microenvironment-mediated drug resistance via balanced inhibition of MET, TIE2, and VEGFR2, *Molecular Cancer Therapeutics*. 14 (2015) 2023–2034.
- [42] J. Zang, X. Liang, Y. Huang, Y. Jia, X. Li, W. Xu, C.J. Chou, Y. Zhang, Discovery of novel pazopanib-based HDAC and VEGFR dual inhibitors targeting cancer epigenetics and angiogenesis simultaneously, *Journal of Medicinal Chemistry*. 61 (2018) 5304–5322.
- [43] L.-L. Yang, G.-B. Li, S. Ma, C. Zou, S. Zhou, Q.-Z. Sun, C. Cheng, X. Chen, L.-J. Wang, S. Feng, L.-L. Li, S.-Y. Yang, Structure–Activity Relationship Studies of Pyrazolo[3,4-*d*]pyrimidine Derivatives Leading to the Discovery of a Novel Multikinase Inhibitor That Potently Inhibits FLT3 and VEGFR2 and Evaluation of Its Activity against Acute Myeloid Leukemia in Vitro and in Vivo, *J. Med. Chem.* 56 (2013) 1641–1655. <https://doi.org/10.1021/jm301537p>.
- [44] E.G. Yang, N. Mustafa, E.C. Tan, A. Poulsen, P.M. Ramanujulu, W.J. Chng, J.J. Yen, B.W. Dymock, Design and synthesis of janus kinase 2 (JAK2) and histone deacetylase (HDAC) bispecific inhibitors based on pacritinib and evidence of dual pathway inhibition in hematological cell lines, *Journal of Medicinal Chemistry*. 59 (2016) 8233–8262.
- [45] L. Yao, N. Mustafa, E.C. Tan, A. Poulsen, P. Singh, M.-D. Duong-Thi, J.X. Lee, P.M. Ramanujulu, W.J. Chng, J.J. Yen, Design and synthesis of ligand efficient dual inhibitors of janus kinase (JAK) and histone deacetylase (HDAC) based on ruxolitinib and vorinostat, *Journal of Medicinal Chemistry*. 60 (2017) 8336–8357.
- [46] C. Tang, C. Li, S. Zhang, Z. Hu, J. Wu, C. Dong, J. Huang, H.-B. Zhou, Novel bioactive hybrid compound dual targeting estrogen receptor and histone deacetylase for the treatment of breast cancer, *Journal of Medicinal Chemistry*. 58 (2015) 4550–4572.
- [47] Y. Ling, C. Xu, L. Luo, J. Cao, J. Feng, Y. Xue, Q. Zhu, C. Ju, F. Li, Y. Zhang, Novel  $\beta$ -carboline/hydroxamic acid hybrids targeting both histone deacetylase and DNA display high anticancer activity via regulation of the p53 signaling pathway, *Journal of Medicinal Chemistry*. 58 (2015) 9214–9227.
- [48] G. Dong, W. Chen, X. Wang, X. Yang, T. Xu, P. Wang, W. Zhang, Y. Rao, C. Miao, C. Sheng, Small molecule inhibitors simultaneously targeting cancer metabolism and epigenetics: discovery of novel nicotinamide phosphoribosyltransferase (NAMPT) and histone deacetylase (HDAC) dual inhibitors, *Journal of Medicinal Chemistry*. 60 (2017) 7965–7983.
- [49] L. Xian-Ping, L. Zhi-Bin, N. Zhi-Qiang, 2-INDOLINONE DERIVATIVES AS MULTITARGET PROTEINKINASE INHIBITORS AND HISTONE DEACETYLASE INHIBITORS, *US 20090298886A1*, 2009.
- [50] V. Monga, U. Swami, M. Tanas, A. Bossler, S.L. Mott, B.J. Smith, M. Milhem, A Phase I/II Study Targeting Angiogenesis Using Bevacizumab Combined with Chemotherapy and a Histone Deacetylase Inhibitor (Valproic Acid) in Advanced Sarcomas, *Cancers*. 10 (2018) 53. <https://doi.org/10.3390/cancers10020053>.
- [51] C. Ding, C. Zhang, M. Zhang, Y.Z. Chen, C. Tan, Y. Tan, Y. Jiang, Multitarget inhibitors derived from crosstalk mechanism involving VEGFR2, *Future Medicinal Chemistry*. 6 (2014) 1771–1789. <https://doi.org/10.4155/fmc.14.112>.
- [52] C.B. Botta, W. Cabri, E. Cini, L. De Cesare, C. Fattorusso, G. Giannini, M. Persico, A. Petrella, F. Rondinelli, M. Rodriguez, A. Russo, M. Taddei, Oxime Amides as a Novel Zinc Binding Group in Histone Deacetylase Inhibitors: Synthesis, Biological Activity, and Computational Evaluation, *J. Med. Chem.* 54 (2011) 2165–2182. <https://doi.org/10.1021/jm101373a>.
- [53] L. Goracci, N. Deschamps, G.M. Randazzo, C. Petit, C. Dos Santos Passos, P.-A. Carrupt, C. Simões-Pires, A. Nurisso, A Rational Approach for the Identification of Non-Hydroxamate HDAC6-Selective Inhibitors, *Sci Rep*. 6 (2016) 29086. <https://doi.org/10.1038/srep29086>.
- [54] Y. Li, P.M. Woster, Discovery of a new class of histone deacetylase inhibitors with a novel zinc binding group, *MedChemComm*. 6 (2015) 613–618.

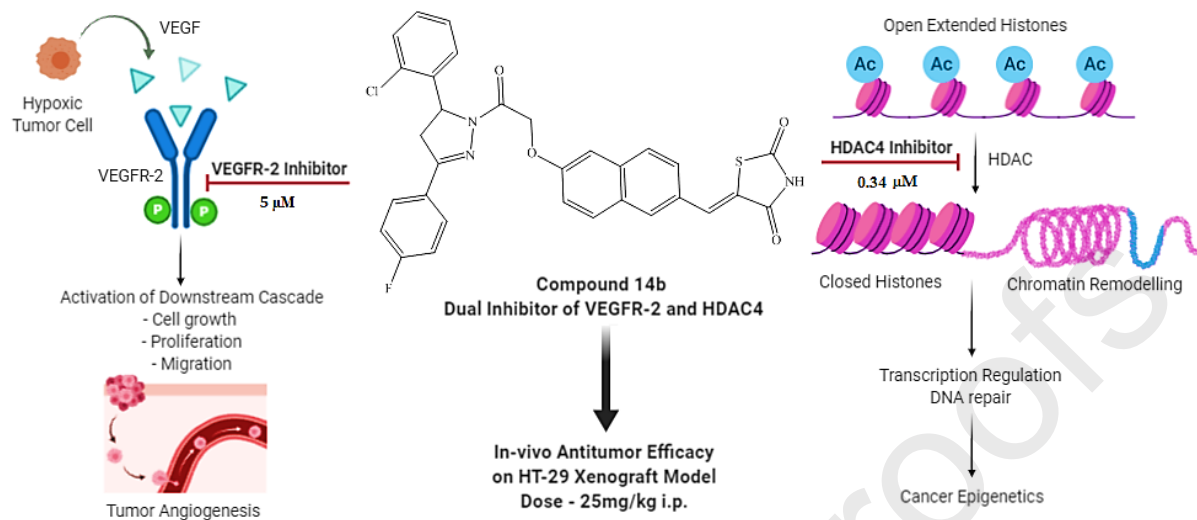
- [55] R.S.K. Vijayan, P. He, V. Modi, K.C. Duong-Ly, H. Ma, J.R. Peterson, R.L. Dunbrack Jr, R.M. Levy, Conformational analysis of the DFG-out kinase motif and biochemical profiling of structurally validated type II inhibitors, *Journal of Medicinal Chemistry*. 58 (2014) 466–479.
- [56] M.A. Zeidan, A.S. Mostafa, R.M. Gomaa, L.A. Abou-zeid, M. El-Mesery, M.A.-A. El-Sayed, K.B. Selim, Design, synthesis and docking study of novel picolinamide derivatives as anticancer agents and VEGFR-2 inhibitors, *European Journal of Medicinal Chemistry*. 168 (2019) 315–329. <https://doi.org/10.1016/j.ejmech.2019.02.050>.
- [57] H.T. Abdel-Mohsen, M.A. Omar, A.M. El Kerdawy, A.E.E. Mahmoud, M.M. Ali, H.I. El Diwani, Novel potent substituted 4-amino-2-thiopyrimidines as dual VEGFR-2 and BRAF kinase inhibitors, *European Journal of Medicinal Chemistry*. 179 (2019) 707–722. <https://doi.org/10.1016/j.ejmech.2019.06.063>.
- [58] Y. Zhang, Y. Chen, D. Zhang, L. Wang, T. Lu, Y. Jiao, Discovery of Novel Potent VEGFR-2 Inhibitors Exerting Significant Antiproliferative Activity against Cancer Cell Lines, *J. Med. Chem.* 61 (2018) 140–157. <https://doi.org/10.1021/acs.jmedchem.7b01091>.
- [59] U. Bhanushali, S. Rajendran, K. Sarma, P. Kulkarni, K. Chatti, S. Chatterjee, C.S. Ramaa, 5-Benzylidene-2, 4-thiazolidenedione derivatives: Design, synthesis and evaluation as inhibitors of angiogenesis targeting VEGFR-2, *Bioorganic Chemistry*. 67 (2016) 139–147.
- [60] U. Bhanushali, S. Kalekar-Joshi, R. Kulkarni-Munshi, S. Yellanki, R. Medishetty, P. Kulkarni, R. Subramanian Chelakara, Design, Synthesis and Evaluation of 5-pyridin-4-yl-2-thioxo-[1, 3, 4]oxadiazol-3-yl Derivatives as Anti-angiogenic Agents Targeting VEGFR-2, *Anti-Cancer Agents in Medicinal Chemistry (Formerly Current Medicinal Chemistry-Anti-Cancer Agents)*. 17 (2017) 67–74.
- [61] R. Neelapapu, D.L. Holzle, S. Velaparthi, H. Bai, M. Brunsteiner, S.Y. Blond, P.A. Petukhov, Design, Synthesis, Docking, and Biological Evaluation of Novel Diazide-Containing Isoxazole- and Pyrazole-Based Histone Deacetylase Probes, *J. Med. Chem.* 54 (2011) 4350–4364. <https://doi.org/10.1021/jm2001025>.
- [62] J. Wen, Q. Niu, J. Liu, Y. Bao, J. Yang, S. Luan, Y. Fan, D. Liu, L. Zhao, Novel thiol-based histone deacetylase inhibitors bearing 3-phenyl-1H-pyrazole-5-carboxamide scaffold as surface recognition motif: Design, synthesis and SAR study, *Bioorganic & Medicinal Chemistry Letters*. 26 (2016) 375–379. <https://doi.org/10.1016/j.bmcl.2015.12.007>.
- [63] J. Yang, G. Cheng, Q. Xu, S. Luan, S. Wang, D. Liu, L. Zhao, Design, synthesis and biological evaluation of novel hydroxamic acid based histone deacetylase 6 selective inhibitors bearing phenylpyrazol scaffold as surface recognition motif, *Bioorganic & Medicinal Chemistry*. 26 (2018) 1418–1425. <https://doi.org/10.1016/j.bmc.2017.08.029>.
- [64] C. Zagni, A. Citarella, M. Oussama, A. Rescifina, A. Maugeri, M. Navarra, A. Scala, A. Piperno, N. Micale, Hydroxamic Acid-Based Histone Deacetylase (HDAC) Inhibitors Bearing a Pyrazole Scaffold and a Cinnamoyl Linker, *IJMS*. 20 (2019) 945. <https://doi.org/10.3390/ijms20040945>.
- [65] X. Liang, J. Zang, X. Li, S. Tang, M. Huang, M. Geng, C.J. Chou, C. Li, Y. Cao, W. Xu, H. Liu, Y. Zhang, Discovery of Novel Janus Kinase (JAK) and Histone Deacetylase (HDAC) Dual Inhibitors for the Treatment of Hematological Malignancies, *J. Med. Chem.* 62 (2019) 3898–3923. <https://doi.org/10.1021/acs.jmedchem.8b01597>.
- [66] C. Dominguez, I. I. M. Maillard, Histone deacetylase inhibitors and compositions and methods of use thereof., WO2014159214A1, 2014.
- [67] J. Pan, X. Wang, J. Barbosa, Preparation of heterocyclic compounds as HDAC modulators., WO2017030938A1, 2017.
- [68] A. Sharma, T. Pathan, R. Mohan, C. S Ramaa, Synthesis and in vitro antitumor activity of novel fluorine containing pyrazoles and pyrazolines, *Letters in Drug Design & Discovery*. 8 (2011) 843–849.
- [69] D. Havrylyuk, B. Zimenkovsky, O. Vasylenko, A. Gzella, R. Lesyk, Synthesis of New 4-Thiazolidinone-, Pyrazoline-, and Isatin-Based Conjugates with Promising Antitumor Activity, *J. Med. Chem.* 55 (2012) 8630–8641. <https://doi.org/10.1021/jm300789g>.
- [70] H. Fahmy, N. Khalifa, M. Ismail, H. El-Sahrawy, E. Nossier, Biological Validation of Novel Polysubstituted Pyrazole Candidates with in Vitro Anticancer Activities, *Molecules*. 21 (2016) 271. <https://doi.org/10.3390/molecules21030271>.
- [71] G. Nitulescu, C. Draghici, O. Oлару, New Potential Antitumor Pyrazole Derivatives: Synthesis and Cytotoxic Evaluation, *IJMS*. 14 (2013) 21805–21818. <https://doi.org/10.3390/ijms141121805>.
- [72] M. Hale, J. Janetka, F. Maltais, J. Cao, Pyrazole compositions useful as inhibitors of ERK, (2004). US6784195B2.

- [73] R.C. Altisen, J.F. Constansa, R.M. Bafalluy, I.C. Rigal, Pyrazoline derivatives useful for the treatment of cancer, US20070066651A1, 2007. <https://patents.google.com/patent/US20070066651A1/en> (accessed June 28, 2020).
- [74] J.L. ADAMS, T. GALLAGHER, I. KELLY OSIFO, NOVEL PYRAZOLE AND PYRAZOLINE SUBSTITUTED COMPOUNDS, US 2002/0156104A1, 2002.
- [75] K.M. Kasiotis, E.N. Tzanetou, S.A. Haroutounian, Pyrazoles as potential anti-angiogenesis agents: a contemporary overview, *Front. Chem.* 2 (2014). <https://doi.org/10.3389/fchem.2014.00078>.
- [76] N. Miyamoto, N. Sakai, T. Hirayama, K. Miwa, Y. Oguro, H. Oki, K. Okada, T. Takagi, H. Iwata, Y. Awazu, Discovery of N-[5-(\$2-[(cyclopropylcarbonyl) amino] imidazo [1, 2-b] pyridazin-6-yl)\$ oxy)-2-methylphenyl]-1, 3-dimethyl-1H-pyrazole-5-carboxamide (TAK-593), a highly potent VEGFR2 kinase inhibitor, *Bioorganic & Medicinal Chemistry*. 21 (2013) 2333–2345.
- [77] M. Wang, S. Xu, H. Lei, C. Wang, Z. Xiao, S. Jia, J. Zhi, P. Zheng, W. Zhu, Design, synthesis and antitumor activity of Novel Sorafenib derivatives bearing pyrazole scaffold, *Bioorganic & Medicinal Chemistry*. 25 (2017) 5754–5763.
- [78] N. Mainolfi, R. Karki, F. Liu, K. Anderson, Evolution of a new class of VEGFR-2 inhibitors from scaffold morphing and redesign, *ACS Medicinal Chemistry Letters*. 7 (2016) 363–367.
- [79] D.J. George, Phase 2 studies of sunitinib and AG013736 in patients with cytokine-refractory renal cell carcinoma, *Clinical Cancer Research*. 13 (2007) 753s–757s.
- [80] B.I. Rini, G.T. Wilding, G. Hudes, W.M. Stadler, S. Kim, J.C. Tarazi, P.W. Bycott, K.F. Liao, J.P. Dutcher, Axitinib (AG-013736; AG) in patients (pts) with metastatic renal cell cancer (RCC) refractory to sorafenib, *Journal of Clinical Oncology*. 25 (2007) 5032–5032.
- [81] R. Kumar, V.B. Knick, S.K. Rudolph, J.H. Johnson, R.M. Crosby, M.-C. Crouthamel, T.M. Hopper, C.G. Miller, L.E. Harrington, J.A. Onori, Pharmacokinetic-pharmacodynamic correlation from mouse to human with pazopanib, a multikinase angiogenesis inhibitor with potent antitumor and antiangiogenic activity, *Molecular Cancer Therapeutics*. 6 (2007) 2012–2021.
- [82] G. Ranieri, M. Mammi, E.D. Di Paola, E. Russo, L. Gallelli, R. Citraro, C.D. Gadaleta, I. Marech, M. Ammendola, G. De Sarro, Pazopanib a tyrosine kinase inhibitor with strong anti-angiogenetic activity: a new treatment for metastatic soft tissue sarcoma, *Critical Reviews in Oncology/Hematology*. 89 (2014) 322–329.
- [83] A. Kabir, K. Tilekar, N. Upadhyay, C.S. Ramaa, Novel Anthraquinone Derivatives as Dual Inhibitors of Topoisomerase 2 and Casein Kinase 2: In Silico Studies, Synthesis and Biological Evaluation on Leukemic Cell Lines, *Anti-Cancer Agents in Medicinal Chemistry (Formerly Current Medicinal Chemistry-Anti-Cancer Agents)*. 18 (2018) 1551–1562.
- [84] V. Patil, K. Tilekar, S. Mehendale-Munj, R. Mohan, C.S. Ramaa, Synthesis and primary cytotoxicity evaluation of new 5-benzylidene-2, 4-thiazolidinedione derivatives, *European Journal of Medicinal Chemistry*. 45 (2010) 4539–4544.
- [85] R. Mohan, A.K. Sharma, S. Gupta, C.S. Ramaa, Design, synthesis, and biological evaluation of novel 2, 4-thiazolidinedione derivatives as histone deacetylase inhibitors targeting liver cancer cell line, *Medicinal Chemistry Research*. 21 (2012) 1156–1165.
- [86] D.T. Hieu, D.T. Anh, N.M. Tuan, P.-T. Hai, L.-T.-T. Huong, J. Kim, J.S. Kang, T.K. Vu, P.T.P. Dung, S.-B. Han, N.-H. Nam, N.-D. Hoa, Design, synthesis and evaluation of novel N -hydroxybenzamides/ N -hydroxypropenamides incorporating quinazolin-4(3 H )-ones as histone deacetylase inhibitors and antitumor agents, *Bioorganic Chemistry*. 76 (2018) 258–267. <https://doi.org/10.1016/j.bioorg.2017.12.007>.
- [87] S. Minucci, P.G. Pelicci, Histone deacetylase inhibitors and the promise of epigenetic (and more) treatments for cancer, *Nat Rev Cancer*. 6 (2006) 38–51. <https://doi.org/10.1038/nrc1779>.
- [88] P. Tessier, D.V. Smil, A. Wahhab, S. Leit, J. Rahil, Z. Li, R. Déziel, J.M. Besterman, Diphenylmethylen hydroxamic acids as selective class IIa histone deacetylase inhibitors, *Bioorganic & Medicinal Chemistry Letters*. 19 (2009) 5684–5688. <https://doi.org/10.1016/j.bmcl.2009.08.010>.
- [89] K. Tilekar, N. Upadhyay, N. Jansch, M. Schweipert, P. Mrowka, F.J. Meyer-Almes, C.S. Ramaa, Discovery of 5-naphthylidene-2,4-thiazolidinedione derivatives as selective HDAC8 inhibitors and evaluation of their cytotoxic effects in leukemic cell lines, *Bioorganic Chemistry*. 95 (2020) 103522. <https://doi.org/10.1016/j.bioorg.2019.103522>.
- [90] L. Ellis, H. Hammers, R. Pili, Targeting tumor angiogenesis with histone deacetylase inhibitors, *Cancer Letters*. 280 (2009) 145–153. <https://doi.org/10.1016/j.canlet.2008.11.012>.
- [91] K. Tilekar, N. Upadhyay, F.-J. Meyer-Almes, F. Loiodice, A.N. Yu, S. Tatiana, D.V. Sokolova, G.B. Smirnova, J. Choe, V.S. Pokrovsky, A. Lavecchia, R. C S, Synthesis and biological evaluation of

- pyrazoline and pyrrolidine-2,5-dione hybrids as potential antitumor agents., *ChemMedChem*. (2020) cmdc.202000458. <https://doi.org/10.1002/cmdc.202000458>.
- [92] R.W. Bürli, C.A. Luckhurst, O. Aziz, K.L. Matthews, D. Yates, Kathy.A. Lyons, M. Beconi, G. McAllister, P. Breccia, A.J. Stott, S.D. Penrose, M. Wall, M. Lamers, P. Leonard, I. Müller, C.M. Richardson, R. Jarvis, L. Stones, S. Hughes, G. Wishart, A.F. Haughan, C. O'Connell, T. Mead, H. McNeil, J. Vann, J. Mangette, M. Maillard, V. Beaumont, I. Munoz-Sanjuan, C. Dominguez, Design, Synthesis, and Biological Evaluation of Potent and Selective Class IIa Histone Deacetylase (HDAC) Inhibitors as a Potential Therapy for Huntington's Disease, *J. Med. Chem.* 56 (2013) 9934–9954. <https://doi.org/10.1021/jm4011884>.
- [93] M. Adel, R.A.T. Serya, D.S. Lasheen, K.A.M. Abouzid, Identification of new pyrrolo[2,3-d]pyrimidines as potent VEGFR-2 tyrosine kinase inhibitors: Design, synthesis, biological evaluation and molecular modeling, *Bioorganic Chemistry*. 81 (2018) 612–629. <https://doi.org/10.1016/j.bioorg.2018.09.001>.
- [94] H.-J. Park, Y. Zhang, S.P. Georgescu, K.L. Johnson, D. Kong, J.B. Galper, Human umbilical vein endothelial cells and human dermal microvascular endothelial cells offer new insights into the relationship between lipid metabolism and angiogenesis, *Stem Cell Reviews*. 2 (2006) 93–101.
- [95] D.Y. Kim, J.A. Park, Y. Kim, M. Noh, S. Park, E. Lie, E. Kim, Y. Kim, Y. Kwon, SALM4 regulates angiogenic functions in endothelial cells through VEGFR2 phosphorylation at Tyr1175, *FASEB j.* 33 (2019) 9842–9857. <https://doi.org/10.1096/fj.201802516RR>.
- [96] Q. Zhang, S. Lu, T. Li, L. Yu, Y. Zhang, H. Zeng, X. Qian, J. Bi, Y. Lin, ACE2 inhibits breast cancer angiogenesis via suppressing the VEGFa/VEGFR2/ERK pathway, *J Exp Clin Cancer Res.* 38 (2019) 173. <https://doi.org/10.1186/s13046-019-1156-5>.
- [97] A.M. Goodwin, In vitro assays of angiogenesis for assessment of angiogenic and anti-angiogenic agents, *Microvascular Research*. 74 (2007) 172–183. <https://doi.org/10.1016/j.mvr.2007.05.006>.
- [98] J. Li, X. Sun, Z. Wang, L. Chen, D. Li, J. Zhou, M. Liu, Regulation of Vascular Endothelial Cell Polarization and Migration by Hsp70/Hsp90-Organizing Protein, *PLoS ONE*. 7 (2012) e36389. <https://doi.org/10.1371/journal.pone.0036389>.
- [99] Z. Li, C. Zhu, B. An, Y. Chen, X. He, L. Qian, L. Lan, S. Li, Indirubin inhibits cell proliferation, migration, invasion and angiogenesis in tumor-derived endothelial cells, *OTT*. Volume 11 (2018) 2937–2944. <https://doi.org/10.2147/OTT.S157949>.
- [100] C.A. Staton, M.W.R. Reed, N.J. Brown, A critical analysis of current in vitro and in vivo angiogenesis assays: Current in vitro and in vivo angiogenesis assays, *International Journal of Experimental Pathology*. 90 (2009) 195–221. <https://doi.org/10.1111/j.1365-2613.2008.00633.x>.
- [101] C.S. Abhinand, R. Raju, S.J. Soumya, P.S. Arya, P.R. Sudhakaran, VEGF-A/VEGFR2 signaling network in endothelial cells relevant to angiogenesis, *J. Cell Commun. Signal.* 10 (2016) 347–354. <https://doi.org/10.1007/s12079-016-0352-8>.
- [102] N.I. Marín-Ramos, D. Alonso, S. Ortega-Gutiérrez, F.J. Ortega-Nogales, M. Balabasquer, H. Vázquez-Villa, C. Andradas, S. Blasco-Benito, E. Pérez-Gómez, A. Canales, J. Jiménez-Barbero, A. Marquina, J.M. del Prado, C. Sánchez, M. Martín-Fontecha, M.L. López-Rodríguez, New Inhibitors of Angiogenesis with Antitumor Activity in Vivo, *J. Med. Chem.* 58 (2015) 3757–3766. <https://doi.org/10.1021/jm5019252>.
- [103] B. Philip, K. Ito, R. Moreno-Sanchez, S.J. Ralph, HIF expression and the role of hypoxic microenvironments within primary tumours as protective sites driving cancer stem cell renewal and metastatic progression., *Carcinogenesis*. 34 (2013) 1699–1707.
- [104] P.-F. Liu, Y.-C. Hu, B.-H. Kang, Y.-K. Tseng, P.-C. Wu, C.-C. Liang, Y.-Y. Hou, T.-Y. Fu, H.-H. Liou, I.-C. Hsieh, L.-P. Ger, C.-W. Shu, Expression levels of cleaved caspase-3 and caspase-3 in tumorigenesis and prognosis of oral tongue squamous cell carcinoma, *PLoS ONE*. 12 (2017) e0180620. <https://doi.org/10.1371/journal.pone.0180620>.
- [105] N. O'Donovan, J. Crown, H. Stunell, A.D. Hill, E. McDermott, N. O'Higgins, M.J. Duffy, Caspase 3 in breast cancer, *Clinical Cancer Research*. 9 (2003) 738–742.
- [106] M. Olsson, B. Zhivotovsky, Caspases and cancer, *Cell Death & Differentiation*. 18 (2011) 1441–1449. <https://doi.org/10.1038/cdd.2011.30>.
- [107] N. Upadhyay, K. Tilekar, F. Loiodice, N. Yu. Anisimova, T.S. Spirina, D.V. Sokolova, G.B. Smirnova, J. Choe, F.-J. Meyer-Almes, V.S. Pokrovsky, A. Lavecchia, C.S. Ramaa, Pharmacophore Hybridization Approach To Discover Novel Pyrazoline-Based Hydantoin Analogs With Anti-tumor Efficacy, *Bioorganic Chemistry*. (2020) 104527. <https://doi.org/10.1016/j.bioorg.2020.104527>.

- [108] N. Jänsch, C. Meyners, M. Muth, A. Koprancovic, O. Witt, I. Oehme, F.-J. Meyer-Almes, The enzyme activity of histone deacetylase 8 is modulated by a redox-switch, *Redox Biology*. 20 (2019) 60–67. <https://doi.org/10.1016/j.redox.2018.09.013>.
- [109] B. Wolff, N. Jänsch, W.O. Sugiarto, S. Frühschulz, M. Lang, R. Altintas, I. Oehme, F.-J. Meyer-Almes, Synthesis and structure activity relationship of 1, 3-benzo-thiazine-2-thiones as selective HDAC8 inhibitors, *European Journal of Medicinal Chemistry*. 184 (2019) 111756. <https://doi.org/10.1016/j.ejmech.2019.111756>.
- [110] A. Volund, Application of the Four-Parameter Logistic Model to Bioassay: Comparison with Slope Ratio and Parallel Line Models, *Biometrics*. 34 (1978) 357. <https://doi.org/10.2307/2530598>.
- [111] M.R. Peram, S. Jalalpure, V. Kumbar, S. Patil, S. Joshi, K. Bhat, P. Diwan, Factorial design based curcumin ethosomal nanocarriers for the skin cancer delivery: in vitro evaluation, *Journal of Liposome Research*. (2019) 1–21.
- [112] K. Tilekar, N. Upadhyay, J.D. Hess, L.H. Macias, P. Mrowka, R.J. Aguilera, F.-J. Meyer-Almes, C.V. Iancu, J.-Y. Choe, C.S. Ramaa, Structure guided design and synthesis of furyl thiazolidinedione derivatives as inhibitors of GLUT 1 and GLUT 4, and evaluation of their anti-leukemic potential, *Eur J Med Chem*. 202 (2020) 112603. <https://doi.org/10.1016/j.ejmech.2020.112603>.

## GRAPHICAL ABSTRACT



- Design and synthesis of diaryl pyrazoline TZD derivatives as dual inhibitors of HDAC and VEGFR-2.
- Lead compound 14b inhibited HUVECs proliferation, migration, and tube formation.
- CAM assay revealed *in-vivo* anti-angiogenic potential of 14b.
- 14b displayed cytotoxicity to different cancer cell lines and
- 14b modulated the expression of proteins, VEGFR-2 and Caspase 3 in western blotting.
- 14b displayed the tumor regression capacity in HT29 mice xenografts.